

Press Fit Design: Force and Torque Testing of
Steel Dowel Pins in Brass and Nylon Samples

by

Alexandra T. Nelson

SUBMITTED TO THE DEPARTMENT OF MECHANICAL ENGINEERING IN
PARTIAL FULFILLMENT OF THE REQUIREMENTS FOR THE DEGREE OF

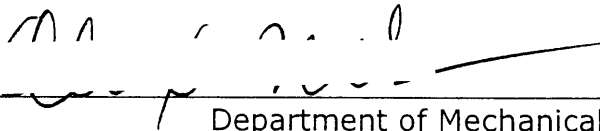
BACHELOR OF SCIENCE IN MECHANICAL ENGINEERING
AT THE
MASSACHUSETTS INSTITUTE OF TECHNOLOGY

FEBRUARY 2006

©2005 Alexandra T. Nelson. All rights reserved.

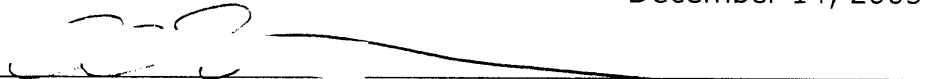
The author hereby grants to MIT permission to reproduce
and to distribute publicly paper and electronic
copies of this thesis document in whole or in part
in any medium now known or hereafter created.

Signature of Author: _____



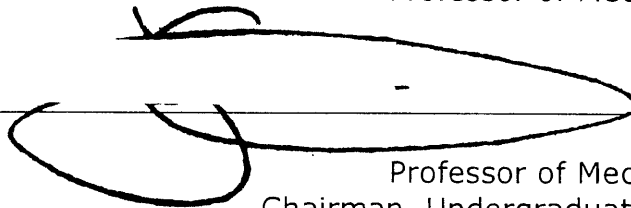
Department of Mechanical Engineering
December 14, 2005

Certified by: _____



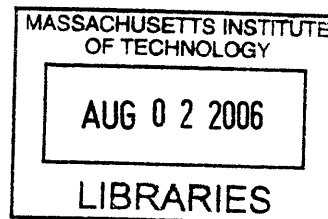
Alexander H. Slocum
Professor of Mechanical Engineering
Thesis Supervisor

Accepted by: _____



John H. Lienhard V
Professor of Mechanical Engineering
Chairman, Undergraduate Thesis Committee

ARCHIVES



Press Fit Design: Force and Torque Testing of Steel Dowel Pins in Brass and Nylon Samples

by

Alexandra T. Nelson

Submitted to the Department of Mechanical Engineering
on December 14, 2005 in Partial Fulfillment of the
Requirements for the Degree of Bachelor of Science in
Mechanical Engineering

ABSTRACT

An experimental study was conducted to determine the accuracy of current press fit theory when applied to press fit design. Brass and nylon hex samples were press fitted with hardened steel dowel pins. Press fit force and torque required to induce slipping were measured experimentally. Sample dimensions and material properties were utilized to predict expected force and torque levels, which were then measured experimentally.

Brass press fit forces proved difficult to predict due to plowing effects in tight interference press fits where material yielding was observed. However, once vertical force was removed, torque was applied to each sample. The observed torque values matched press fit theory well suggesting that the interface pressure of the press fit can be accurately predicted by theory. The brass torque samples matched theory well once material yield conditions were taken into account. The creep sensitivity of the nylon samples made predictions over the testing period unreliable.

Results show the need for further testing with specific attention to precision in sample machining and measurements. Other considerations include press fit interface roughness and plowing effects during press fitting.

Thesis Supervisor: Alexander H. Slocum

Title: Professor of Mechanical Engineering

Acknowledgements

Professor Alexander H. Slocum, Thesis Advisor: For allowing me the opportunity to work with two of his graduate students and to develop part of my research into an undergraduate thesis. His advice and insight have been invaluable in completing the press fit data analysis.

Pierce Hayward: For his assistance with lab set-up, experimentation, and results interpretation.

Jaime Werkmeister: For providing guidance in the press fit experiments.

Table of Contents

ABSTRACT	2
1. Introduction.....	6
2. Experimentation.....	6
2.1 Sample Design.....	6
2.2 Force Experiments.....	8
Nylon Samples.....	8
Testing Apparatus.....	8
Methods	8
Data Analysis.....	10
Brass Samples.....	10
Testing Apparatus.....	10
Methods	10
Data Analysis.....	11
2.3 Torque Experiments.....	12
Brass Samples.....	12
Testing Apparatus.....	12
Methods	12
Nylon Samples.....	13
Testing Apparatus.....	13
Methods	13
Torque Data Analysis	13
3. Theoretical Predictions	14
Von Mises Yield Criterion.....	18
4. Results.....	19
4.1 Experimental Results.....	19
Nylon Experimental Results.....	19
Brass Experimental Results	25
4.2 Theoretical Predictions	28
Nylon Theoretical Predictions	28
Brass Theoretical Predictions	29
4.3 Comparison of Experiment to Theory	31
Brass Sample Results.....	31
Nylon Sample Results.....	40
5. Conclusion	50
Appendix 1: Calculation of Friction Coefficient.....	52
Appendix 2: Nylon and Brass Sample Measurements	54

Appendix 3: Nylon Experimental Force Data	56
Appendix 4: Brass Experimental Force Data	72
Appendix 5: Brass Torque Data	89

1. Introduction

A press fit is created by placing a shaft into a hole that is slightly smaller than the shaft diameter. This difference in shaft and hole diameter is known as the interference. The shaft is slowly pressed into the hole, causing an elastic deformation in the shaft and hole-piece. The deformation in both pieces results in “large normal and frictional forces between the parts.”¹

A simple press-fit calculation based on shaft and hole diameters, material properties, and shaft depth into the part can yield a nominal value for a force and torque approximation. Using an interference fit calculator, such as the one found on <http://www.tribology-abc.com/calculators/default.htm>, one will obtain a result based on the interference between the parts. While this is extremely useful for ideal press fit calculations, this simplified calculator fails to take into account tolerances of all measurements or material yield limits.

In reality, press fitting is not a perfect science. One may use current press fit equations to design a press fit to meet a specific application, but it is difficult to meet precise design targets due to the sensitivity of press fitting. To better understand the variables that influence press fit design, press fit theory has been applied to laboratory samples to determine accuracy and precision of current design methods. By reviewing the experimental results and theoretical predictions for a series of laboratory samples, the true complexity of press fits becomes clear.

2. Experimentation

In order to determine the accuracy of press fit force and torque predictions, an experiment was conducted to compare experimental results to theoretical results predicted by the press fit equations.

2.1 Sample Design

For the press fit experiment, hex pieces, shown in Figure 1, were chosen of two materials: brass and nylon. Samples were designed and acquired by Jaime Werkmeister, a graduate student in the MIT Precision Engineering Research Group.

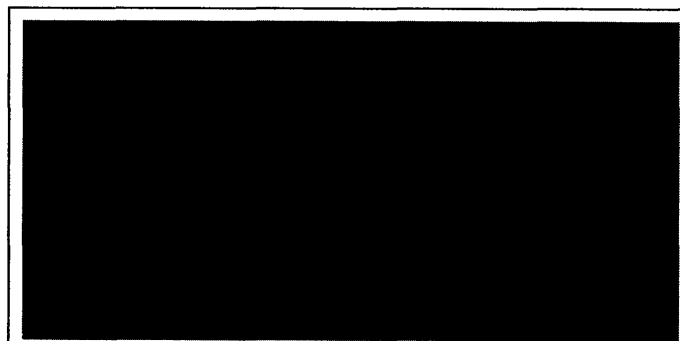


Figure 1. Hex pieces made of brass or nylon were tested to determine press fit force and required torque to cause slipping.

¹ http://www.engineerstoobox.com/doc/etb/mod/stat1/interference/interference_help.html

For each material, one of three hole sizes was drilled: 0.368", 0.374", 0.375". The first group of samples, with diameter on the order of 0.368", has the greatest interference with the steel dowel pin and thus should yield the highest forces and torques experimentally. Nylon samples 1N – 8N and brass samples 1B – 12B belong to group 1. The second group of samples, with diameter close to 0.374", has a small interference approximately equal to 0.001". The press fit forces and torques in group 2 should be much less than for the group 1. Nylon samples 9N – 13N and brass samples 13B – 23B are in group 2. The third group of samples have an inner hole diameter the same size as the steel dowel pin outer diameter. The press fit forces or torques for these samples should be nominally zero. Due to tolerances of the hex pieces, the hole sizes within a group varied up to 0.001".

Table 1. Material properties of brass and nylon utilized in press fit force and torque prediction.²

	Brass	Nylon	Stainless Steel
Modulus of elasticity (N/mm ²)	130000	1200	200000
Yield strength (N/mm ²)	310	78	538
Poisson's ratio	0.33	0.41	0.3
Coefficient of thermal expansion (1/°C)	20.0 x 10 ⁻⁶	90.0 x 10 ⁻⁶	16 x 10 ⁻⁶
Density (g/cm ³)	8.4	1.14	7.78
Coefficient of friction ³ (Material vs. Steel)	0.14	0.1884	-

Thirty-four brass samples were tested. Eighteen nylon samples were tested. For each sample, the hex length was measured with a micrometer and recorded. The nylon inner hole diameters were measured with a micrometer.⁴ The nylon and brass inner hole diameters were measured with a precision CMM machine ± 0.0002" (A-2).

Using a drill press, a short counterbore was added to each sample on the topside. A 0.377" reamer was used to enlarge the existing holes. The purpose of the counterbore was to facilitate pin alignment in the hex piece during press fitting. The length of each counterbore was recorded for each sample (A-2).

Stainless steel precision dowel pins of 0.375" ± 0.0002" were chosen for the press fit inner-body. The CMM machine was also used to measure the steel dowel pins. Based on calibration of the CMM machine, the dowel pins were measured to be 9.53 mm, which is slightly larger than 0.375".

² Source: Crandall, S. H., T. J. Lardner, and N. C. Dahl. An Introduction to the Mechanics of Solids. 2nd ed. McGraw Hill, 1999.

³ Coefficient of friction for brass on steel and nylon on steel were calculated experimentally. Detailed explanation given in A-1.

⁴ All precision CMM measurements were taken post-testing. However, these diameters are less accurate for the nylon pieces due to creep and thermal variations. The micrometer measurements were taken between force and torque testing and are a more accurate measurement of the actual hole diameter during testing. Theoretical predictions for both sets of nylon measurements will be presented in the results section.

2.2 Force Experiments

First, each sample was press fitted with a precision steel dowel pin. The maximum force to press fit was recorded along with the press fit length for use in the theoretical equations.

Nylon Samples

The nylon samples were tested twice. First, the pins were inserted and the force versus distance data was collected. Five weeks later, the pins were removed by pressing the pins out of the nylon hexes and recording the force required to do so. The second force experiment, removal of the dowel pins, was performed in order to correlate maximum press fit forces at both periods in time. Because nylon is subject to creep over time and is thermally sensitive, it is important to determine the magnitude of these effects in the experiment.

Testing Apparatus

A Zwick/Roell Z2.5 compression/tension tester (Serial #155820) controlled by testXpert V9.01 software was used to conduct force testing for the nylon hex samples. The test set-up is shown in Figure 2. The maximum linearity of the test equipment is $\pm 0.01\%$ of the measurement end value, while the position accuracy is $\pm 2 \mu\text{m}$. The machine was run using a 2.5 kN load cell. The machine was calibrated using the software to zero the force reading. When testing, the machine was set to begin recording upon detecting a preload force of +0.2 N or greater. An attachment was added to the upper crosshead of the machine. The attachment, shown below in Figure 3, contains a small recess slightly larger than the end of the dowel pin. This attachment allowed the pin to be aligned directly beneath the location of applied force. Data was collected at 100 Hz. Displacement (mm), force (N), and time (s) data were recorded in spreadsheet format.

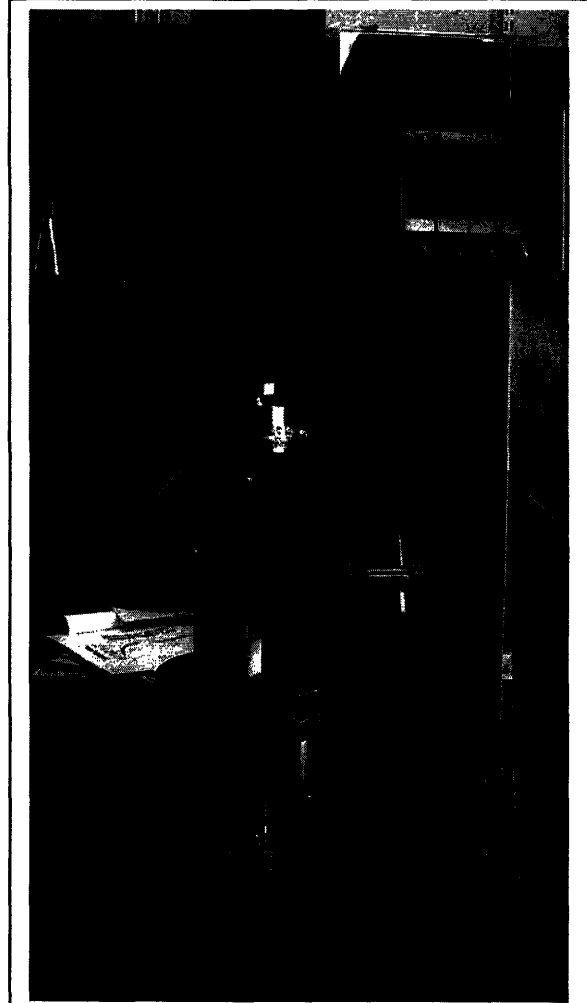


Figure 2. A Zwick/Roell Z2.5 testing device was utilized for the nylon press fits.

Methods

The precision dowel pins were inserted into the counterbore of each nylon hex piece prior to testing. These pieces were inserted by hand, requiring no more than 5 lbs. of force. The initial

pin height, the distance of the dowel pin from the bottom of the hex piece, was measured using dial calipers and recorded for each sample (A-2).⁵

The height of the crosshead was adjusted according to the initial pin depth. To begin testing, the machine was initialized by selecting “run test” on the software. The machine began to slowly displace downwards until detecting a force of 0.1N starting the data collection. Tests were conducted at a crosshead speed of 20 mm/min. The test was stopped manually before displacing the total distance, which was the initial height of the dowel pin. The sample was removed from the test machine and the final height of the dowel pin was recorded (A-2). The press fit distance that the pin traveled is therefore the difference between the initial height and final height of the dowel pin.

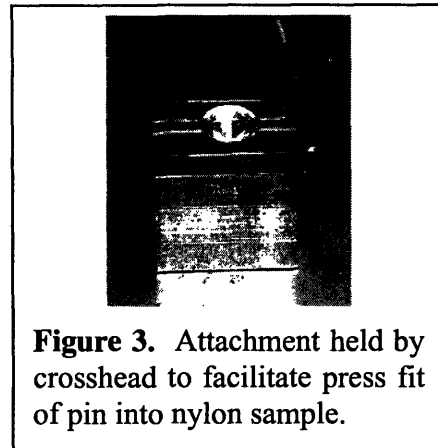


Figure 3. Attachment held by crosshead to facilitate press fit of pin into nylon sample.

For removal of the dowel pins, the same test equipment is required. A hollow brass block and a smaller diameter steel pin are needed to remove the dowel pin from each nylon hex sample. The nylon sample to be tested is placed pin side down into the brass block (Figure 4). The smaller steel pin is then placed on top of the press-fitted dowel pin. The crosshead is then lowered to the appropriate height. Force and distance data is collected over the length of the press fit until the pin completely dislodges.

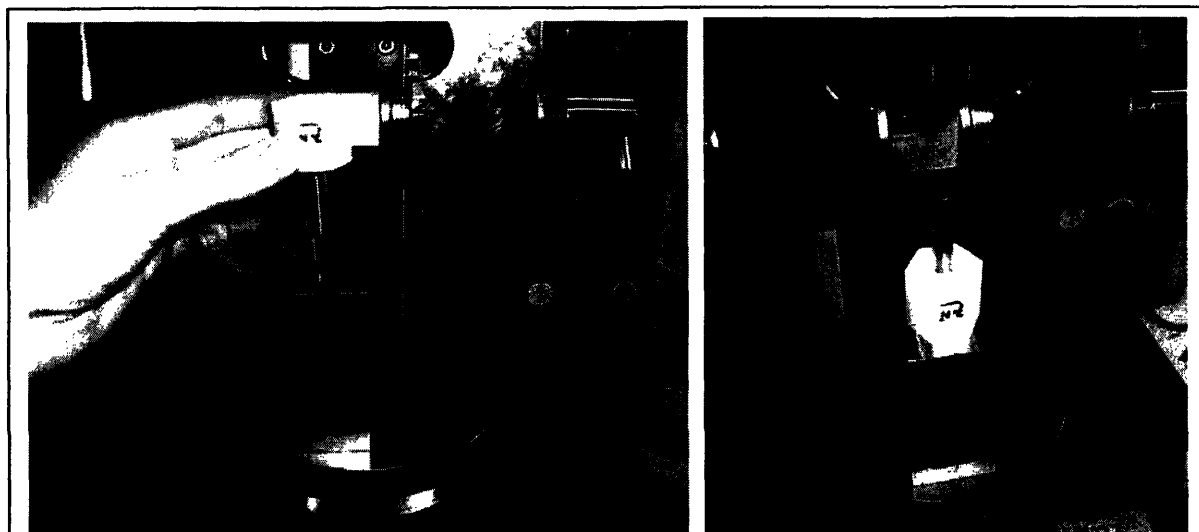


Figure 4. Experimental test set-up to remove dowel pins from nylon samples. Press-fitted nylon hex pieces were inserted with the dowel pin into a hollow brass support as shown on left. Force was applied via a smaller diameter steel pin to remove the press-fitted dowel pin from the nylon sample as shown on right.

⁵ The nylon pieces have shown a tendency towards shrinkage/expansion with changes in climate. Although a 0.377” counterbore was added, the fit of a 0.375”-diameter dowel pin was tight. Therefore, it was necessary to measure the initial pin height since this position may or may not have coincided with the counterbore length.

Data Analysis

After testing, the spreadsheet files were analyzed to determine the maximum press fitting force achieved for the total displacement length of each sample. The force data from the second test, to remove the dowel pin, was plotted on the same graph as the initial press fit data to compare maximum press fit forces.

Brass Samples

For the brass samples, an instron machine, capable of imparting greater vertical forces, was required. Each dowel pin was press fitted with a brass hex piece at each end. This procedure was chosen in order to facilitate torque testing experiments.

Testing Apparatus

An Instron test machine model 1125 (Serial #6214) was used to conduct force testing for the brass hex samples. A voltage reading of $\pm 10.0\text{V}$ was output to the laptop testing software, Labtech Controlpro version 12.1. The machine was run using a 20kN load cell. The accuracy of the force reading is given by the larger of the following values: $\pm 0.5\%$ of indicated load or $\pm 0.25\%$ of load range. The initial machine calibration was performed by zeroing the amplified voltage reading. The machine was set to displace downwards at a rate of $0.2''/\text{min}$. The displacement distance for each test was $0.2''$. After displacing this distance, the machine was set to retract quickly to the initial height. Data was collected at 100 Hz. Force (kN) data was recorded in spreadsheet format.

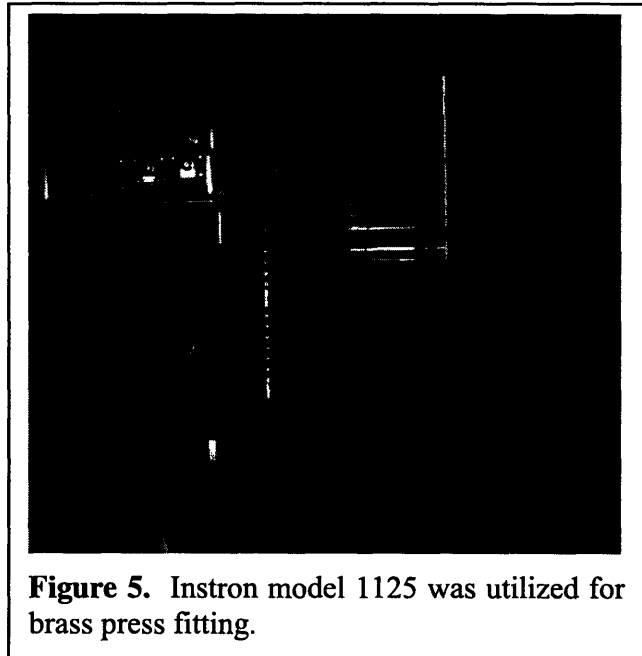


Figure 5. Instron model 1125 was utilized for brass press fitting.

Methods

Before testing, a dowel pin was placed in each odd-numbered brass hex piece. The pins inserted loosely to the depth of the counterbore. The initial height of the pin was known based on the length of the hex piece and the depth of the counterbore:

$$H_i = L_{hex} - L_{CB} \quad (1)$$

Each odd-numbered sample was tested first. The sample was placed on the machine and the crosshead was moved to the correct height. The data collection was started and the machine started. After the machine retracted from the $0.2''$ displacement depth, the data collection was stopped manually.

For the even-numbered brass hex pieces, an odd-numbered hex piece (already press fit) was inserted into the counterbore of the even-numbered sample. The dowel pin of the odd-numbered piece was then press fit into the even-numbered piece using a smaller steel shaft. The use of the

steel shaft prevented disruption of the previous press fit. The test was run following the same procedure from above. The final height of the dowel pin in each hex sample was measured after press fitting and recorded (A-2).

Data Analysis

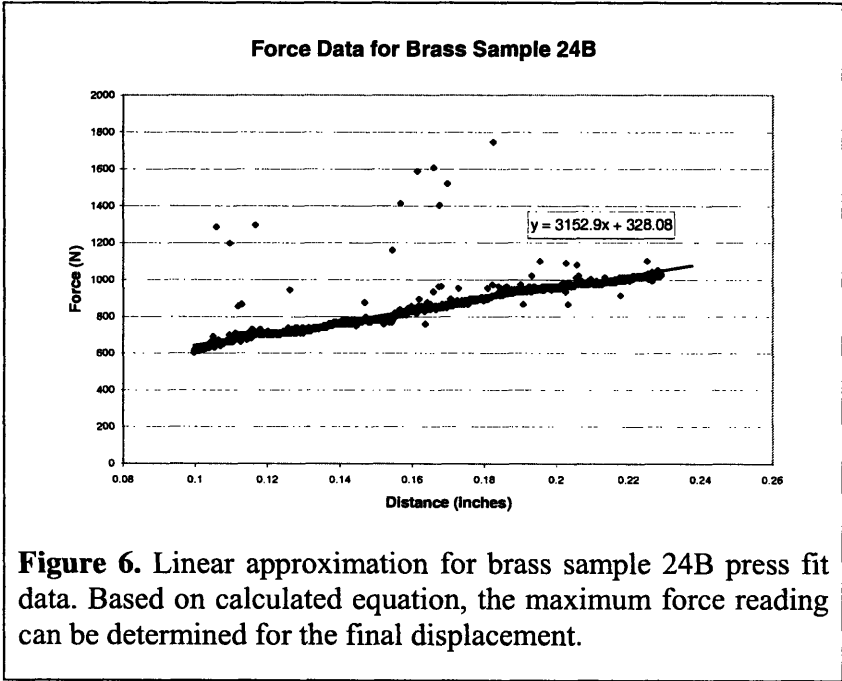
Following testing, the data files were analyzed to determine the press fit distance. To determine time (s) and displacement (in.), the displacement rate and frequency of data collection were employed. The test displacement d_n at the n th data position is equal to

$$d_n = n * 1/f * \text{feed rate} * 1/60 \tag{2}$$

where f is the frequency of data collection (100 Hz) and the feed rate is 0.2"/min.

The test displacement was zeroed according to the position of the first non-zero force reading. The force readings were zeroed by subtracting the noise in the signal. The average value of the measured noise was calculated in the testing region before the first non-zero force reading. This portion of the test, before contact was made with the press fit piece, should have registered a 0.0 V reading (0.0 N) when no force was being applied.

The maximum force reading was determined by a linear approximation at the maximum press fit displacement. Figure 6 below shows the force versus distance data measured experimentally for the brass sample 24B. It is clear that there is a strong linear correlation between force and displacement.



The least-squares regression line was the best method for determining the maximum press fit force from the data because it was insensitive to large value fluctuations. The data results from the Instron machine were noisier than from the Zwick-Roell tester. The linear fit method reduced possible signal variations, which otherwise would have lead to inflated maximum force values.

2.3 Torque Experiments

The torque was transmitted on each hex piece via a lever device inserted over each hex piece. For the brass samples, two hex pieces were press fit onto the same dowel pin. A double hex set-up was chosen to allow for better gripping during testing. The nylon samples were individually inserted into dowel pins. Because much less torque is required to dislodge the nylon pieces, the dowel pins were held in the clamp without slipping.

Brass Samples

Testing Apparatus

The same Instron machine was used to conduct torque testing for the brass hex samples as was used for the brass hex force testing. The brass hex torque testing was conducted using a 1 kN load cell. The load cell was calibrated using the procedure mentioned previously. The machine was set to displace downwards at a rate of 1"/min. The displacement distance for each test was 2.2". After displacing this distance, the machine was set to retract quickly to the initial height. Data was collected at 6 Hz. Force (N) data was recorded in spreadsheet format.

The test set-up is shown in Figure 7. One end of the brass hex pair was clamped loosely. A 1.0" socket with a 0.5" drive was placed over the other hex piece. A welded steel lever was fitted into the socket drive to deliver the required torque. The length of the lever is 500 mm. The point of force application was 400 mm from the socket. The mass of the socket is 134 g. The mass of the lever is 660 g. An aluminum stand was placed under the socket to ensure that the force exerted through the lever caused the sample to rotate and not to displace vertically.

Methods

After positioning a brass hex pair in the clamp and socket, the lever was inserted into the socket drive. The testing apparatus was lowered to < 1 cm above the lever at the 400 mm mark. A black permanent marker was used to mark the centerline of each hex piece and its intersection with the centerline of the dowel pin. These marks were used post-testing to determine which hex piece had slipped under the applied torque.

To run the test, data collection was started and the machine initialized. After the machine reached its maximum distance and retracted, data collection was manually stopped. The



Figure 7. The Instron testing device model 1125 was utilized for the brass and nylon torque testing. The brass sample is shown with one hex piece held by the clamp and the other inserted into the socket.

markings on the test pieces were examined to determine which hex piece had slipped with respect to the dowel pin.

Nylon Samples

Testing Apparatus

The same Instron machine was used to conduct torque testing for the nylon hex samples as was used for the brass hex torque and force testing. The brass nylon torque testing was conducted using a 50 N load cell. The load cell was calibrated using the procedure mentioned previously. All other testing parameters were the same as in the brass torque testing.

The dowel pin of each hex piece was tightly clamped to prevent slipping. The same socket and lever system employed in the brass torque testing was utilized for the nylon samples.

Methods

The same testing methods were employed for the nylon samples as were used for the brass torque samples. After running the test, the centerline marking on each sample was examined to determine whether the nylon hex piece was slipping on the dowel pin or if the dowel pin had slipped in the clamp. Tests where the dowel pin slipped in the clamp were not used.

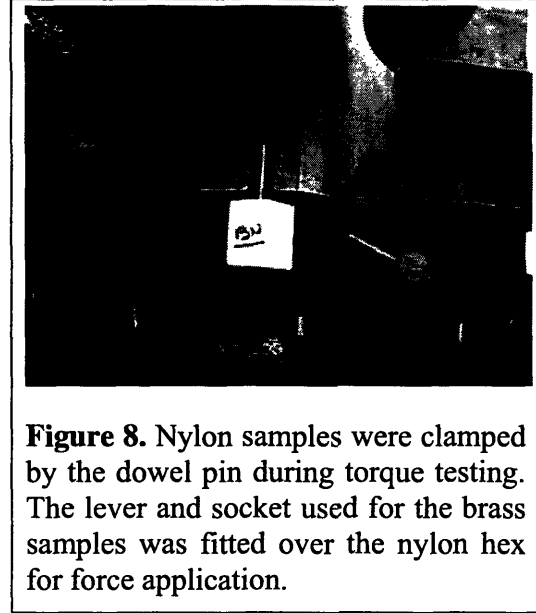


Figure 8. Nylon samples were clamped by the dowel pin during torque testing. The lever and socket used for the brass samples was fitted over the nylon hex for force application.

Torque Data Analysis

The Instron machine data measured the force applied at the end of the lever. The torque $\tau_{instron}$ transmitted at the socket must be calculated from the maximum measured force F_{max} and the distance r from the pivot point:

$$\tau_{instron} = r \times F_{max}, \quad (3)$$

where $r = 408 \text{ mm}$.

The weight of the bar F_{bar} must be considered because it contributes additional torque τ_{bar} to the socket. The mass of the bar $m = 0.660 \text{ kg}$ and the gravitational force $g = 9.8 \text{ m/s}^2$ are multiplied to determine F_{bar} .

$$F_{bar} = m g = 6.47 \text{ N}. \quad (4)$$

From F_{bar} , τ_{bar} can be determined with the weight applied at the position of the center of mass r_{cm} , where

$$\tau_{bar} = r_{cm} \times F_{bar} = 1617 \text{ N-mm}. \quad (5)$$

with r_{cm} equal to half of the length of the bar or 250 mm.

Therefore, the total applied torque τ_{socket} is the sum of $\tau_{instron}$ and τ_{bar} and is

$$\tau_{socket} = 400 \text{ mm} \times F_{max} + 1617 \text{ N-mm}. \quad (6)$$

There is also a residual torque effect due to the horizontal offset of the lever arm.

$$\tau_{resid} = (F_{bar} + F_{max}) D/2 \mu (1 + 2 l_2 / l_1). \tag{7}$$

Thus, the total force transmitted experimentally is the difference between the torque at the socket and the residual torque, which can be considered the net torque,

$$\tau_{net} = \tau_{socket} - \tau_{resid}. \tag{8}$$

3. Theoretical Predictions

Theoretical predictions were made to determine the required force to press fit the pin a distance L and the required torque to turn the hex independent of the pin. Press fit calculations were based on a spreadsheet available on the MIT 2.007 website.⁶

The Excel spreadsheet, compiled by Professor Alexander H. Slocum, is shown below in Figure 9. For each sample, the material properties and dimensions were inputted to determine desired static properties.

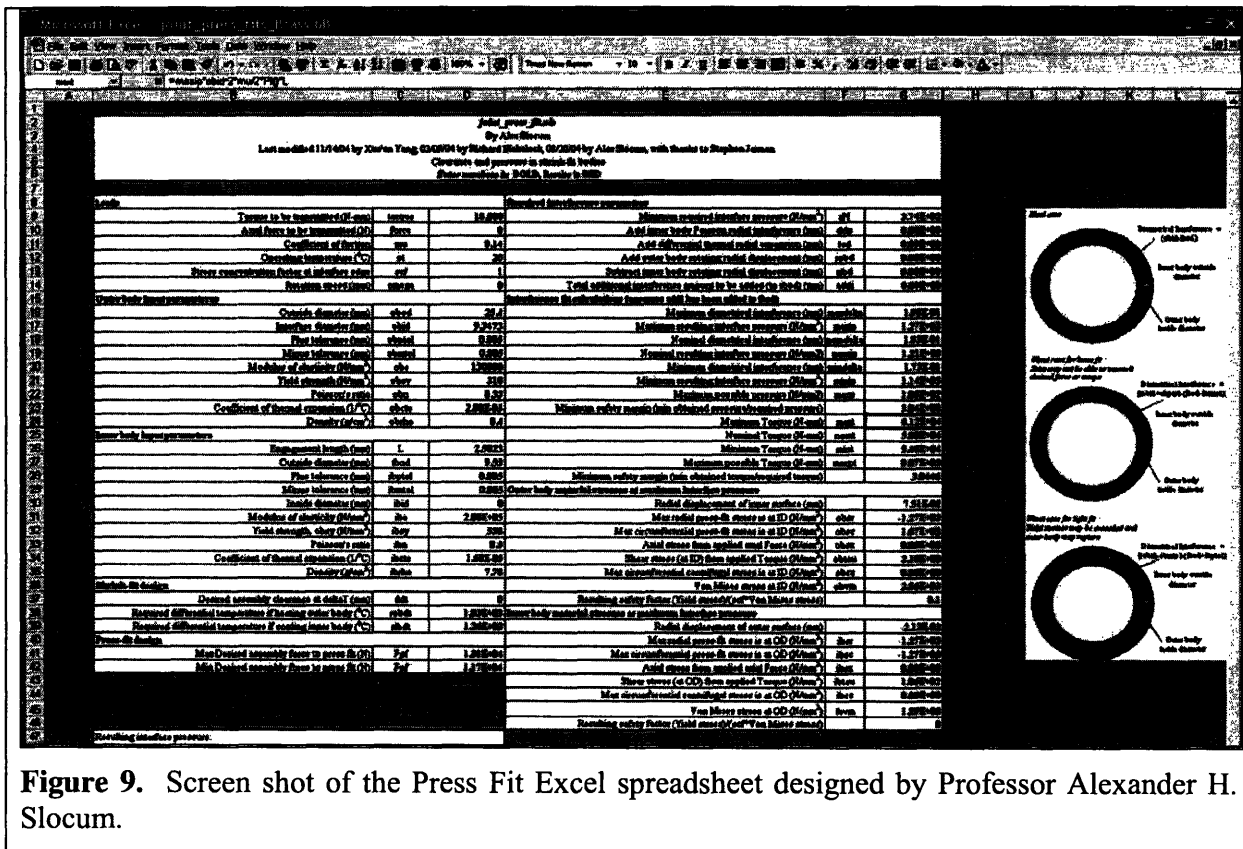


Figure 9. Screen shot of the Press Fit Excel spreadsheet designed by Professor Alexander H. Slocum.

The spreadsheet takes into account dimensional tolerances for the hex inner hole diameter and the dowel pin outer diameter. Based on these tolerances, an upper bounds calculation, nominal value, and lower bounds calculation are made for both force and torque predictions.

⁶ http://pergatory.mit.edu/2.007/software_tools/excel/manufacturing/Joint_press_fit.xls

For each press fit sample, the diametrical interference Δ , defined by the outer body inner diameter subtracted from the inner body outer diameter, was calculated as follows:

$$\Delta = D_{O,inner} - D_{I,outer}. \quad (9)$$

However, the tolerances of the outer body hole \varnothing_{outer} and inner body hole \varnothing_{inner} must also be considered. Refer to Figure 10 for a detailed view of the three possible interference types. The maximum diametrical interference is

$$\Delta_{max} = (D_{O,inner} + \varnothing_{inner}) - (D_{I,outer} - \varnothing_{outer}). \quad (10)$$

The minimum diametrical interference is

$$\Delta_{min} = (D_{O,inner} - \varnothing_{inner}) - (D_{I,outer} + \varnothing_{outer}). \quad (11)$$

For each press fit, three force values were calculated based on the tolerances of the hole diameter and dowel pin diameter. A maximum press fit force F_{max} was determined from the greatest possible diametrical interference Δ_{max} and the corresponding maximum interference pressure P_{max} .

$$F_{max} = \mu P_{max} \pi D_{I,outer} L. \quad (12)$$

A nominal press fit force F_{nom} was determined from the nominal diametrical interference Δ and the corresponding nominal interference pressure P_{nom} .

$$F_{nom} = \mu P_{nom} \pi D_{I,outer} L. \quad (13)$$

A minimum press fit force F_{min} was determined from the smallest diametrical interference Δ_{min} and the corresponding minimum interference pressure P_{min} .

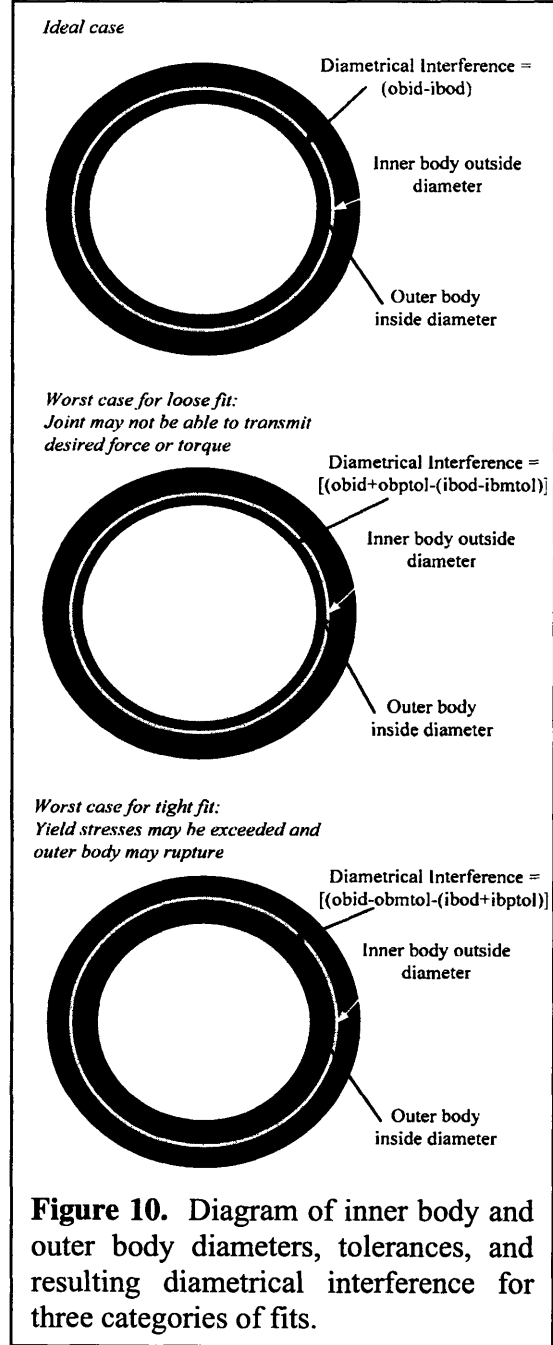
$$F_{min} = \mu P_{min} \pi D_{I,outer} L. \quad (14)$$

For each press fit sample, the force at yielding F_{yield} was determined from the maximum interface pressure at yielding.

$$F_{yield} = \mu P \pi D_{I,outer} L. \quad (15)$$

If $F_{min} > F_{yield}$, then the material is yielding and a maximum press fit force of F_{yield} should be assumed.

The torque predictions were calculated in a similar manner with respect to diametrical interference. The maximum, nominal, and minimal torque were calculated with respect to the corresponding diametrical interference and pressures.



$$\tau_{max} = P_{max} D_{I,outer}^2 \mu / 2 \pi L. \quad (16)$$

$$\tau_{nom} = P_{nom} D_{I,outer}^2 \mu / 2 \pi L. \quad (17)$$

$$\tau_{min} = P_{min} D_{I,outer}^2 \mu / 2 \pi L. \quad (18)$$

For each press fit sample, the torque at yielding τ_{yield} was determined from the maximum interface pressure at yielding.

$$\tau_{yield} = P D_{I,outer}^2 \mu / 2 \pi L. \quad (19)$$

If $\tau_{min} > \tau_{yield}$, then the material is yielding and a maximum press fit torque of τ_{yield} should be assumed.

The following equations were used to calculate stresses, pressures, and torques on both the inner and outer body based on dimensions and material properties.

Radial displacements due to Poisson effect, thermal expansion and rotation

Inner body Poisson radial displacement

$$u_{Poisson} = \frac{-2F\eta_{inner}D_{O,inner}}{\pi(D_{O,inner}^2 - D_{I,inner}^2)E_{inner}} \quad (20)$$

Thermal radial mismatch

$$u_{thermal} = \Delta T(CTE_{outer} - CTE_{inner}) \cdot D_{interface} / 2, \text{ use } D_{interface} = D_{I,outer} \quad (21)$$

Outer body radial displacement caused by rotation

$$u_{centri,outer} = \frac{\rho\omega^2}{8E^*} \left\{ -\left(\frac{D_{I,outer}}{2}\right)^3 + (3 + \eta_{outer}) \left[\frac{(D_{O,outer}^2 + D_{I,outer}^2)}{4(1 + \eta_{outer})} \cdot \frac{D_{I,outer}}{2} + \frac{D_{O,outer}^2 D_{I,outer}}{8(1 - \eta_{outer})} \right] \right\} \quad (22)$$

Inner body radial displacement caused by rotation

$$u_{centri,inner} = \frac{\rho\omega^2}{8E^*} \left\{ -\left(\frac{D_{O,inner}}{2}\right)^3 + (3 + \eta_{inner}) \left[\frac{(D_{O,inner}^2 + D_{I,inner}^2)}{4(1 + \eta_{inner})} \cdot \frac{D_{O,inner}}{2} + \frac{D_{O,inner} D_{I,inner}^2}{8(1 - \eta_{inner})} \right] \right\} \quad (23)$$

Interface pressure as a result of diametrical interference

$$P = \frac{\Delta}{\frac{D_{I,outer}}{E_{outer}} \left(\frac{D_{O,outer}^2 + D_{I,outer}^2}{D_{O,outer}^2 - D_{I,outer}^2} + \eta_{outer} \right) + \frac{D_{O,inner}}{E_{inner}} \left(\frac{D_{O,inner}^2 + D_{I,inner}^2}{D_{O,inner}^2 - D_{I,inner}^2} - \eta_{inner} \right)} \quad (24)$$

For the outer body subjected to internal pressure, axial force, torque and rotation

The radial displacement of the inner surface caused by internal pressure

$$u_{inner} = \frac{D_{I,outer} P}{2E_{outer}} \left(\frac{D_{I,outer}^2 - D_{O,outer}^2}{D_{O,outer}^2 - D_{I,outer}^2} + \eta_{outer} \right) \quad (25)$$

Radial stress caused by internal pressure

$$\sigma_{r,pressure} = \frac{D_{I,outer}^2 P}{D_{O,outer}^2 - D_{I,outer}^2} \left(1 - \frac{D_{O,outer}^2}{D_{I,outer}^2} \right) \quad (26)$$

Circumferential stress caused by internal pressure

$$\sigma_{\theta,pressure} = \frac{D_{I,outer}^2 P}{D_{O,outer}^2 - D_{I,outer}^2} \left(1 + \frac{D_{O,outer}^2}{D_{I,outer}^2} \right) \quad (27)$$

Axial stress caused by axial force

$$\sigma_z = \frac{4F}{\pi(D_{O,outer}^2 - D_{I,outer}^2)} \quad (28)$$

Shear stress caused by torque

$$\tau = \frac{16TD_{I,outer}}{\pi(D_{O,outer}^4 - D_{I,outer}^4)} \quad (29)$$

Circumferential centrifugal stress at the inner surface

$$\sigma_{\theta,centrifugal} = \frac{\rho\omega^2(3+\eta_{outer})}{8} \left(\frac{D_{I,outer}^2}{4} + \frac{D_{O,outer}^2}{2} - \frac{(1+3\eta_{outer})}{(3+\eta_{outer})} \frac{D_{I,outer}^2}{4} \right) \quad (30)$$

Von Mises stress at the inner surface

$$\sigma_{VonMises} = \sqrt{\frac{(\sigma_r - \sigma_{\theta,pressure} - \sigma_{\theta,centrifugal})^2 + (\sigma_{\theta,pressure} + \sigma_{\theta,centrifugal} - \sigma_r)^2 + (\sigma_r - \sigma_z)^2}{2}} + 3\tau^2 \quad (31)$$

For the inner body subjected to external pressure, axial force, torque and rotation

The radial displacement of the outer surface caused by internal pressure

$$u_{outer} = -\frac{D_{O,inner} P}{2E_{outer}} \left(\frac{D_{O,inner}^2 - D_{I,inner}^2}{D_{O,inner}^2 - D_{I,inner}^2} - \eta_{inner} \right) \quad (32)$$

Radial stress caused by internal pressure

$$\sigma_{r,pressure} = -\frac{D_{O,inner}^2 P}{D_{O,inner}^2 - D_{I,inner}^2} \left(1 - \frac{D_{I,inner}^2}{D_{O,inner}^2} \right) \quad (33)$$

Circumferential stress caused by internal pressure

$$\sigma_{\theta,pressure} = \frac{D_{O,inner}^2 P}{D_{O,inner}^2 - D_{I,inner}^2} \left(1 + \frac{D_{I,inner}^2}{D_{O,inner}^2} \right) \quad (34)$$

Axial stress caused by axial force

$$\sigma_z = \frac{4F}{\pi(D_{O,inner}^2 - D_{I,inner}^2)} \quad (35)$$

Shear stress caused by torque

$$\tau = \frac{16TD_{O,inner}}{\pi(D_{O,inner}^4 - D_{I,inner}^4)} \quad (36)$$

Circumferential centrifugal stress at the outer surface

$$\sigma_{\theta,centrifugal} = \frac{\rho\omega^2(3 + \eta_{inner})}{8} \left(\frac{D_{I,inner}^2}{2} + \frac{D_{O,inner}^2}{4} - \frac{(1 + 3\eta_{inner})D_{O,inner}^2}{(3 + \eta_{inner})4} \right) \quad (37)$$

Von Mises stress at the outer surface

$$\sigma_{VonMises} = \sqrt{\frac{(\sigma_r - \sigma_{\theta,pressure} - \sigma_{\theta,centrifugal})^2 + (\sigma_{\theta,pressure} + \sigma_{\theta,centrifugal} - \sigma_r)^2 + (\sigma_r - \sigma_z)^2}{2} + 3\tau^2} \quad (38)$$

Refence: Slocum A.H., Precision Machine Design, Prentice Hall, Eaglewood Cliffs, New Jersey 1992, pp 387-399.

Von Mises Yield Criterion

Adaptations were made to the Excel spreadsheet by Alexandra Nelson to include yield criterion for both press fit force and torque. Equation 31, the Von Mises stress condition at the inner surface, was manipulated to solve for the maximum interface pressure at yielding. By definition, Von Mises stress is equal to the yield strength once a material undergoes plastic deformation. The yield strength is also the maximum possible stress a material can withstand before plastically deforming.

To determine the maximum interference pressure, set equation 31 equal to the yield strength of the material. Substitute σ_r with equation 33, $\sigma_{\theta,pressure}$ with equation 34, $\sigma_{\theta,centrifugal}$ with equation 37, and τ with equation 36. For the experimental torque test, $\sigma_r = P$, $\sigma_{\theta,centrifugal} = 0$, and $\tau = 0$ since there is no rotational velocity ($\omega = 0$).

Solving for the interference pressure gives

$$P = \frac{\sigma_y}{\sqrt{1 + \left(\frac{D_{O,outer}^2 + D_{I,outer}^2}{D_{O,outer}^2 - D_{I,outer}^2} \right)^2 + \left(\frac{2D_{I,outer}^2}{D_{O,outer}^2 - D_{I,outer}^2} \right)^2}} \quad (39)$$

Therefore the maximum press fit force at yielding F_{yield} and the maximum torque at yielding τ_{yield} can be calculated as described above in equations 15 and 19 respectively in conjunction with equation 39.

In order to determine whether a sample is yielding plastically, the spreadsheet is used to calculate both the force and torque due to the interference and the due to the yield strength of the material. If the interference prediction exceeds that given by the Von Mises yield strength criterion, the material is yielding plastically and the force or torque defined by the yield condition should be assumed. If F_{min} exceeds F_{yield} , then the material is yielding. If τ_{min} exceeds τ_{yield} , then the material is yielding.

4. Results

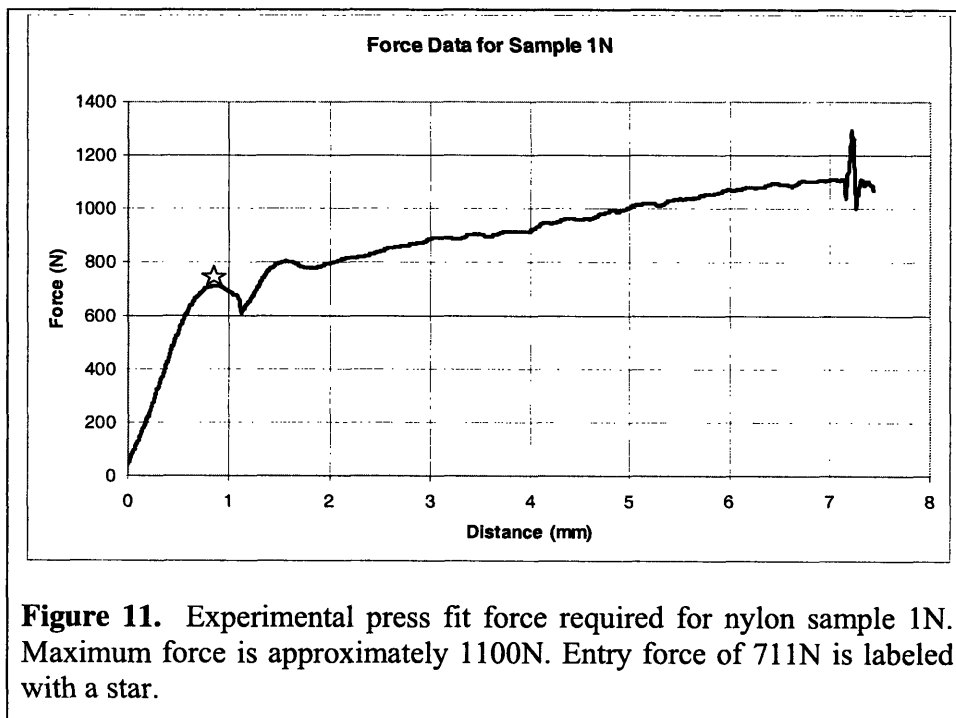
From the hex samples, experimental data was collected and theoretical predictions were made for both press fit force and torque. The results will be presented in three parts: the experimental results, the theoretical predictions, and comparisons between experiment and theory.

4.1 Experimental Results

Data collected experimentally will be presented for each sample. A representative press fit force and torque graph will be shown and described. Graphs for all data collected are available in the appendix.

Nylon Experimental Results

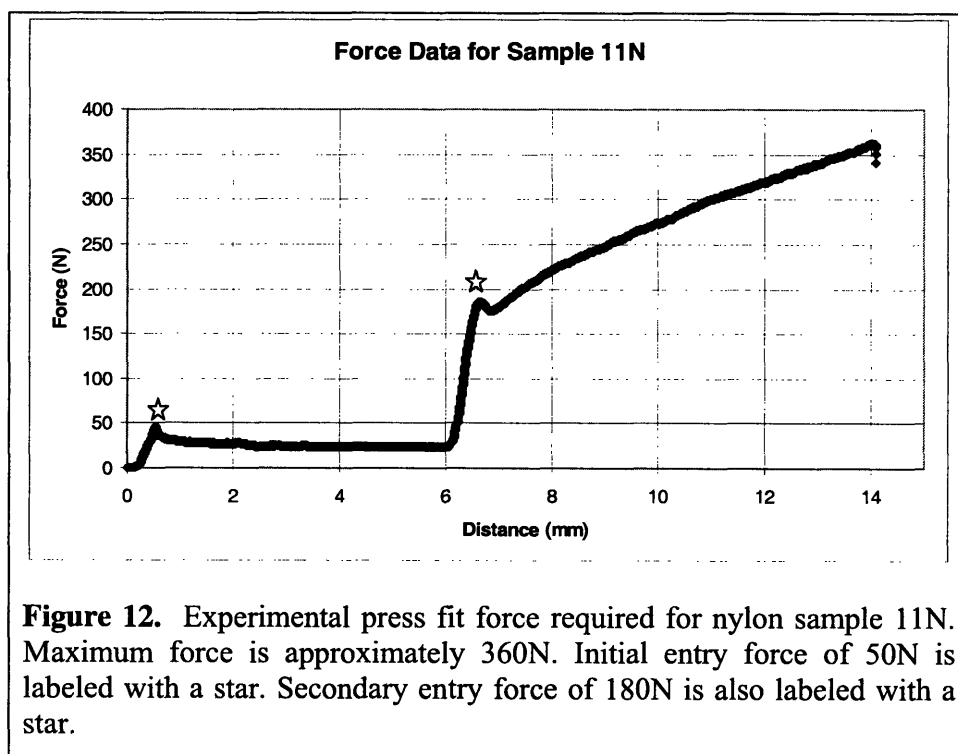
Nylon data includes press fit force, torque, and pin removal force for all 18 samples. Nylon force graphs are available in A-2. Nylon torque graphs are available in A-3. Experimental data for sample 1N will be considered throughout this section. First the press fit force will be examined.



From Figure 11, it is easy to see that the force graph is divided into two parts: the entry and the press fit. For the nylon pieces, an initial entry effect due to misalignment and/or the counterbore is observed. The entry effect appears to add an additional force to the press fit data. The press fit is characterized by a clear change in slope from the entry effect region. The press fit slope varies linearly with displacement making it possible to determine the “starting point” of the press fit. As shown in Figure 10, the entry effects occur from 0 to 1 mm and must be subtracted

from total press fit force. The force due to entry effects is approximately 711 N and is labeled with a star on the graph. The maximum force at 7.4 mm displacement is 1145 N. To determine the press fit force, the entry effects must be subtracted from the maximum force, which results in a press fit force of 434 N for nylon sample 1N.

The graphical data for sample 1N is quite clear to read and relatively linear in both the entry effects and the press fit force vs. displacement slope. This is not the case for all of the nylon force data. As described in Sect. 2.1, the nylon samples had an initial counterbore added to the hex to allow the pin to be easily inserted prior to press fitting. Due to the sensitivity of the nylon pieces, both the hex hole and counterbore diameter changed during testing. It was found in many cases that although the nylon hexes had been reamed with a 0.377" drill, the 0.375" dowel pins could not easily fit into the counterbore. Therefore, the material had expanded and the hole had shrunk. Before press fitting each nylon hex, the pins were inserted into the hex. It was intended that the pin would rest at the bottom of the counterbore. However, because a slight force was required to insert the pins into the tightened counterbore, the pins did not always align at the intended position. In these cases, a graph with multiple press fit regions was obtained. An example of this phenomenon is shown in Figure 12.



As seen in Figure 12, two entry regions and two press fit regions are observed. The first entry and press fit region from 0mm – 6mm corresponds to the counterbore length of the nylon hex. The second entry and press fit region from 6mm – 14mm corresponds to the intended press fit region. For data such as this, the second press fit region is considered the actual press fit under test.

Next the torque data for sample 1N will be examined. Torque testing was performed on all nylon samples. Figure 13 graphs torque vs. time data for sample 1N. For each torque experiment, the maximum torque was determined and recorded. Outlier data points are not considered.

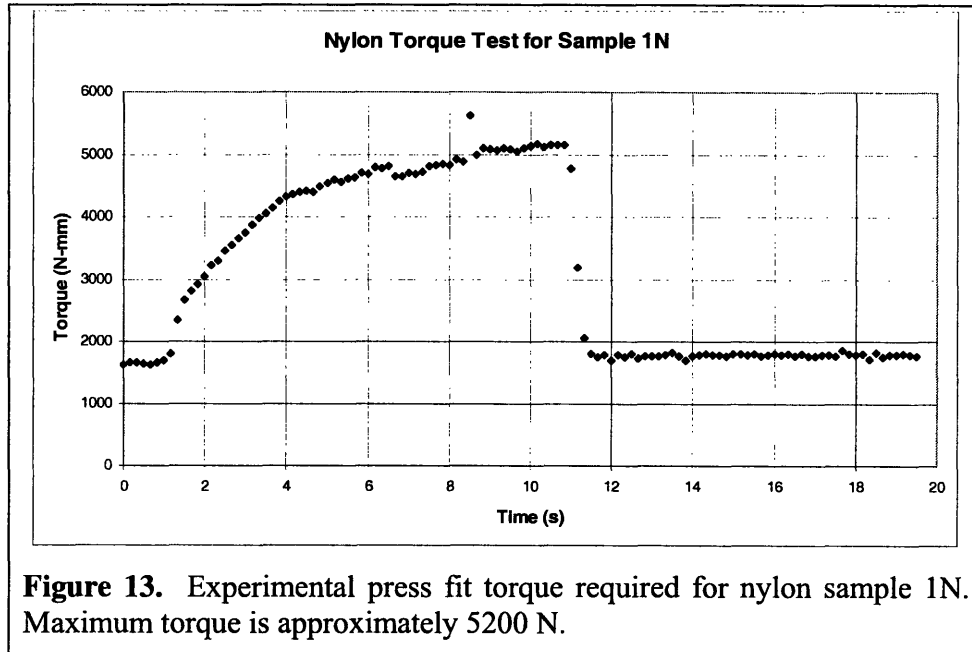


Figure 13. Experimental press fit torque required for nylon sample 1N. Maximum torque is approximately 5200 N.

The maximum torque measured for sample 1N was 5155 N. To determine the press fit torque, a lever effect must be subtracted from this value as described in Sect. 2.3 Torque Data Analysis. From equation 7, the residual torque can be calculated to be 587 N. The net torque, determined from equation 8, is therefore 4466 N.

After the completion of torque testing, a press fit removal test was performed to correlate press fit force over time. The press fit removal experiment was only conducted for the nylon samples due to the sensitive nature of the material. How well this data correlates with the initial press fit forces (including entry effects) will help to determine the accuracy of the theoretical predictions for nylon samples. It will also increase our understanding of the sensitivity of nylon dimensions over time. Shown below is a graph of the pin removal force required for sample 1N.

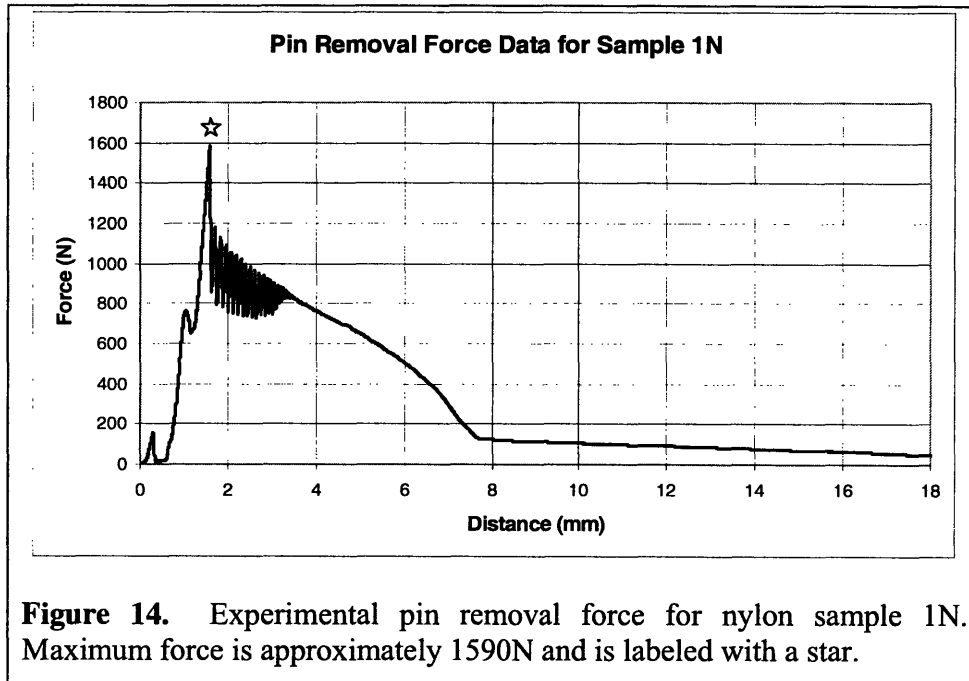


Figure 14. Experimental pin removal force for nylon sample 1N. Maximum force is approximately 1590N and is labeled with a star.

The force required to remove the dowel pin for sample 1N was 1590 N. This is almost 500 N greater than the initial force (1145 N) required to press fit the dowel pin. It is likely that sample 1N experienced significant creep over the testing period. Creep would normally lessen the force, yet the data shows a tightening. This indicates something strange about the data or that the nylon under pressure crept into surface features on the pin and formed an interface.

For the nylon hex pieces, the maximum press fit force and torque obtained experimentally were recorded in Table 2. The hex inner hole diameters are recorded for micrometer and CMM measurements. Although the CMM machine is more precise, these measurements were taken approximately 5 months after testing and may not accurately reflect the diameter of the nylon during testing. The press fit distance is defined as the length of the pin along the diameter described. These nylon hex pieces include a preliminary counterbore, which was not considered part of the press fit distance. Experimental torque values include correction factor from offset lever arm (see Sect. 2.3 Torque Data Analysis).

Table 2. Nylon hex hole diameter measured by micrometer and CMM, press fit distance, measured force, and measured torque.

Sample	Hex Inner Diameter (in) Micrometer	Hex Inner Diameter (mm) CMM	Press Fit Distance (in)	Experimental Press Fit Force (N)	Experimental Torque (N-mm)
1N	0.366	9.3420	0.293	433.9	4382
2N	0.366	9.3284	0.333	1555.0	6059
3N*	0.365	9.3248	0.275	N/A	3808
4N	0.365	9.3327	0.282	617.0	5751
5N	0.366	9.3415	0.264	550.8	5769
6N	0.366	N/A	0.253	386.4	2916
7N	0.365	9.3531	0.106	1561.0	2047
8N	0.365	9.3308	0.259	600.9	2361
9N	0.371	9.4988	0.443	183.3	2973
10N	0.372	9.4955	0.405	156.7	2636
11N	N/A	9.4881	0.412	178.6	<1617
12N	0.371	9.4929	0.417	148.4	<1617
13N	0.371	9.4934	0.705	385.0	3831
14N	0.374	9.5337	0.400	19.0	<1617
15N	0.374	9.5246	0.636	124.3	<1617
16N	0.373	9.5305	0.621	31.2	<1617
17N	0.374	9.5397	0.705	10.0	<1617
18N	0.372	9.5257	0.638	83.7	<1617

*Force data for sample 3N was lost.

For sample 6N, hole diameter was not measured with the CMM machine.

Samples 11N, 12N, 14N, 15N, 16N, 17N, and 18N required less than the torque of the lever to cause the hex to rotate independent of the dowel pin. Therefore, since the torque of the lever arm is 1617 N-mm, these samples required less than 1617 N-mm.

Several important relationships can be seen from the data recorded in Table 2. First, smaller hole diameters (note samples are arranged roughly in ascending order of hole size) have greater interferences with the pin and thus larger forces and torques result. Second, the magnitude of the force and torque measured varies linearly with press fit distance. Therefore for the same hex inner diameter, a larger press fit distance requires a greater force and torque. For example, samples 12N and 13N have hole diameters of 0.371", but the press fit distance for 13N is roughly twice the length of that for 12N. A similar relationship can be seen from the force data, where the force for 13N is roughly twice that of 12N.

As mentioned earlier, press fit removal force values are useful for determining whether the nylon material has undergone significant changes over the course of testing. If no changes have occurred in the material, the force required to press fit the piece, the maximum experimental force, should be the same as the removal force. The maximum experimental force includes the forces due to entry effects and the press fit. Table 3 compares the maximum experiment force upon entry and the removal force for the nylon samples.

Table 3. Nylon hex maximum experimental force, removal force, difference, and % difference.

Sample	Maximum Experimental Force (N)	Removal Force (N)	Absolute Difference	% Difference
1N	1145.0	1587.3	-442.3	-38.6
2N	2037.0	1989.2	47.8	2.3
3N*	N/A	1848.2	N/A	N/A
4N	1590.3	2222.1	-631.8	-39.7
5N	1342.3	1802.5	-460.2	-34.3
6N	2180.3	2247.5	-67.2	-3.1
7N	2037.0	2275.0	-238.0	-11.7
8N	1514.9	1510.4	4.5	0.3
9N	353.1	504.1	-151.0	-42.8
10N	300.7	420.0	-119.3	-39.7
11N	362.2	536.9	-174.7	-48.2
12N	268.4	371.2	-102.8	-38.3
13N	489.5	679.5	-190.0	-38.8
14N	34.5	106.3	-71.8	-208.1
15N	124.3	245.1	-120.8	-97.2
16N	62.0	77.3	-15.3	-24.7
17N	10.0	22.2	-12.2	-122.3
18N	131.7	174.7	-43.0	-32.6

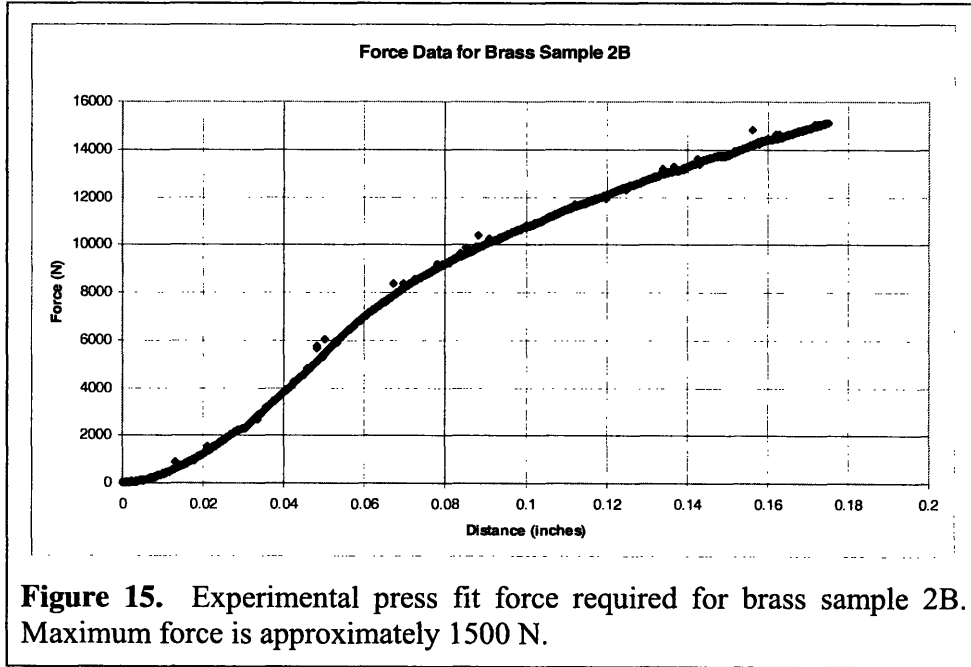
*Force data for sample 3N was lost.

From Table 3, it is clear that the majority of the pieces have undergone changes on the order of 40%. Some samples have not been affected, such as 2N, 6N, and 8N. But substantial effects are seen in 14N and 17N. The average calculated difference is determined to be -48.1%. Because the average removal force for the eighteen nylon samples is 48.1% greater, this would suggest that the material could be creeping into features creating an interlock between the nylon and the steel dowel pin. The data suggests that over time nylon is extremely sensitive. For future press fit testing, I would not recommend it as a material that is easy to use or one that is reliable over the testing period.

Brass Experimental Results

Brass data includes press fit force and torque. Brass force graphs are available in A-4. Brass torque graphs are available in A-5. Experimental data for sample 2B will be considered throughout this section. First the press fit force will be examined.

The maximum press fit force varied linearly with displacement into the hex piece.



The maximum press fit force measured for sample 2B was 15134 N. It is clear from Figure 15 that there is little entry effect seen in the brass samples as compared to the nylon press fit. The material proved to press fit more linearly overall. No counterbore effect is observed because the pin always inserted easily into the brass hex and was positioned in the correct location prior to testing (A-2).

Recall from the experimental set-up (Sect. 2.2) that brass hexes were press fitted two to each dowel pin. Torque testing was performed on each pair of brass hex pieces. Due to the strength of the brass press fits, only one sample was tested from each pair, while the other served as a holding device in the clamp. Therefore, approximately half of the brass samples were tested for maximum torque. For each torque experiment, the maximum torque was determined graphically and recorded. Outlier data points are not considered.

Torque data for sample 2B is shown below in Figure 16.

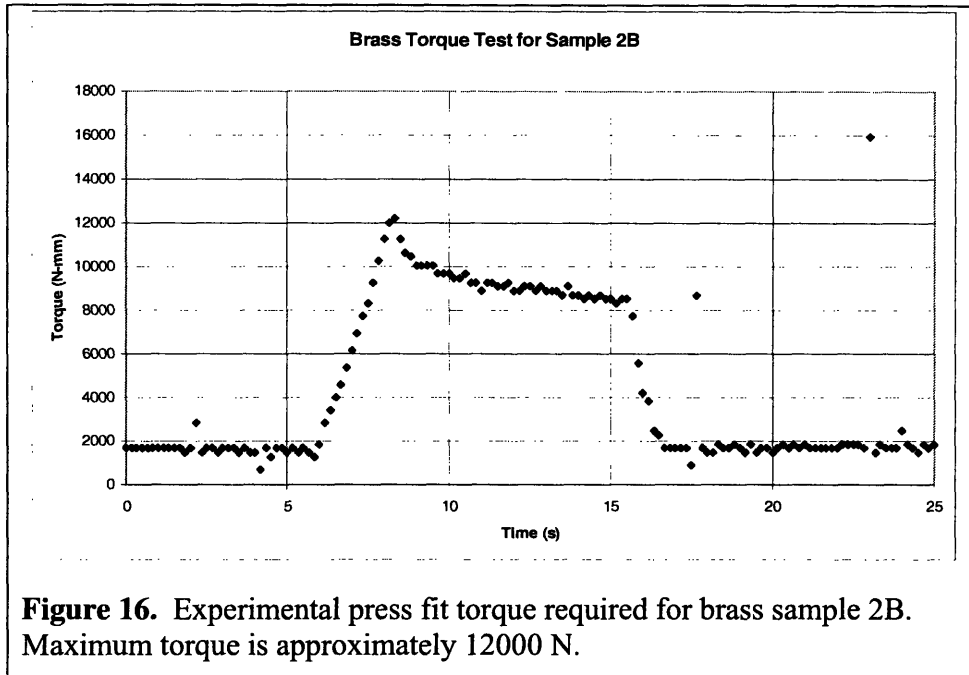


Figure 16. Experimental press fit torque required for brass sample 2B. Maximum torque is approximately 12000 N.

The maximum torque measured for sample 2B was 12216 N. To determine the press fit torque, a lever effect must be subtracted from this value as described in Sect. 2.3 Torque Data Analysis. From equation 7, the residual torque can be calculated to be 195 N. The net torque, determined from equation 8, is therefore 12021 N.

Figure 16 shows a linear increase in torque that peaks initially, then decreases slightly before reducing to the weight of the bar (1617 N-mm). This initial peak is not seen in all samples, but is most noticeable in group 1 brass samples that deformed plastically during press fitting. An effect that would be interesting to consider is the possibility of surface abrasion or particles on the interface between the steel and brass press fit. The radial stress between the materials could lead to a relative interlocking at the abrasive interface. When applying torque to the press fit, a greater initial torque would be required to dislodge the interlocked surfaces. This phenomenon would cause the experimental results to be greater than the theoretical predictions. In order to gain understanding of these surface effects, a study could be performed comparing press fit torque required for various surface roughnesses.

For the brass hex pieces, the press fit force and torque obtained experimentally were recorded in Table 3. Samples 28B, 30B, 32B and 33B required less than the torque of the lever to cause the hex to rotate independent of the dowel pin. Therefore, since the torque of the lever arm is 1617 N-mm, these samples required less than 1617 N-mm.

Table 4. Brass hex hole diameter, press fit distance, measured force, and measured torque.

Sample	Hex Inner Diameter (in) Micrometer	Hex Inner Diameter (mm) CMM	Distance (mm)	Experimental Force (N)	Experimental Torque (N-mm)
1B	0.368	9.3403	2.25	8351	
2B	0.3688	9.3383	3.64	15134	12021
3B	0.3658	9.3331	6.08	19936	18152
4B	0.369	9.3342	3.95	10398	
5B	0.369	9.3467	6.03	13737	
6B	0.3689	9.3473	2.45	11102	23285
7B	0.3687	9.3360	4.85	13261	27860
8B	0.369	9.3318	4.11	15269	
9B	0.3689	9.3357	4.02	14392	
10B	0.3687	9.3145	4.87	18013	29605
11B	0.3685	9.3347	N/A	N/A	
12B	0.3685	9.3374	4.94	12816	
13B	0.3755	9.5129	5.77	2374	8504
14B	0.3755	9.5158	5.40	2517	
15B	0.376	9.5154	5.30	1540	
16B	0.3755	9.5165	5.59	1528	5691
17B	0.376	9.5146	9.32	1683	
18B	0.3759	9.5194	6.09	1708	6441
19B	0.376	9.5224	5.78	1617	
20B	0.3755	9.5171	6.08	2000	6921
21B	0.3761	9.5206	5.71	1879	7017
22B	0.3755	9.5165	5.11	1807	
23B	0.376	9.5205	5.73	1604	
24B	0.376	9.5364	5.91	1033	4399
25B	0.376	9.5389	4.79	1344	
26B	0.376	9.5266	6.00	800	3952
27B	0.3763	9.5305	7.08	300	
28B	0.376	9.5300	5.74	701	<1617
29B	0.3762	9.5311	6.37	1384	
30B	0.3765	9.5369	N/A	0	<1617
31B	0.376	9.5374	5.52	815	
32B	0.376	9.5312	6.24	523	<1617
33B	0.3762	9.5387	5.44	567	<1617
34B	0.3765	9.5358	5.91	1164	

4.2 Theoretical Predictions

For each sample, theoretical calculations were performed to predict the force and torque required. Measured dimensions and corresponding tolerances, material properties, and press fit length for each sample were inputted into a series of equations from Sect. 3. The theoretical predictions will be presented here in tabular format for all nominal values. Theoretical predictions including tolerances can be viewed in Sect. 4.3.

Nylon Theoretical Predictions

Table 5. Nylon theoretical predictions for force and torque are shown below for the micrometer diameter measurements and the experimentally measured press fit distance.

Sample	Hex Inner Diameter (in) Micrometer	Distance (in)	Predicted Force (N)	Predicted Torque (N-mm)
1N	0.366	0.329	700.5	3256
2N	0.366	0.014	795.5	3698
3N	0.365	0.002	733.1	3398
4N	0.365	0.301	750.4	3478
5N	0.366	0.557	631.6	2936
6N	0.366	0.177	601.7	2797
7N	0.365	0.108	280.4	1300
8N	0.365	0.103	686.4	3182
9N	0.371	0.452	466.0	2196
10N	0.372	0.417	319.2	1508
11N*	N/A	0.447	N/A	N/A
12N	0.371	0.435	438.8	2067
13N	0.371	0.677	230.0	1092
14N	0.374	0.435	105.0	499
15N	0.374	0.678	166.9	793
16N	0.373	0.696	326.4	1546
17N	0.374	0.677	184.9	878
18N	0.372	0.689	502.9	2376

*The micrometer diameter measurement for sample 11N was not taken at the same time as all other nylon samples, therefore no predictions were made.

Table 6. Nylon theoretical predictions for force and torque are shown below for the CMM diameter measurements and the experimentally measured press fit distance.

Sample	Hex Inner Diameter (mm) CMM	Distance (in)	Predicted Force (N)	Predicted Torque (N-mm)
1N	9.3420	0.329	574.9	2685
2N	9.3284	0.014	700.6	3268
3N	9.3248	0.002	590.8	2755
4N	9.3327	0.301	581.3	2712
5N	9.3415	0.557	519.8	2428
6N*	N/A	0.177	N/A	N/A
7N	9.3531	0.108	194.6	910
8N	9.3308	0.103	536.9	2505
9N	9.4988	0.452	142.6	677
10N	9.4955	0.417	144.2	685
11N	9.4881	0.447	178.3	846
12N	9.4929	0.435	-20263.3	758
13N	9.4934	0.677	230.0	1092
14N	9.5337	0.435	-15.3	-73
15N	9.5246	0.678	35.4	169
16N	9.5305	0.696	-3.2	-15
17N	9.5397	0.677	-70.5	-336
18N	9.5257	0.689	28.3	135

*The diameter measurement for sample 6N was not taken by the CMM machine, therefore no predictions were made.

It is interesting to note that the predictions based on measurements taken by the CMM machine have yielded several negative values for both forces and torques. This may be attributed to one of two things. First, as mentioned in the introduction, the CMM measurements were taken 5 months after the nylon testing and may not accurately reflect the nylon diameter measurements during testing due to creep and thermal variation sensitivity. Second, the CMM machine may differ in its precision to measure inner diameters or outer diameter circles. It is likely that these two issues in conjunction have led to lower accuracy in predictions.

Brass Theoretical Predictions

Table 7. Brass theoretical predictions for force and torque are shown below for the CMM diameter measurements and the experimentally measured press fit distance.

Sample	Hex Inner Diameter (in) Micrometer	Hex Inner Diameter (mm) CMM	Distance (mm)	Predicted Force (N)	Predicted Torque (N-mm)
1B	0.368	9.3403	2.25	11885	55504
2B	0.3688	9.3383	3.64	19235	89813
3B	0.3658	9.3331	6.08	32797	153051
4B	0.369	9.3342	3.95	20539	95856
5B	0.369	9.3467	6.03	30278	141499
6B	0.3689	9.3473	2.45	12405	57977
7B	0.3687	9.3360	4.85	25829	120568
8B	0.369	9.3318	4.11	22418	104598
9B	0.3689	9.3357	4.02	21501	100362
10B	0.3687	9.3145	4.87	28826	134249
11B	0.3685	9.3347	N/A	26925	125669
12B	0.3685	9.3374	4.94	26121	121950
13B	0.3755	9.5129	5.77	2690	12793
14B	0.3755	9.5158	5.40	2091	9949
15B	0.376	9.5154	5.30	2115	10065
16B	0.3755	9.5165	5.59	2064	9819
17B	0.376	9.5146	9.32	3914	18621
18B	0.3759	9.5194	6.09	1762	8388
19B	0.376	9.5224	5.78	1197	5700
20B	0.3755	9.5171	6.08	2137	10169
21B	0.3761	9.5206	5.71	1462	6959
22B	0.3755	9.5165	5.11	1882	8955
23B	0.376	9.5205	5.73	1484	7063
24B	0.376	9.5364	5.91	-1032	-4922
25B	0.376	9.5389	4.79	-1166	-5563
26B	0.376	9.5266	6.00	557	2655
27B	0.3763	9.5305	7.08	-97	-460
28B	0.376	9.5300	5.74	0	0
29B	0.3762	9.5311	6.37	-191	-909
30B	0.3765	9.5369	N/A	-949	-4523
31B	0.376	9.5374	5.52	-1116	-5320
32B	0.376	9.5312	6.24	-205	-975
33B	0.3762	9.5387	5.44	-1291	-6157
34B	0.3765	9.5358	5.91	-937	-4465

Once again, negative values are seen for torque predictions based on the CMM measurements. The CMM machine is measuring the hex inner hole diameters to be larger than the steel dowel pin outer diameters, where in reality this is not the case. A simple test to prove this is that if one tries to place the dowel pin into the hole of the hex piece, one cannot because the hole is indeed smaller than the pin diameter. From this testing, it is apparent that the CMM is old and should be recalibrated.

4.3 Comparison of Experiment to Theory

After presenting the experimental and theoretical results separately, both sets of data will now be considered together.

Brass Sample Results

Shown below in Figure 17 are the results for the brass press fit testing. All samples are shown with experimental values and theoretical prediction ranges (due to dimensional tolerances).

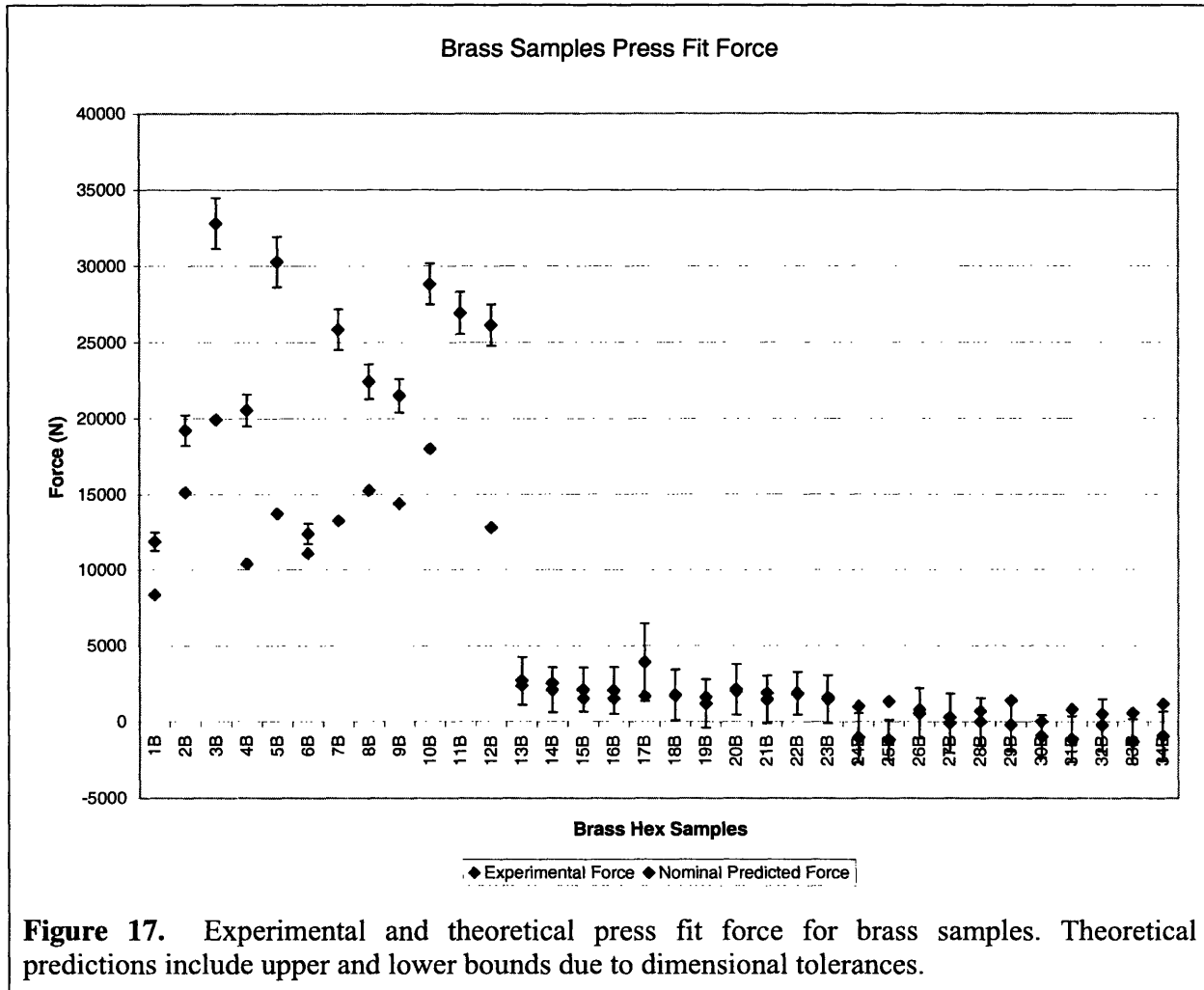


Figure 17. Experimental and theoretical press fit force for brass samples. Theoretical predictions include upper and lower bounds due to dimensional tolerances.

From Figure 17, it is possible to determine which samples belong to which inner diameter group: 0.368", 0.374", or 0.375". The first group of samples is characterized by high press fit forces, 10 – 100 times greater than the other sample groups. In this first group, it is also interesting that the theoretical prediction is grossly overestimating the experimentally observed values. After careful consideration, it was determined that the cause of this over prediction was failure to take into account the yield strength of the materials. For large interferences, as exhibited by group 1, the sample will actually yield plastically. To take this phenomenon into account, the spreadsheet was updated to include the Von Mises stress-based yield criterion for both force and torque predictions (Eq. 37). These calculations are described in Sect. 3.

For the remainder of the samples in groups 2 and 3, nearly all samples fell within the predicted press fit force range. By further examining those samples in groups 2 and 3, it is possible to get a better impression of the accuracy of the press fit predictions for the elastically deforming brass samples. Figure 18 shows a closer look at the brass samples from groups 2 and 3 which have looser interference fits.

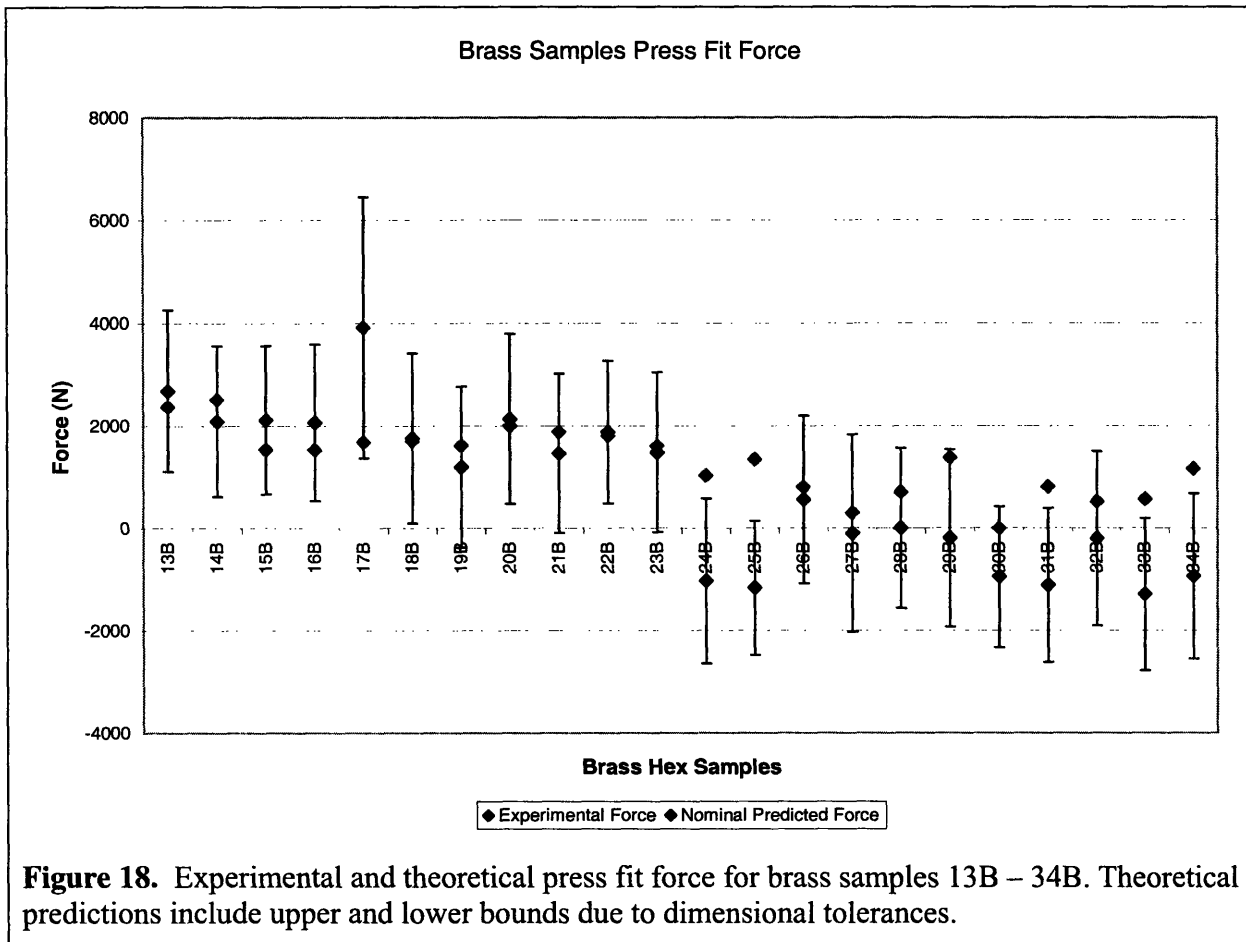


Figure 18. Experimental and theoretical press fit force for brass samples 13B – 34B. Theoretical predictions include upper and lower bounds due to dimensional tolerances.

From Figure 18, it is clear that of the 22 samples shown, 17 samples fall within the predicted press fit force. Samples 13B – 23B, which make up group 2, all have experimental press fit

forces that lie within the predicted range. Samples 24B – 34B, which make up group 3, are predicting press fit forces lower than what is observed experimentally. Only about half of the samples fall within the predicted range. As mentioned in Sect. 4.2, it appears that the CMM measurements are not entirely accurate when comparing inner diameter measurements to outer diameter measurements.

Figure 19 displays the brass force samples in group 1, which are thought to have plastically yielded during press fitting. This graph includes new theoretical forces at yielding, derived from the adapted spreadsheet.

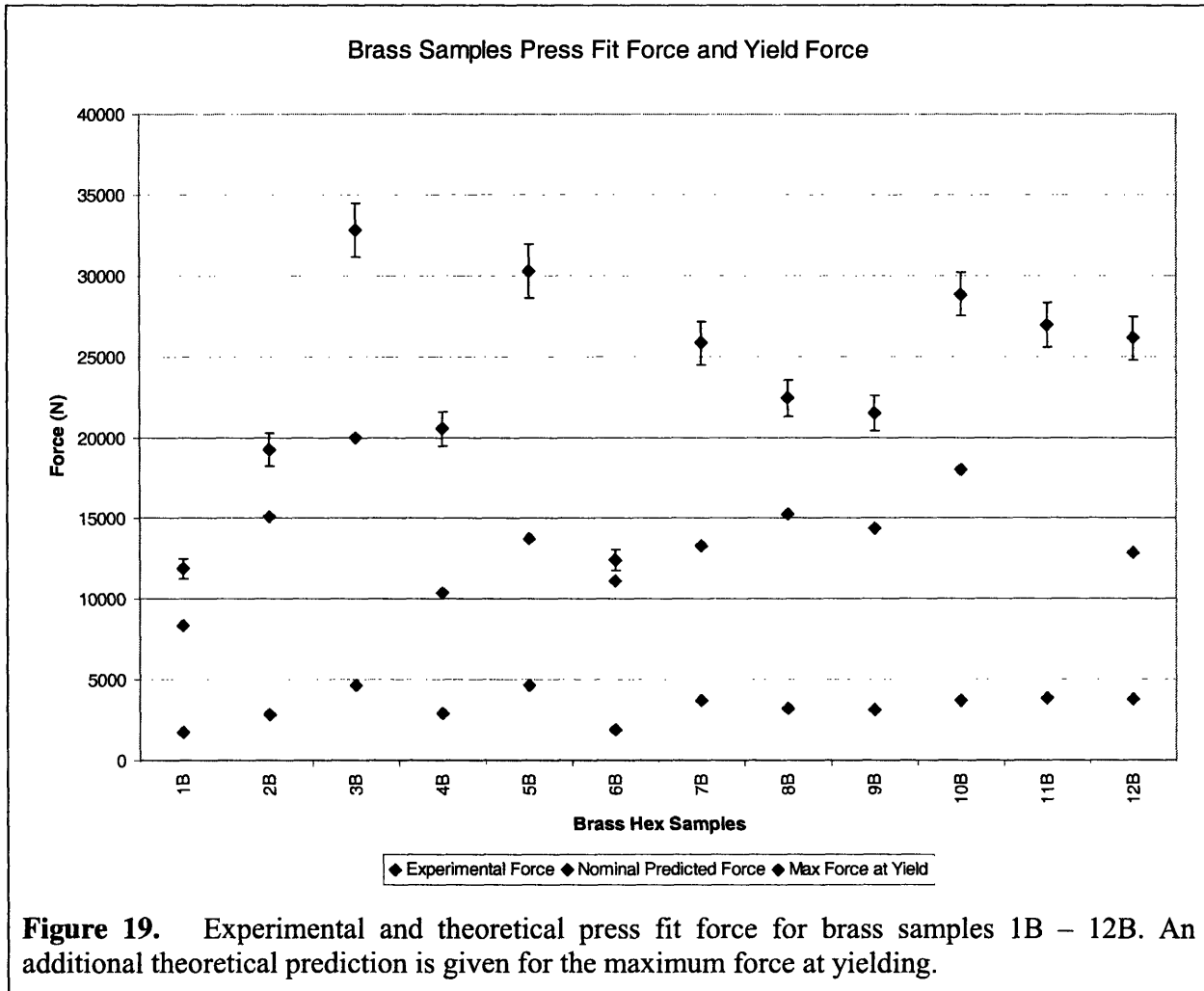


Figure 19. Experimental and theoretical press fit force for brass samples 1B – 12B. An additional theoretical prediction is given for the maximum force at yielding.

It appears from Figure 19 that the experimental press fit forces are half-way between the originally-predicted press fit forces and the maximum force at material yield. It is not totally clear what may be the cause of this spread in the experiment and theory. One potential cause could be misalignment of the dowel pin, which could lead to plowing along the inside of the brass hex piece and therefore higher forces than would be expected under plastic deformation. In other cases, more substantial plowing is seen for the tighter interference fits. In some of the hex

pieces, it was possible to look at the bottom of the dowel pin and visibly see the effects of plowing. Some of the brass material was in fact bubbled around the bottom of the dowel pin.

Shown below in Figure 20 are the results for the brass press fit torque testing. All samples are shown with experimental values and theoretical prediction ranges (due to dimensional tolerances).

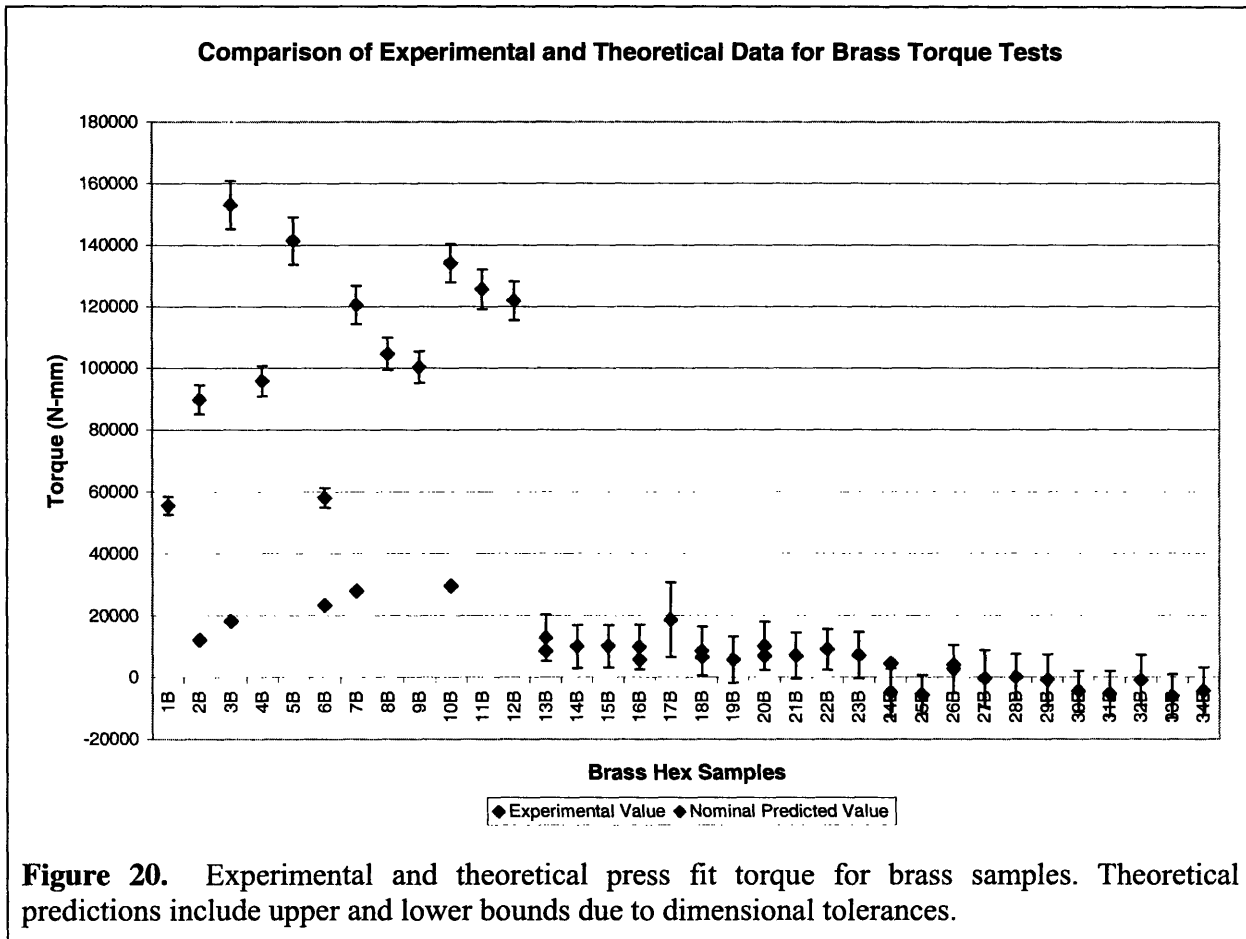


Figure 20. Experimental and theoretical press fit torque for brass samples. Theoretical predictions include upper and lower bounds due to dimensional tolerances.

Once again it is possible to determine from Figure 20 which samples belong to which inner diameter group: 0.368", 0.374", or 0.375". The first group of samples, 1B – 13B, is characterized by high torque, up to 20 times greater than the other sample groups. As concluded in the press fit testing, the first group's torque predictions also fail to take into account the yield strength of the materials. For large interferences or tight fits, as exhibited by group 1, the samples yield plastically. To take this phenomenon into account, the spreadsheet was updated to include the Von Mises stress-based yield criterion for both force and torque predictions (Sect. 3).

For the remainder of the samples in groups 2 and 3, nearly all samples fell within the predicted press fit torque range. By further examining those samples in groups 2 and 3, it is possible to get a better impression of the accuracy of the torque predictions for the elastically deforming brass samples.

Figure 21 shows a closer look at torque results for the brass samples from groups 2 and 3 which have looser interference fits. In the third group, the majority of the test samples had torque values below 1617 N-mm. These samples failed to support the weight of the lever arm during testing. Because their exact torque value is unknown, samples 28B, 30B, 32B and 33B do not have an experimental data point represented on the graph. However, judging from the torque prediction ranges depicted on the graph, one can conclude that these data points would fall within the predicted ranges, which include 1617 N-mm and 0 N-mm.

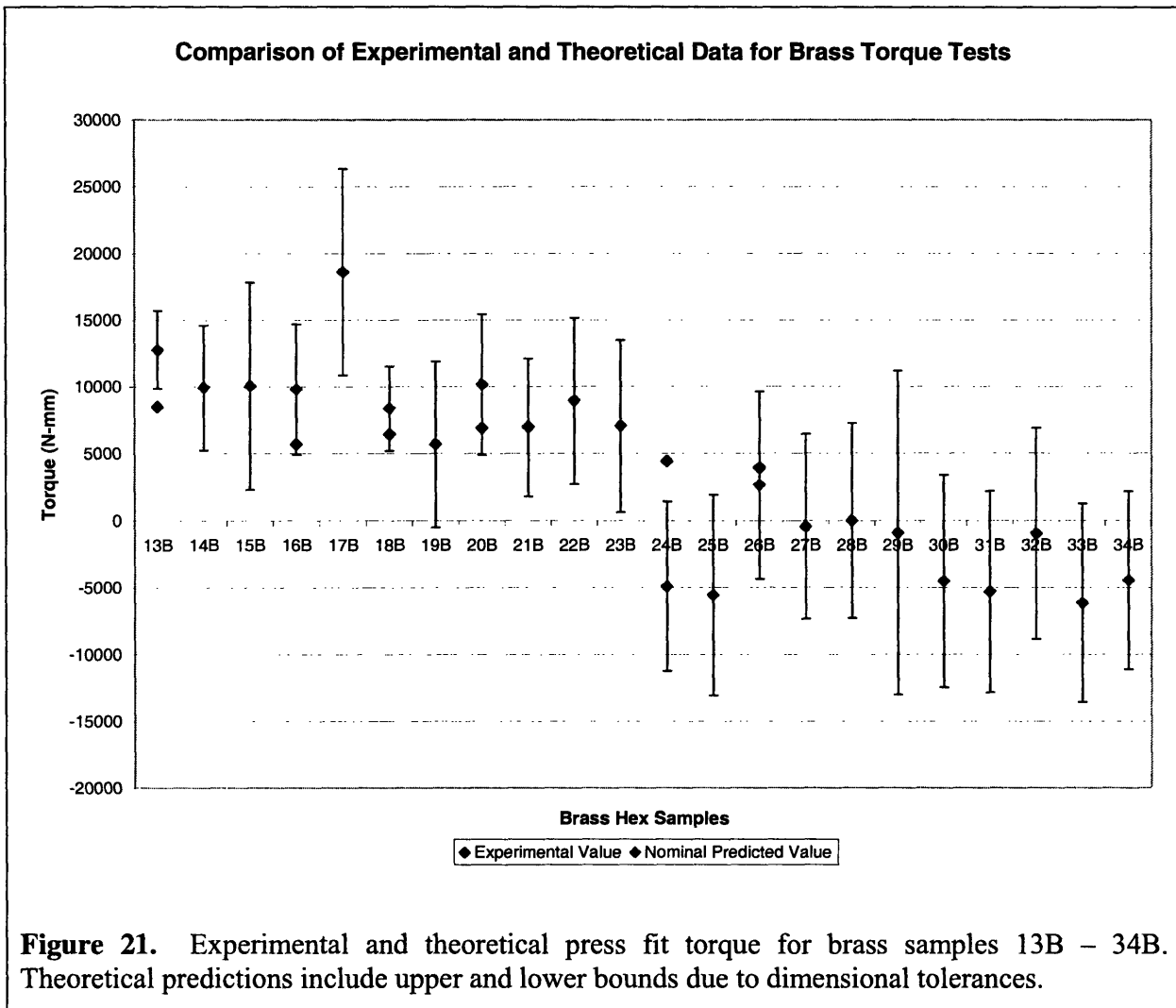


Figure 21. Experimental and theoretical press fit torque for brass samples 13B – 34B. Theoretical predictions include upper and lower bounds due to dimensional tolerances.

From Figure 21, it is clear that of the six experimental data points shown, four samples fall within the predicted torque range. This does not include the four additional data points mentioned above, for which the weight of the lever arm was sufficient torque. Therefore, of the ten samples that deformed elastically, only two fell outside of the predicted torque range.

If the data is considered once again by diameter dimensions, experimental data from group 2, samples 13B – 23B, tends to fall on the low end of the prediction ranges. This suggests that

perhaps for this group the theoretical predictions are overestimating the observed torques. For the third group, samples 24B – 34B, the opposite is true. The experimental values tend to fall on the upper end of the torque range. For the loosest interference fits, the torque predictions underestimate the experimental values, which may be due to issues surrounding the CMM measurements.

Figure 22 displays the brass torque samples in group 1, which are thought to have plastically yielded during press fitting. This graph includes new theoretical forces at yielding, derived from the adapted spreadsheet.

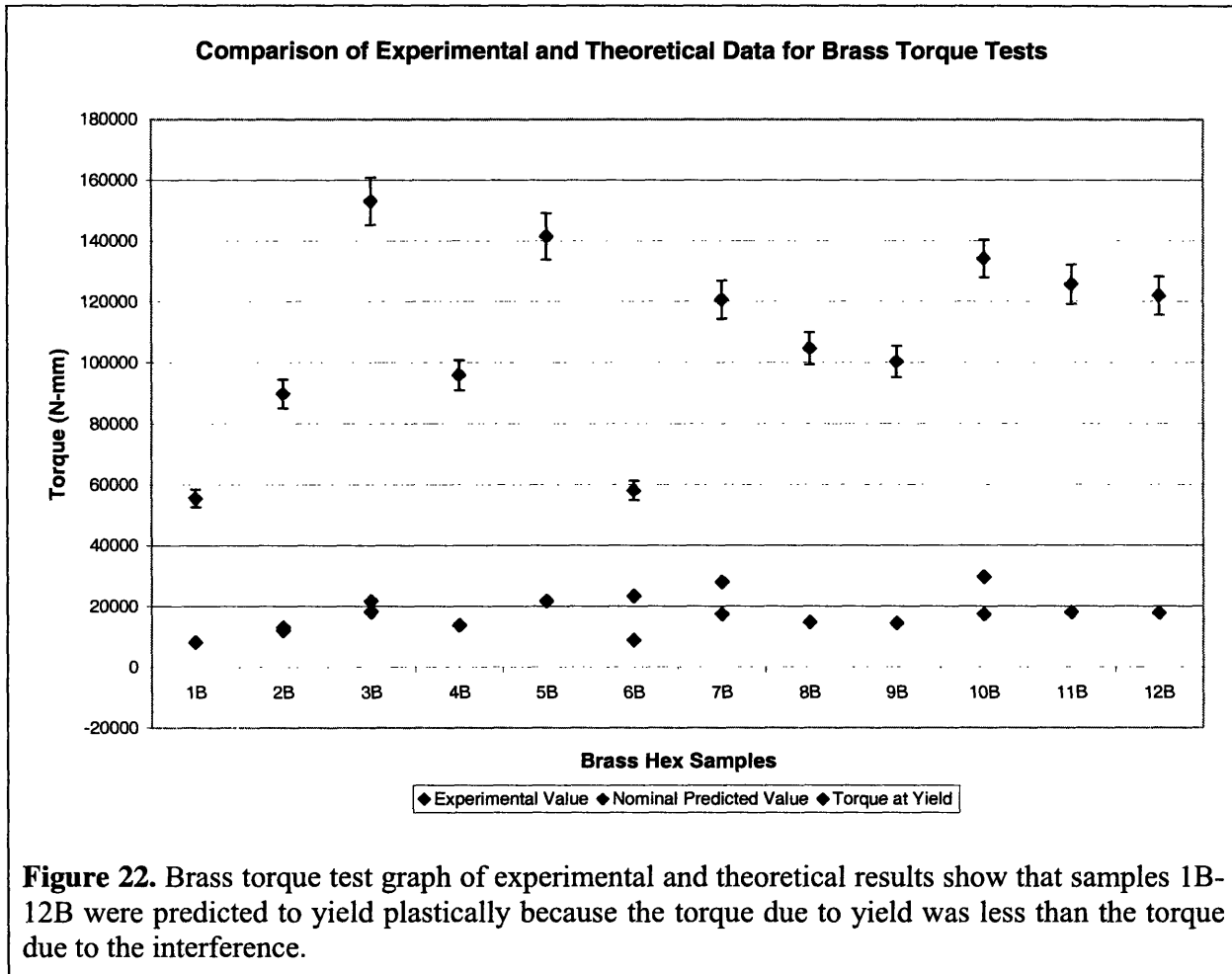


Figure 22. Brass torque test graph of experimental and theoretical results show that samples 1B-12B were predicted to yield plastically because the torque due to yield was less than the torque due to the interference.

It appears from Figure 22 that the Von Mises yield criterion is a very accurate way of predicting the experimental torque values. This criterion did not predict the press fit forces nearly as accurately as it has predicted the torque values. The potential cause of inaccuracy in predicting the press fit forces through the yield criterion method was the presence of shearing of the brass by the steel dowel pin. However, in testing the required torque, one may conclude that although the brass inner shaft had been sheared during press fit entry it does not adversely affect the torque required to rotate the pin.

The following tables include a summary of theoretical results for the brass samples. For each test, a maximum, nominal, and minimum predicted value (for force or torque) are given based on diametrical interference and tolerances. A fourth predicted value is given based on the Von Mises yield criterion. A sample is yielding plastically if the Von Mises yield criterion value is less than the minimum predicted value. In this case, the yield predicted value should be assumed.

Table 8. Comparison of experiment to theory for brass force samples based on CMM measurements.

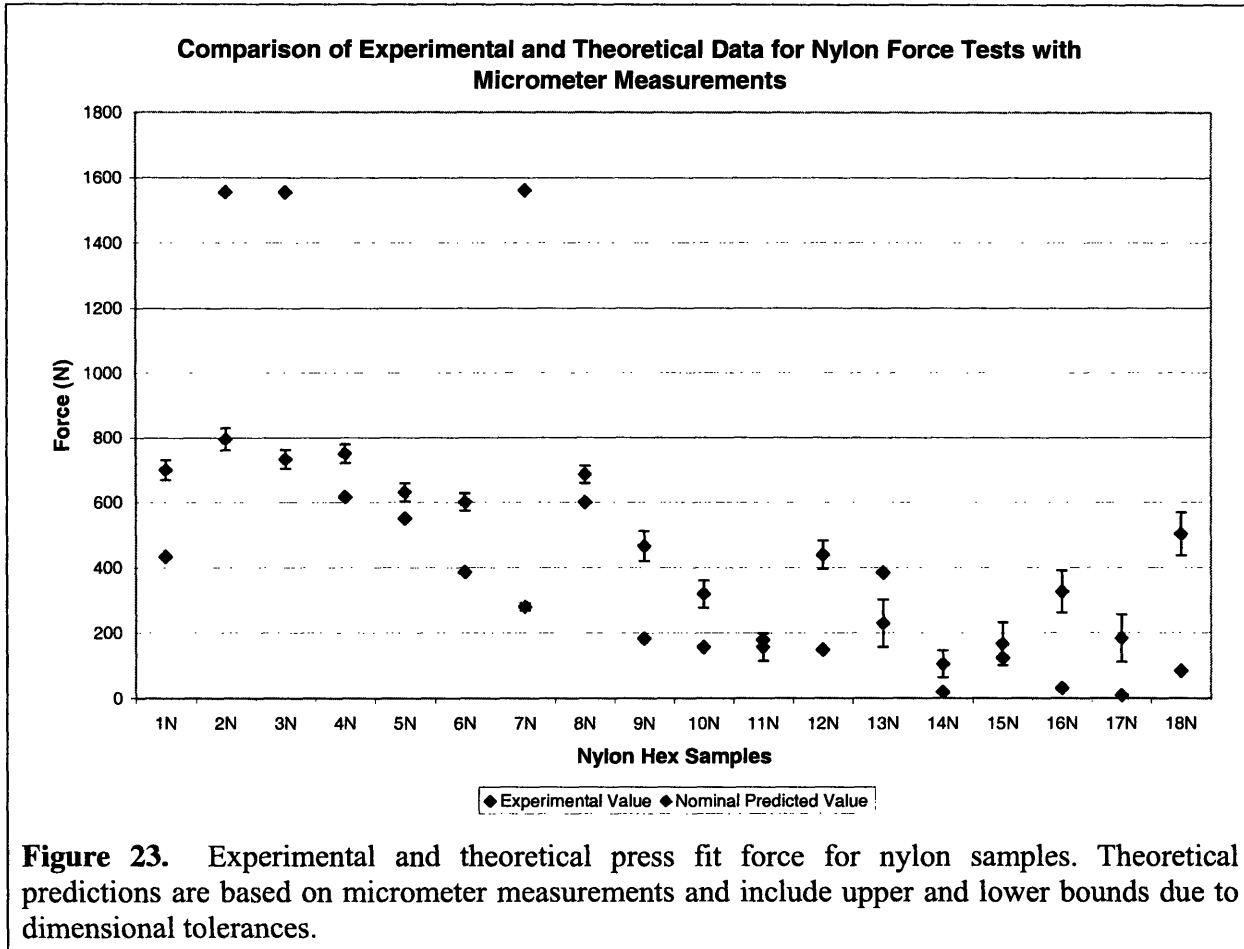
Sample	Hex Inner Diameter (mm) CMM	Distance (mm)	Maximum Predicted Force (N)	Nominal Predicted Force (N)	Minimum Predicted Force (N)	Yield Predicted Force (N)	Experimental Force (N)
1B	9.3403	2.25	12511.20	11885.01	11258.82	1749.57	8351
2B	9.3383	3.64	20238.88	19235.47	18232.05	2803.15	15134
3B	9.3331	6.08	34463.08	32797.39	31131.70	4651.45	19936
4B	9.3342	3.95	21587.59	20538.63	19489.67	2929.47	10398
5B	9.3467	6.03	31929.73	30277.90	28626.08	4617.48	13737
6B	9.3473	2.45	13084.04	12405.06	11726.07	1898.11	11102
7B	9.3360	4.85	27160.07	25828.70	24497.32	3718.70	13261
8B	9.3318	4.11	23548.64	22417.58	21286.52	3158.18	15269
9B	9.3357	4.02	22607.35	21500.77	20394.20	3090.73	14392
10B	9.3145	4.87	30163.39	28825.76	27488.14	3730.06	18013
11B	9.3347	N/A	28303.86	26925.20	25546.54	3850.38	N/A
12B	9.3374	4.94	27477.03	26120.81	24764.59	3788.49	12816
13B	9.5129	5.77	4262.33	2689.52	1116.70	4451.68	2374
14B	9.5158	5.40	3563.67	2091.08	618.49	4168.89	2517
15B	9.5154	5.30	3564.46	2115.49	666.52	4101.89	1540
16B	9.5165	5.59	3592.29	2063.66	535.02	4327.78	1528
17B	9.5146	9.32	6455.77	3914.13	1372.49	7194.74	1683
18B	9.5194	6.09	3424.97	1762.37	99.76	4708.09	1708
19B	9.5224	5.78	2772.52	1197.23	-378.07	4461.84	1617
20B	9.5171	6.08	3793.68	2137.05	480.42	4690.37	2000
21B	9.5206	5.71	3016.88	1461.79	-93.31	4404.03	1879
22B	9.5165	5.11	3276.07	1882.00	487.93	3946.82	1807
23B	9.5205	5.73	3045.53	1483.72	-78.09	4423.01	1604
24B	9.5364	5.91	580.63	-1032.24	-2645.11	4573.01	1033
25B	9.5389	4.79	144.15	-1166.29	-2476.73	3716.20	1344
26B	9.5266	6.00	2196.90	557.42	-1082.05	4645.06	800
27B	9.5305	7.08	1835.08	-96.58	-2028.25	5474.49	300
28B	9.5300	5.74	1566.26	0.00	-1566.26	4438.76	701
29B	9.5311	6.37	1543.34	-190.75	-1924.83	4914.75	1384
30B	9.5369	N/A	426.16	-948.54	-2323.24	3897.85	0
31B	9.5374	5.52	391.99	-1115.66	-2623.30	4274.97	815
32B	9.5312	6.24	1499.80	-204.52	-1908.83	4830.41	523
33B	9.5387	5.44	192.90	-1290.94	-2774.77	4207.86	567
34B	9.5358	5.91	678.18	-936.53	-2551.24	4578.00	1164

Table 9. Comparison of experiment to theory for brass torque samples based on CMM measurements.

Sample	Hex Inner Diameter (mm) CMM	Distance (mm)	Maximum Predicted Torque (N-mm)	Nominal Predicted Torque (N-mm)	Minimum Predicted Torque (N-mm)	Yield Predicted Torque (N-mm)	Experimental Torque (N-mm)
1B	9.3403	2.25	58429	55504	52580	8171	
2B	9.3383	3.64	94498	89813	85128	13088	12021
3B	9.3331	6.08	160824	153051	145278	21706	18152
4B	9.3342	3.95	100751	95856	90960	13672	
5B	9.3467	6.03	149219	141499	133780	21579	
6B	9.3473	2.45	61150	57977	54804	8871	23285
7B	9.3360	4.85	126783	120568	114353	17359	27860
8B	9.3318	4.11	109876	104598	99321	14736	
9B	9.3357	4.02	105528	100362	95197	14427	
10B	9.3145	4.87	140478	134249	128019	17372	29605
11B	9.3347	N/A	132104	125669	119235	17971	
12B	9.3374	4.94	128282	121950	115618	17687	
13B	9.5129	5.77	20274	12793	5312	21174	8504
14B	9.5158	5.40	16956	9949	2943	19835	
15B	9.5154	5.30	16959	10065	3171	19516	
16B	9.5165	5.59	17093	9819	2546	20593	5691
17B	9.5146	9.32	30712	18621	6529	34228	
18B	9.5194	6.09	16302	8388	475	22409	6441
19B	9.5224	5.78	13201	5700	-1800	21244	
20B	9.5171	6.08	18052	10169	2286	22319	6921
21B	9.5206	5.71	14361	6959	-444	20964	7017
22B	9.5165	5.11	15588	8955	2322	18780	
23B	9.5205	5.73	14497	7063	-372	21055	
24B	9.5364	5.91	2769	-4922	-12612	21805	4399
25B	9.5389	4.79	688	-5563	-11813	17724	
26B	9.5266	6.00	10464	2655	-5154	22126	3952
27B	9.5305	7.08	8745	-460	-9665	26087	
28B	9.5300	5.74	7463	0	-7463	21151	<1617
29B	9.5311	6.37	7355	-909	-9173	23422	
30B	9.5369	N/A	2032	-4523	-11078	18587	<1617
31B	9.5374	5.52	1869	-5320	-12510	20386	
32B	9.5312	6.24	7147	-975	-9097	23020	<1617
33B	9.5387	5.44	920	-6157	-13234	20069	<1617
34B	9.5358	5.91	3233	-4465	-12164	21827	

Nylon Sample Results

Shown below in Figures 23 and 24 are the results for the nylon press fit testing based on micrometer and CMM measurements respectively. All samples are shown with experimental values and theoretical prediction ranges (due to dimensional tolerances).



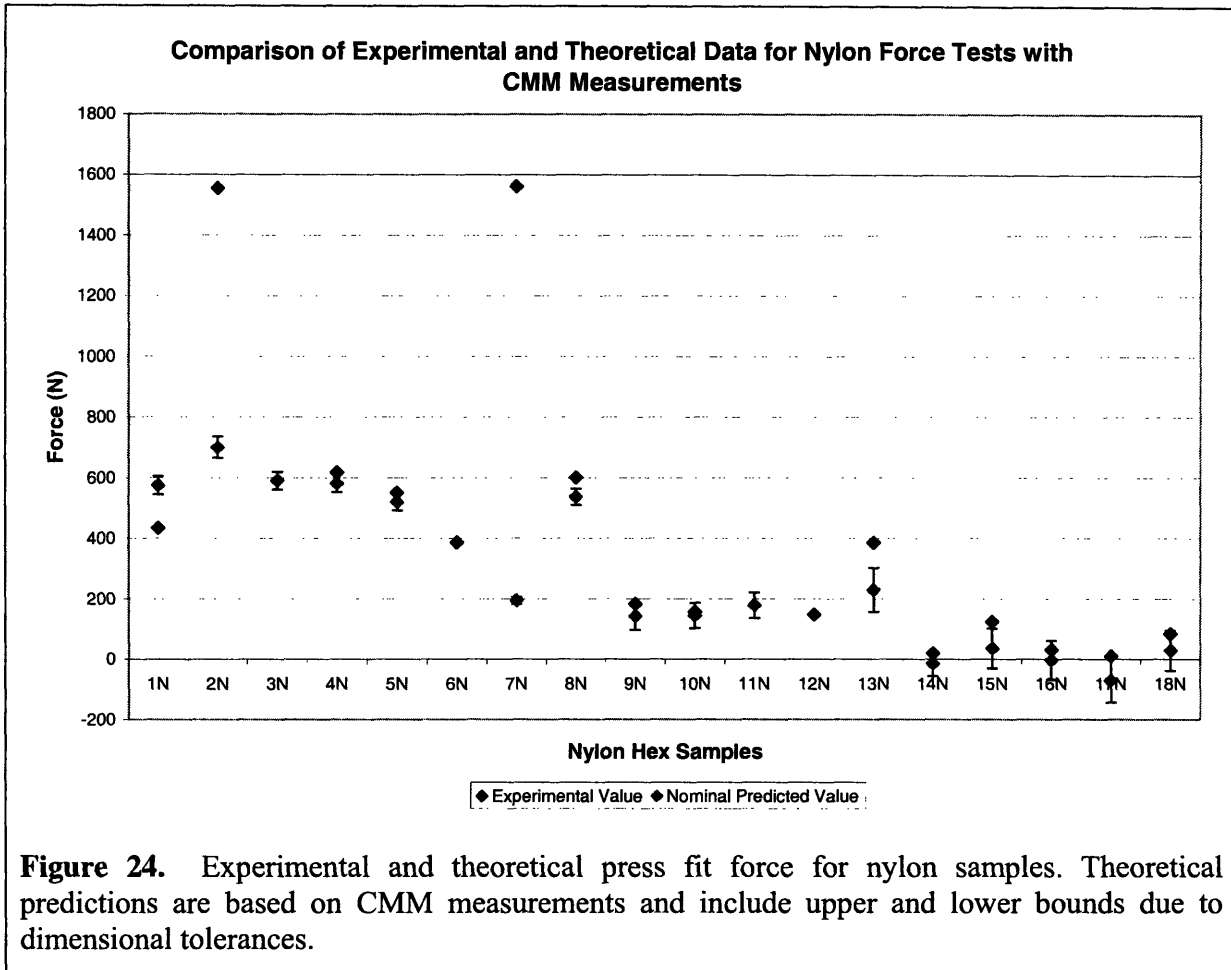


Figure 24. Experimental and theoretical press fit force for nylon samples. Theoretical predictions are based on CMM measurements and include upper and lower bounds due to dimensional tolerances.

Comparing the theoretical predictions in Figures 23 and 24, it is possible to judge which measurements best predict the experimental findings. Looking at the entire set of data, it appears that the CMM measurements have higher prediction accuracy. Once again, the CMM measurements yield several negative value predictions though. Despite this issue, the CMM measurements still are a closer match with the experimental data.

Another interesting thing to consider is the state of deformation for the group 1 samples, those with the tightest interference fit. The brass samples in group 1 were found to be plastically deforming at this interference range. The nylon samples do not reach yielding and therefore the Von Mises yield criterion does not apply.

Shown below in Figures 25 and 26 is a zoomed in view of the nylon press fit testing based on micrometer and CMM measurements respectively. From these graphs, it is possible to determine how many experimental data points fall within the predicted force range for each series of measurements.

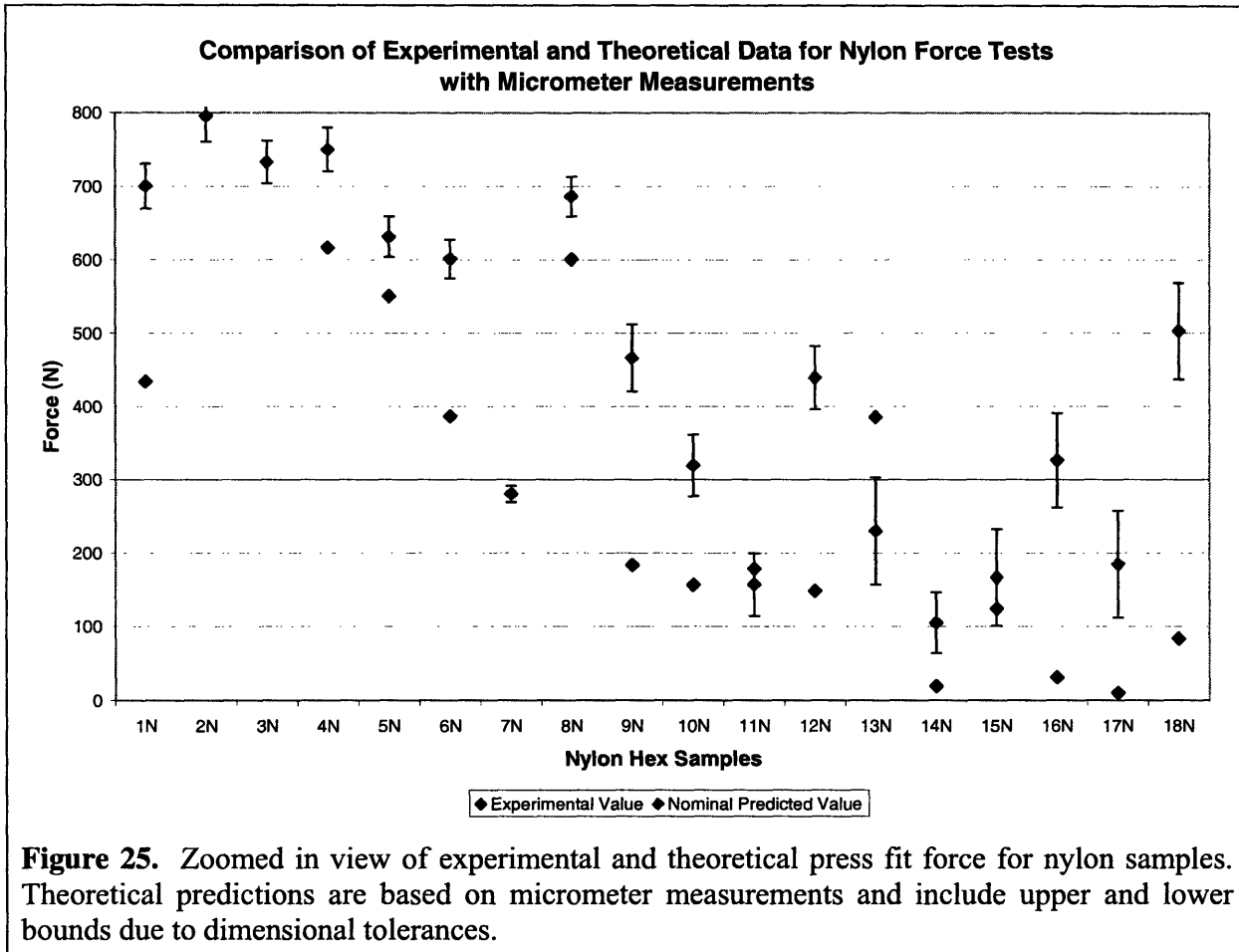


Figure 25. Zoomed in view of experimental and theoretical press fit force for nylon samples. Theoretical predictions are based on micrometer measurements and include upper and lower bounds due to dimensional tolerances.

For the micrometer measurements of Figure 25, only one data point, 15N, out of seventeen data points falls within the predicted range.⁷

⁷ Only seventeen data points are considered because sample 11N does not have predictions for the micrometer measurements.

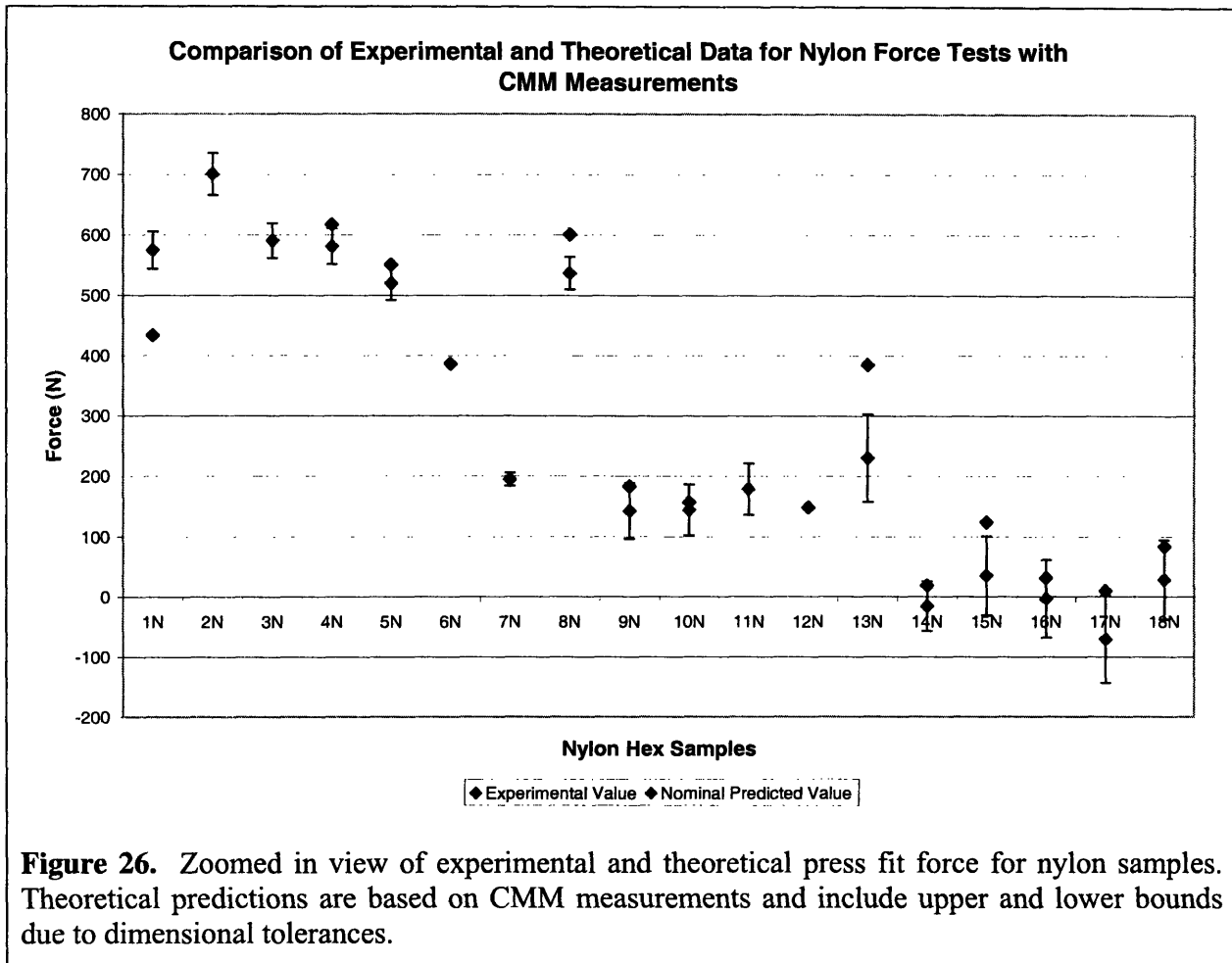


Figure 26. Zoomed in view of experimental and theoretical press fit force for nylon samples. Theoretical predictions are based on CMM measurements and include upper and lower bounds due to dimensional tolerances.

For the CMM measurements of Figure 26, eight data points out of sixteen data points fall within the predicted range.⁸ Once again, the CMM measurements appear to be a better predictor of the experimental data.

⁸ Only sixteen data points are considered because sample 6N does not have predictions for the CMM measurements and sample 3N does not have experimental force data.

Next the torque data results will be considered for the nylon hex samples. For both Figure 27 and 28, samples 11N, 12N, 14N, 15N, 16N, 17N, and 18N which required less than 1617 N-mm of torque are represented by a data point at 1617 N-mm. In reality, this is not an exact experimental value, but an upper bounds for the seven aforementioned samples.

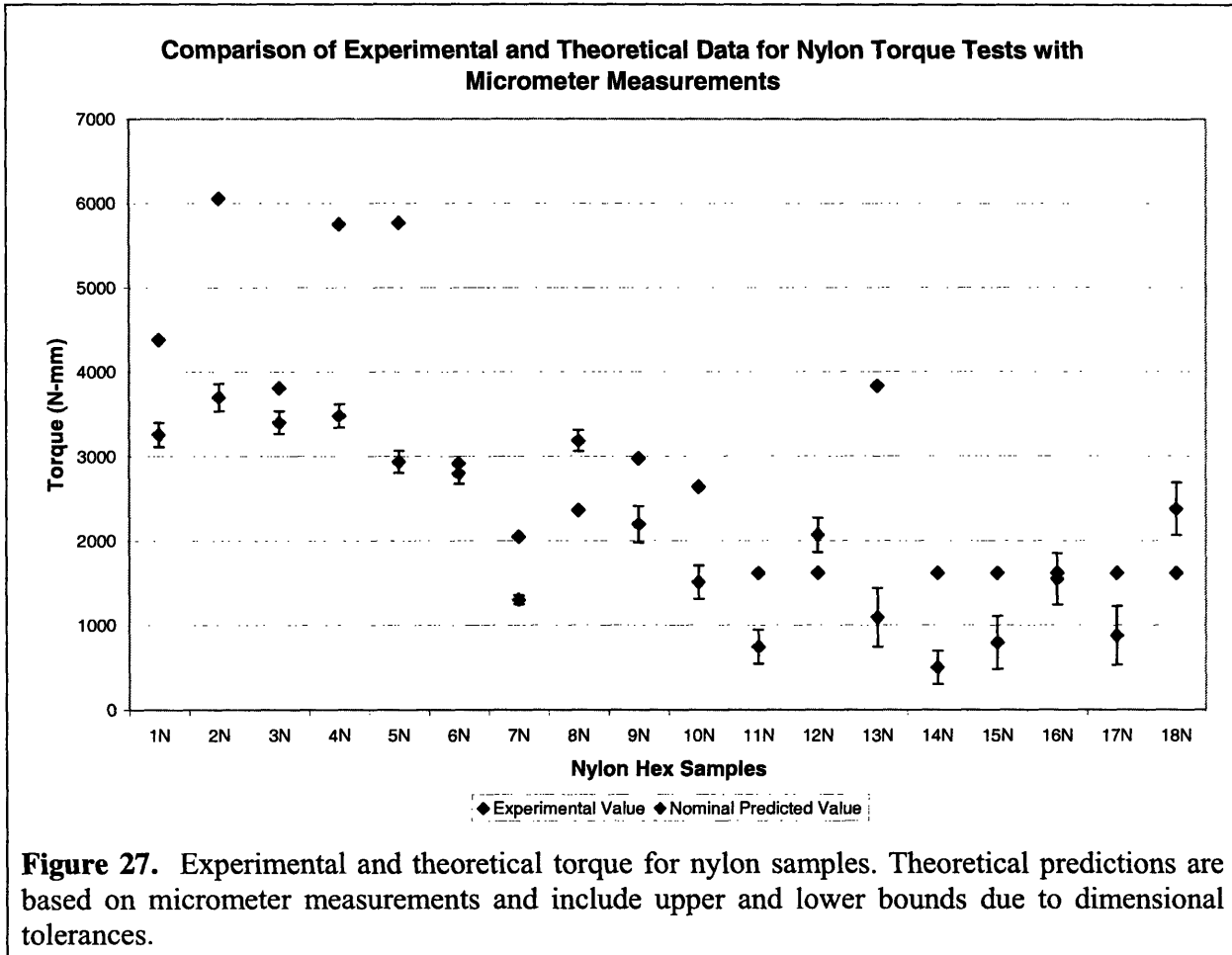


Figure 27. Experimental and theoretical torque for nylon samples. Theoretical predictions are based on micrometer measurements and include upper and lower bounds due to dimensional tolerances.

For the micrometer torque predictions, only sample 6N falls in the predicted range. The accuracy for samples which had torque values less than or equal to 1617 N-mm cannot be determined, except for sample 18N. In the case of 18N, it is clear that the micrometer predictions are over predicting the required torque since the range lies above the 1617 N-mm data point.

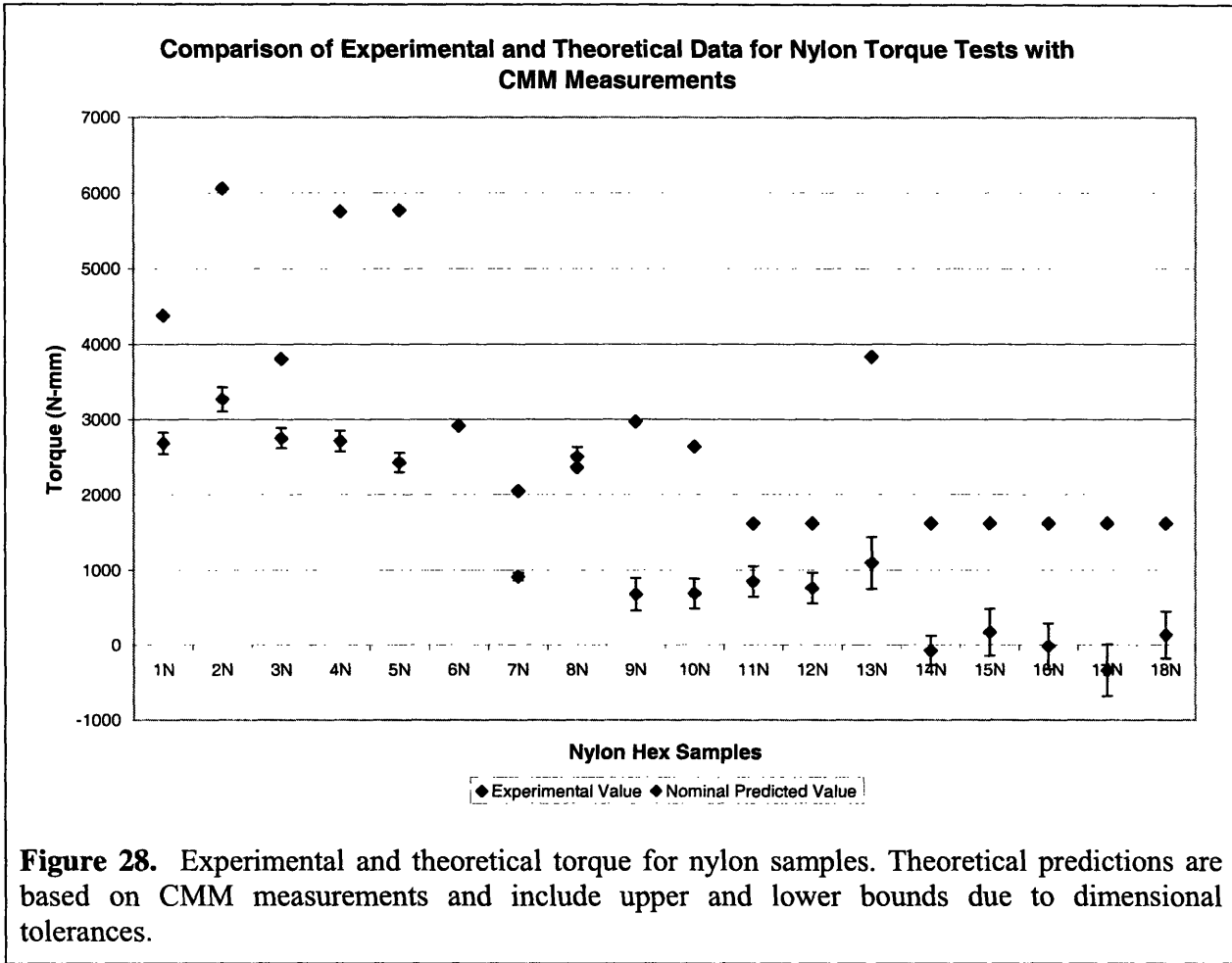


Figure 28. Experimental and theoretical torque for nylon samples. Theoretical predictions are based on CMM measurements and include upper and lower bounds due to dimensional tolerances.

The following tables include a summary of theoretical results for the nylon samples. For each test, a maximum, nominal, and minimum predicted value (for force or torque) are given based on diametrical interference and tolerances. A fourth predicted value is given based on the Von Mises yield criterion. A sample is yielding plastically if the Von Mises yield criterion value is less than the minimum predicted value. In this case, the yield predicted value should be assumed. However, for the nylon data, none of the samples were determined to have yielded plastically during testing.

Table 10. Comparison of experiment to theory for nylon force samples based on micrometer measurements.

Sample	Hex Inner Diameter (in) Micrometer	Maximum Predicted Force (N)	Nominal Predicted Force (N)	Minimum Predicted Force (N)	Yield Predicted Force (N)	Experimental Force (N)
1N	0.366	731.1	700.5	669.8	1903.8	433.9
2N	0.366	830.3	795.5	760.7	2162.2	1555.0
3N	0.365	761.9	733.1	704.2	1788.3	N/A
4N	0.365	779.9	750.4	720.8	1830.6	617.0
5N	0.366	659.3	631.6	604.0	1716.8	550.8
6N	0.366	628.0	601.7	575.4	1642.3	386.4
7N	0.365	291.4	280.4	269.4	687.0	1561.0
8N	0.365	713.4	686.4	659.4	1681.5	600.9
9N	0.371	511.9	466.0	420.1	2900.6	183.3
10N	0.372	361.0	319.2	277.3	2655.9	156.7
11N*	N/A	N/A	N/A	N/A	N/A	178.6
12N	0.371	481.9	438.8	395.6	2731.1	148.4
13N	0.371	302.8	230.0	157.2	4637.1	385.0
14N	0.374	146.3	105.0	63.7	2635.4	19.0
15N	0.374	232.6	166.9	101.2	4189.5	124.3
16N	0.373	390.6	326.4	262.1	4085.0	31.2
17N	0.374	257.7	184.9	112.1	4640.8	10.0
18N	0.372	568.9	502.9	436.9	4185.0	83.7

*The diameter measurement for sample 11N was not taken with the micrometer, therefore no predictions were made.

Table 11. Comparison of experiment to theory for nylon torque samples based on micrometer measurements.

Sample	Hex Inner Diameter (in) Micrometer	Maximum Predicted Torque (N-mm)	Nominal Predicted Torque (N-mm)	Minimum Predicted Torque (N-mm)	Yield Predicted Torque (N-mm)	Experimental Torque (N-mm)
1N	0.366	3398	3256	3113	8849	4382
2N	0.366	3860	3698	3536	10051	6059
3N	0.365	3532	3398	3264	8290	3808
4N	0.365	3615	3478	3341	8486	5751
5N	0.366	3064	2936	2808	7980	5769
6N	0.366	2919	2797	2674	7634	2916
7N	0.365	1351	1300	1249	3184	2047
8N	0.365	3307	3182	3056	7795	2361
9N	0.371	2412	2196	1980	13667	2973
10N	0.372	1706	1508	1310	12548	2636
11N	N/A	N/A	N/A	N/A	N/A	<1617
12N	0.371	2271	2067	1864	12868	<1617
13N	0.371	1437	1092	746	22011	3831
14N	0.374	695	499	302	12517	<1617
15N	0.374	1105	793	481	19899	<1617
16N	0.373	1851	1546	1242	19351	<1617
17N	0.374	1224	878	532	22043	<1617
18N	0.372	2688	2376	2064	19772	<1617

*The diameter measurement for sample 11N was not taken with the micrometer, therefore no predictions were made.

Table 12. Comparison of experiment to theory for nylon force samples based on CMM measurements.

Sample	Hex Inner Diameter (mm) CMM	Distance (in.)	Maximum Predicted Force (N)	Nominal Predicted Force (N)	Minimum Predicted Force (N)	Yield Predicted Force (N)	Experimental Force (N)
1N	9.3420	0.329	605.5	574.9	544.3	1909.3	433.9
2N	9.3284	0.014	735.3	700.6	665.8	2166.6	1555.0
3N	9.3248	0.002	619.6	590.8	562.0	1794.4	1555.0
4N	9.3327	0.301	610.8	581.3	551.8	1837.7	617.0
5N	9.3415	0.557	547.4	519.8	492.2	1721.7	550.8
6N*	N/A	0.177	N/A	N/A	N/A	N/A	386.4
7N	9.3531	0.108	205.6	194.6	183.6	690.5	1561.0
8N	9.3308	0.103	563.8	536.9	509.9	1687.9	600.9
9N	9.4988	0.452	188.3	142.6	96.9	2913.8	183.3
10N	9.4955	0.417	186.0	144.2	102.4	2663.4	156.7
11N	9.4881	0.447	220.9	178.3	135.8	2709.9	178.6
12N	9.4929	0.435	202.8	-20263.3	-40729.3	2742.5	148.4
13N	9.4934	0.677	302.7	230.0	157.2	4638.5	385.0
14N	9.5337	0.435	26.0	-15.3	-56.5	2640.7	19.0
15N	9.5246	0.678	101.1	35.4	-30.2	4195.7	124.3
16N	9.5305	0.696	60.9	-3.2	-67.3	4098.7	31.2
17N	9.5397	0.677	2.2	-70.5	-143.2	4651.8	10.0
18N	9.5257	0.689	94.1	28.3	-37.5	4204.2	83.7

*The diameter measurement for sample 6N was not taken by the CMM machine, therefore no predictions were made.

Table 13. Comparison of experiment to theory for nylon torque samples based on CMM measurements.

Sample	Hex Inner Diameter (mm) CMM	Distance (in.)	Maximum Predicted Torque (N-mm)	Nominal Predicted Torque (N-mm)	Minimum Predicted Torque (N-mm)	Yield Predicted Torque (N-mm)	Experimental Torque (N-mm)
1N	9.3420	0.329	2828	2685	2542	8918	4382
2N	9.3284	0.014	3430	3268	3106	10105	6059
3N	9.3248	0.002	2889	2755	2620	8366	3808
4N	9.3327	0.301	2850	2712	2575	8575	5751
5N	9.3415	0.557	2557	2428	2299	8041	5769
6N*	N/A	0.177	N/A	N/A	N/A	N/A	2916
7N	9.3531	0.108	961	910	859	3229	2047
8N	9.3308	0.103	2631	2505	2379	7875	2361
9N	9.4988	0.452	894	677	460	13839	2973
10N	9.4955	0.417	883	685	486	12645	2636
11N	9.4881	0.447	1048	846	644	12856	<1617
12N	9.4929	0.435	962	758	-193320	13017	<1617
13N	9.4934	0.677	1438	1092	747	22029	3831
14N	9.5337	0.435	124	-73	-270	12588	<1617
15N	9.5246	0.678	481	169	-144	19981	<1617
16N	9.5305	0.696	290	-15	-321	19531	<1617
17N	9.5397	0.677	10	-336	-683	22188	<1617
18N	9.5257	0.689	448	135	-179	20024	<1617

*The diameter measurement for sample 6N was not taken by the CMM machine, therefore no predictions were made.

5. Conclusion

A variety of conclusions can be made for the press fits study. These conclusions can be grouped into several categories based on material, experiment type, and content.

First, the brass samples will be discussed. The most important conclusion from this set of data is the need to determine whether the samples are deforming elastically or plastically. Without the inclusion of the Von Mises yield criterion, the brass predictions would be grossly overestimated for samples in group 1. Addition of the Von Mises yield criterion led to highly accurate predictions for the brass torque testing. However, it was found that the Von Mises yield criterion did not function as well in predicting the force to press fit the brass samples in group 1. It underestimated the force levels. For future studies it would be useful to adapt the spreadsheet to include force due to plowing effects in the press fit force calculations. One would also need to determine in what interference range plowing occurs. From this study, plowing appears to be a consequence of large interferences. Despite difficulty in predicting press fit forces, it is important to underline the degree to which the press fit equations were able to predict the required torque. The highest degree of accuracy was seen in group 2 press fits with interferences on the order of 0.0005". It would be interesting to conduct further experiments on press fits within this interference range and smaller. A future study might also consider the effects of surface particles and abrasion on press fit torque.

Second, the nylon samples will be discussed. The most important conclusion to be made regarding the nylon samples is their sensitivity to variation over time. During the testing period and post-test analysis, it was impossible to reliably determine the state of the nylon samples. If a material such as nylon must be used for testing, it is important to conduct testing in as short a time span as possible. It is also important that the samples remain in a relatively stable environment free of temperature fluctuations. From the data collected, it is difficult to assess to what degree the theory is capable of predicting experimental results. Reliability in the dimensional measurements was low with nylon press fit entry and removal forces varying on average 48.1% over the testing period. Despite this fact, the predictions made were quite close to the experimental values observed.

Third, measurements will be discussed. In press fitting, in order to understand and interpret data, precise measurements must be made. The accuracy of predictions is directly related to the accuracy of the measurements. It is necessary to take measurements for every test. One weakness of the nylon data is that inner hex diameter measurements are not available for each test. Had these measurements been taken, the material changes would be less of a concern had they been accounted for. Another consideration would be the measurement device used. Each set of measurements must be taken by the same method. In using the CMM, it appears, as shown by the data, that the measurements for the inner hole diameters are very precise, but are not accurate when compared to the CMM measurements for the dowel pin outer diameter.

Fourth, overall conclusions regarding press fits will be made. The theoretical predictions, especially for the torque experiments, exhibit a large range of possible values. This is due to the fact that the torque varies proportionately with the square of the diameter, and the diameter measurements have a tolerance of $\pm 0.005\text{mm}$. The large range in predicted values makes it difficult to design for a specific value and to know with much certainty the torque that will result. This brings about a second conclusion about press fit design. Press fits are very sensitive to

dimensions, especially those relating to the interference fit. Precise measurements are needed, and precision machining must be utilized to ensure tighter tolerances and accurate predictions.

Separate conclusions regarding the accuracy of press fit theory can be made for brass and nylon and for the corresponding force and torque experiments. For the brass samples, press fit theory did not accurately predict observed press fit forces due to material plowing effects that were unaccounted for by theory. Given more time, I would be inclined to conduct additional experiments specifically addressing plowing and surface abrasion. The spreadsheet could also be improved by adding parameters to address these effects. Press fit theory when applied to the brass torque measurements was very accurate in conjunction with the Von Mises yield criterion. Quite possibly the most important result of this study is the addition of the yield criterion to the press fit spreadsheet. As evidenced by initial brass press fit predictions, without inclusion of the yield criterion, the press fit forces and torque will be grossly exaggerated at tighter interferences without recognizing that the sample would undergo plastic deformation at a much lower stresses.

For the nylon samples, the most important conclusion of the study is the time-sensitivity of the material due to creep. Over the course of the study, sensitivity of the nylon material would have played a significant role in dimensional measurements, which in turn affects the accuracy of the theoretical predictions. In future testing, I would not recommend the use of viscoelastic materials unless the study is conducted over a short period of time to minimize creep and in a controlled environment with little temperature fluctuation. Nylon force predictions were generally very accurate. However, several extreme outliers out of eighteen data points exist. It would be interesting to consider surface abrasion and other factors that may lead to much higher force values during press fitting. Nylon torque predictions were slightly lower than observed experimentally providing a conservative estimate for press fit design.

Overall, additional modeling is required in the area of press fit force design, but experimental results show that current theory can be used to accurately predict press fit interface pressure and thus press fit torque.

Appendix 1: Calculation of Friction Coefficient

The coefficient of friction between the hardened steel pins and the brass or nylon hexes was calculated based on principles of Newtonian physics.

From the diagram at right, the frictional force F_r and gravitational force F_g on the sample can be defined as:

$$F_r = \mu \cos \theta mg.$$

$$F_g = \sin \theta mg.$$

When the sample begins to slide:

$$F_r = F_g.$$

$$\mu \cos \theta mg = \sin \theta mg.$$

$$\mu = \tan \theta = H / B.$$

To calculate the coefficient of friction an experiment was conducted to measure the distance H which causes the sample to slide. A hex sample was laid flat on an even surface. The hardened steel pin was placed on top of the hex sample lengthwise. The orientation of the steel dowel pin was chosen to minimize rolling and maximize frictional forces between the pin and hex pieces. One edge of the hex sample was raised using a height gauge. When the steel pin began to slip, the height of the gauge was recorded.

From the experimental data shown below in Table 11, the following averages were calculated:

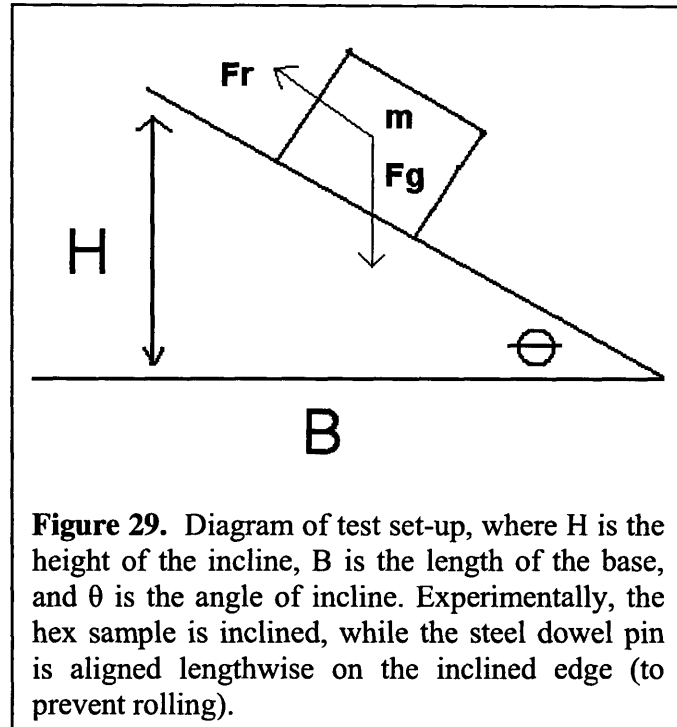
$$\text{Nylon } H_{\text{average}} = 0.187 \text{ inches.}$$

$$\text{Brass } H_{\text{average}} = 0.139 \text{ inches.}$$

Based on the average height calculations and the length of each hex piece (1"), the coefficients of friction were determined to be:

$$\mu_{\text{nylon}} = 0.187.$$

$$\mu_{\text{brass}} = 0.139.$$



The data shown in Table 14 was used to calculate the coefficient of friction for brass on steel and nylon on steel.

Table 14 Experimental data giving height required to induce slipping.

Nylon Height (in.)	Brass Height (in.)
0.174	0.124
0.126	0.178
0.195	0.163
0.183	0.168
0.196	0.158
0.179	0.142
0.202	0.105
0.204	0.090
0.230	0.127
0.161	0.152
0.186	0.121
0.167	0.120
0.165	0.114
0.218	0.163
0.200	0.146
0.141	0.169
0.174	0.156
0.201	0.101
0.210	0.111
0.208	0.163
0.185	0.125
0.114	0.150
0.240	0.160
0.209	
0.216	

Appendix 2: Nylon and Brass Sample Measurements

For each hex sample, the inner diameter and length were measured and recorded. At the time the counterbore was drilled, its length into the hex piece was also recorded. Prior to press fitting the dowel pins, each pin was inserted into a hex sample. The initial pin height is determined as the height of the pin from the bottom of the hex piece. Figure 30 shows a pin inserted in the counterbore section of the hex piece. The larger counterbore region is the larger diameter shown around the pin, and the press fit region is the smaller diameter shown below the pin. The final pin height is defined as the height of the pin after press fitting. The displacement is defined as the displacement of the pin during the press fit test. The press fit distance is defined as the displacement of the pin in the non-counterbore section of the hex piece.

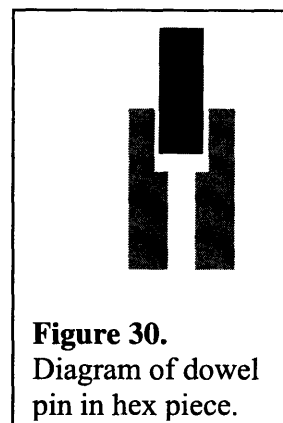


Table 15. Sample data for the nylon hex pieces and measurements for the press fit force test.

Sample	Hex Inner Diameter (mm)	Hex Length (mm)	Counterbore depth (mm)	Initial Pin Height (mm)	Final Pin Height (mm)	Displacement (mm)	Press fit Distance (mm)
1N	9.342	25.60	17.5	7.21	0.00	7.44	7.44
2N	9.328	25.91	17.5	21.87	0.00	13.78	8.45
3N	9.325	25.63	17.5	21.11	1.17	13.00	7.00
4N	9.333	25.65	17.5	22.91	1.03	22.36	7.16
5N	9.342	25.76	19.0	13.92	0.00	21.37	6.71
6N	9.296	25.53	17.5	16.56	1.65	13.00	6.41
7N	9.353	25.40	17.5	18.97	5.25	13.78	2.69
8N	9.331	25.78	17.5	20.19	1.74	14.48	6.58
9N	9.499	25.91	14.3	20.29	0.38	20.16	11.24
10N	9.496	25.65	14.3	20.90	1.09	20.13	10.28
11N	9.488	25.91	14.3	14.35	1.16	14.10	10.46
12N	9.493	25.78	14.3	14.66	0.91	14.22	10.58
13N	9.493	25.83	8.0	21.69	0.00	21.00	17.89
14N	9.534	26.04	14.3	10.87	0.60	10.17	10.17
15N	9.525	25.65	8.0	16.66	0.55	16.16	16.16
16N	9.531	25.91	8.0	16.08	0.41	15.78	15.78
17N	9.540	25.68	8.0	18.34	-0.16	17.79	17.90
18N	9.526	25.86	8.0	16.61	0.69	16.19	16.19

For the brass hex pieces, because the material is less elastic, the counterbore served as a ledge on top of which the dowel pin could rest before testing. Therefore, for the initial pin height is the interface between the counterbore region and the press fit region (See Figure 30).

Table 16. Sample data for the brass hex pieces and measurements for the press fit force test.

Sample	Hex Inner Diameter (mm)	Hex Length (mm)	Initial Pin Height (mm)	Final Pin Height (mm)	Distance (mm)
1B	9.340	25.40	17.5	15.21	2.25
2B	9.335	25.40	17.5	13.82	3.64
3B	9.329	25.40	17.5	11.38	6.08
4B	9.345	25.40	17.5	13.51	3.95
5B	9.342	25.40	17.5	11.43	6.03
6B	9.340	25.65	17.7	15.27	2.45
7B	9.348	25.58	17.6	12.79	4.85
8B	9.341	25.40	17.5	13.35	4.11
9B	9.335	25.40	17.5	13.44	4.02
10B	9.329	25.40	17.5	12.59	4.87
11B	9.335	25.40	17.5	-	-
12B	9.345	25.40	17.5	12.52	4.94
13B	9.513	25.40	12.7	6.93	5.77
14B	9.516	25.40	12.7	7.30	5.40
15B	9.515	25.15	17.2	11.91	5.30
16B	9.517	25.91	18.0	12.38	5.59
17B	9.515	29.72	21.8	12.46	9.32
18B	9.519	25.65	17.7	11.63	6.09
19B	9.522	25.40	12.7	6.92	5.78
20B	9.517	25.40	12.7	6.62	6.08
21B	9.521	25.15	12.5	6.74	5.71
22B	9.517	25.40	12.7	7.59	5.11
23B	9.521	25.40	12.7	6.97	5.73
24B	9.536	25.27	17.3	11.43	5.91
25B	9.539	25.15	17.2	12.42	4.79
26B	9.527	25.40	17.5	11.46	6.00
27B	9.531	25.40	17.5	10.38	7.08
28B	9.530	25.65	14.5	8.80	5.74
29B	9.531	25.40	11.1	4.74	6.37
30B	9.537	25.65	17.7	12.62	5.08
31B	9.537	25.60	17.7	12.15	5.52
32B	9.531	25.40	17.5	11.22	6.24
33B	9.539	25.45	14.3	8.9	5.44
34B	9.536	25.63	17.7	11.78	5.91

Sample 11B was not tested.

Appendix 3: Nylon Experimental Force Data

All experimental press fit data is shown below in Table 17. The hex inner diameter micrometer measurement is given as a reference point. The press fit distance is the measured displacement of the pin into the hex pieces taking into account location of the counterbore. The measured experimental force is the maximum force collected experimentally. The entry effect force is determined graphically for each sample. The experimental press fit force is the force required to insert the pin over the measured press fit distance neglecting any entry effects. The press fit force is calculated by subtracting the entry effects from the measured experimental force. The press fit removal force is the force required to remove the pin over the entire distance of pin insertion, the removal distance.

Table 17. Nylon hex hole diameter measured by micrometer, press fit distance, measured force, entry effect force, press fit force, removal distance, and removal force.

Sample	Hex Inner Diameter (in) Micrometer	Press Fit Distance (in)	Measured Experimental Force (N)	Entry Effect Force (N)	Experimental Press Fit Force (N)	Removal Distance (in)	Press Fit Removal Force (N)
1N	0.366	0.293	1145.0	711.1	433.9	0.293	1587.3
2N	0.366	0.333	2037.0	482.0	1555.0	0.542	1989.2
3N*	0.365	0.275	N/A	N/A	N/A	0.512	1848.2
4N	0.365	0.282	1590.3	973.3	617.0	0.880	2222.1
5N	0.366	0.264	1342.3	791.5	550.8	0.841	1802.5
6N	0.366	0.253	2180.3	1793.9	386.4	0.512	2247.5
7N	0.365	0.106	2037.0	476.0	1561.0	0.542	2275.0
8N	0.365	0.259	1514.9	914.1	600.9	0.570	1510.4
9N	0.371	0.443	353.1	169.8	183.3	0.794	504.1
10N	0.372	0.405	300.7	144.0	156.7	0.792	420.0
11N	N/A	0.412	362.2	183.6	178.6	0.555	536.9
12N	0.371	0.417	268.4	120.0	148.4	0.560	371.2
13N	0.371	0.705	489.5	104.5	385.0	0.827	679.5
14N	0.374	0.400	34.5	15.5	19.0	0.400	106.3
15N	0.374	0.636	124.3	0.0	124.3	0.636	245.1
16N	0.373	0.621	62.0	30.8	31.2	0.621	77.3
17N	0.374	0.705	10.0	0.0	10.0	0.700	22.2
18N	0.372	0.638	131.7	48.0	83.7	0.638	174.7

*Force data for sample 3N was lost.

The following graphs show the force vs. distance graphs for each sample. From these graphs, the maximum press fit force was determined for each test. Data was first collected to measure the force required to press fit the pin. Five weeks later, data was collected to measure the force to remove the pin. Please refer to Sect. 4.1 for interpretation of experimental results.

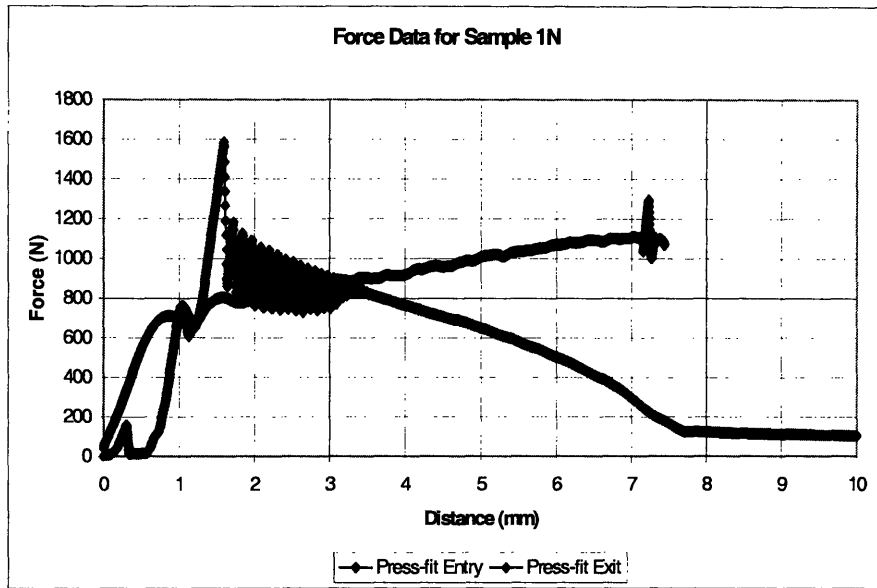


Figure 31. The maximum force measured was 1145.0 N. Subtracting entry effects of 711.1 N, the press fit force for a distance of 7.44 mm was determined to be 433.9 N. Removing the steel dowel pin required 1587.3 N.

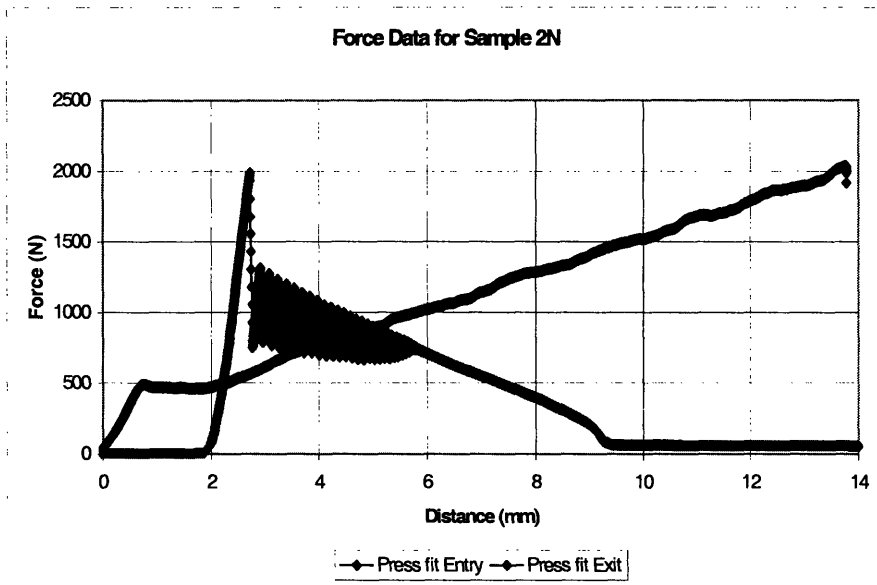


Figure 32. The maximum force measured was 2037.0 N. Subtracting entry effects of 482.0 N, the press fit force for a distance of 8.45 mm was determined to be 1555.0 N. Removing the steel dowel pin required 1989.2 N.

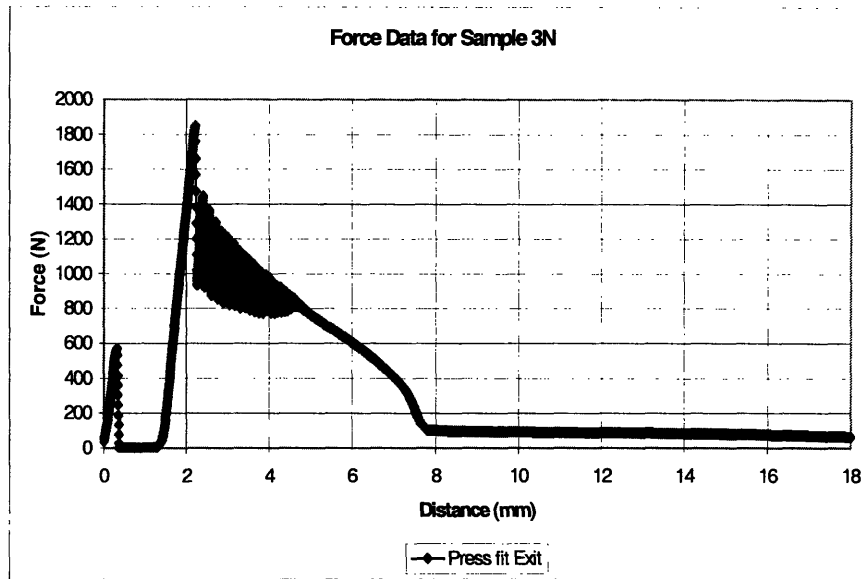


Figure 33. The force data file for the initial press fit is unavailable. Removing the steel dowel pin required 1848.2 N.

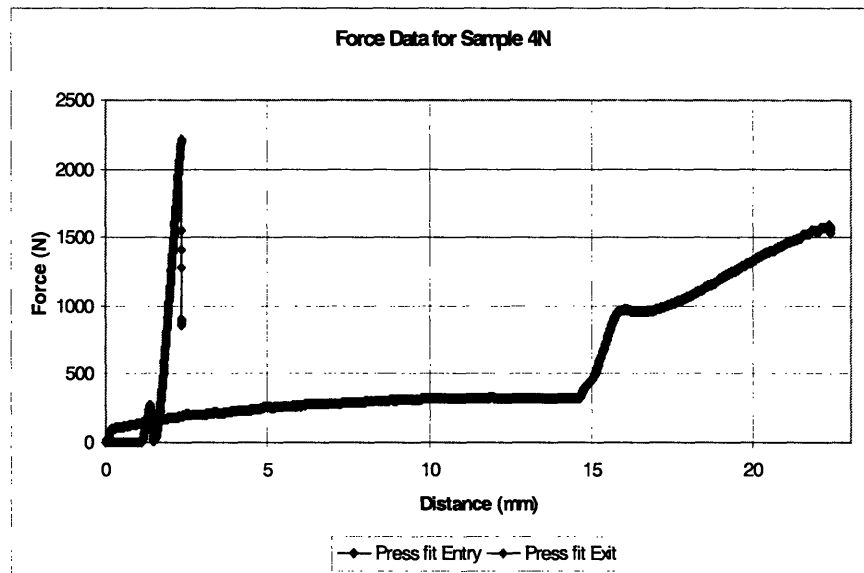


Figure 34. The maximum force measured was 1590.3 N. Subtracting entry effects of 973.3 N, the press fit force for a distance of 7.16 mm was determined to be 617.0 N. Removing the steel dowel pin required 2222.1 N.

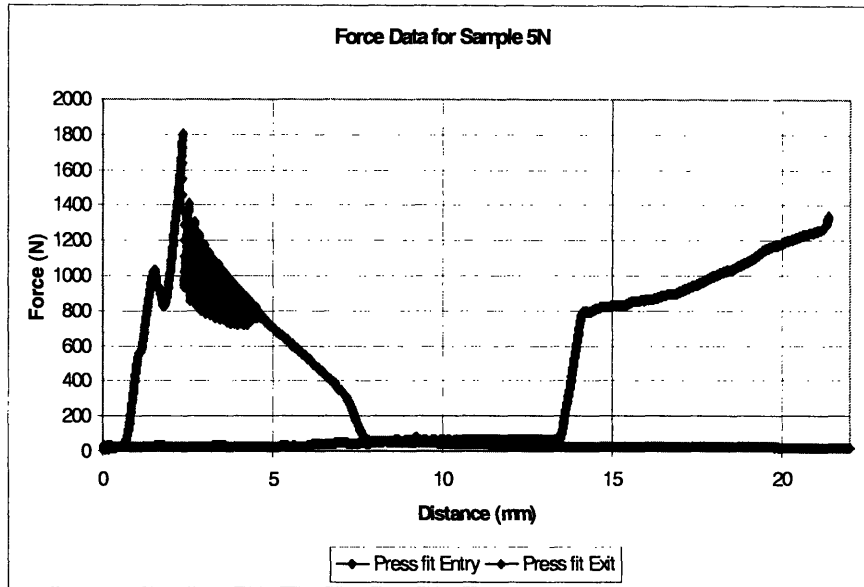


Figure 35. The maximum force measured was 1342.3 N. Subtracting entry effects of 791.5 N, the press fit force for a distance of 6.71 mm was determined to be 550.8 N. Removing the steel dowel pin required 1802.5 N.

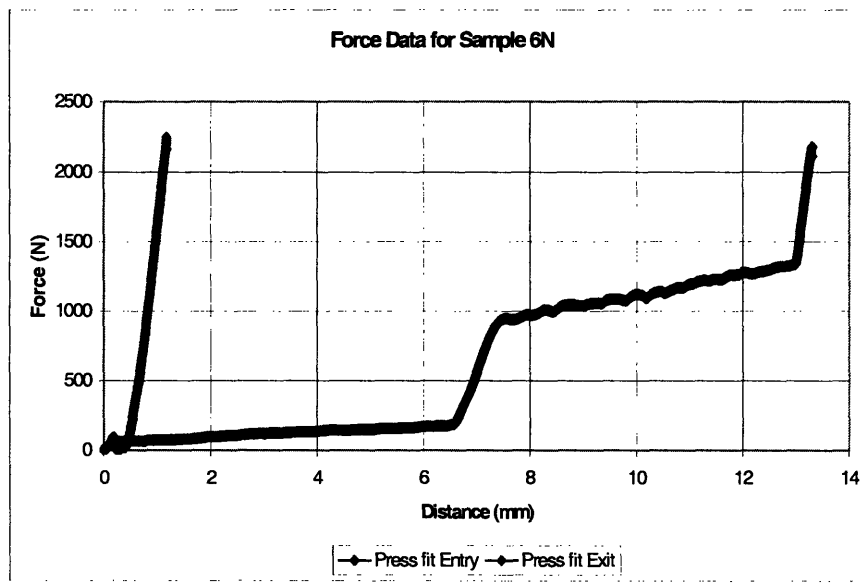


Figure 36. The maximum force measured was 2180.3 N. Subtracting entry effects of 1793.9 N, the press fit force for a distance of 6.41 mm was determined to be 386.4 N. Removing the steel dowel pin required 2247.5 N.

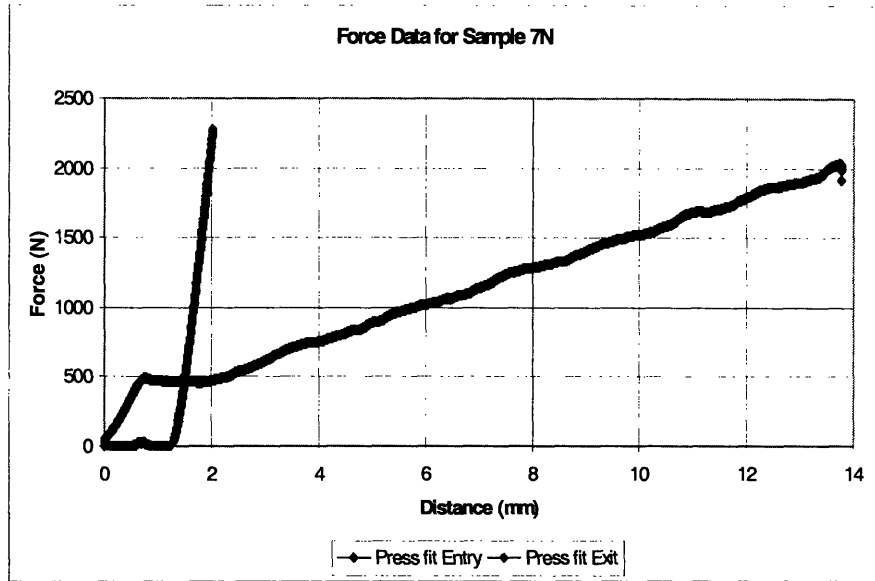


Figure 37. The maximum force measured was 2037.0 N. Subtracting entry effects of 476.0 N, the press fit force for a distance of 2.69 mm was determined to be 1561.0 N. Removing the steel dowel pin required 2275.0 N.

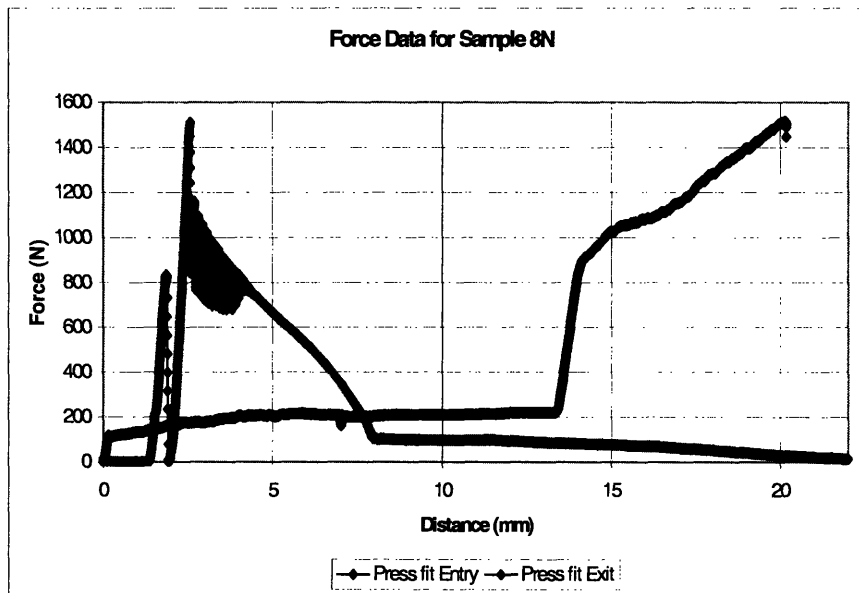


Figure 38. The maximum force measured was 1514.9 N. Subtracting entry effects of 914.1 N, the press fit force for a distance of 6.58 mm was determined to be 600.9 N. Removing the steel dowel pin required 1510.4 N.

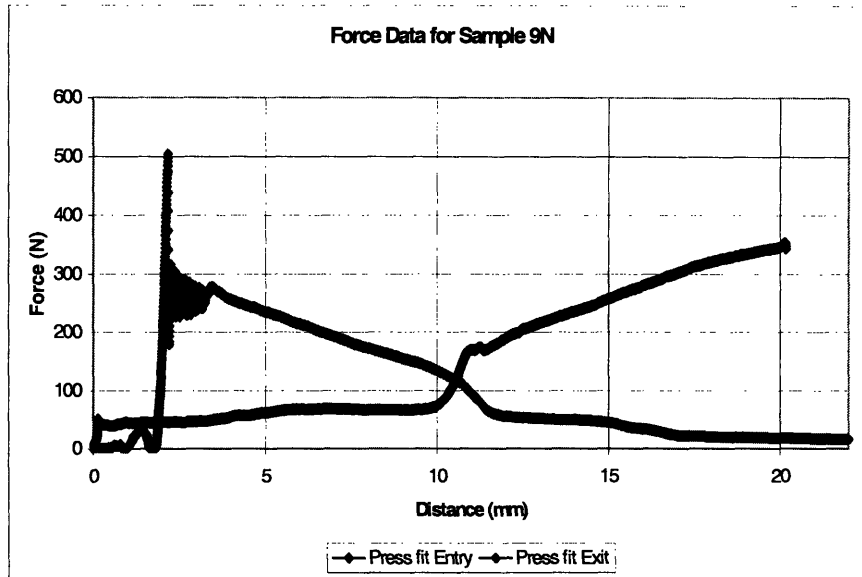


Figure 39. The maximum force measured was 353.1 N. Subtracting entry effects of 169.8 N, the press fit force for a distance of 11.24 mm was determined to be 183.3 N. Removing the steel dowel pin required 504.1 N.

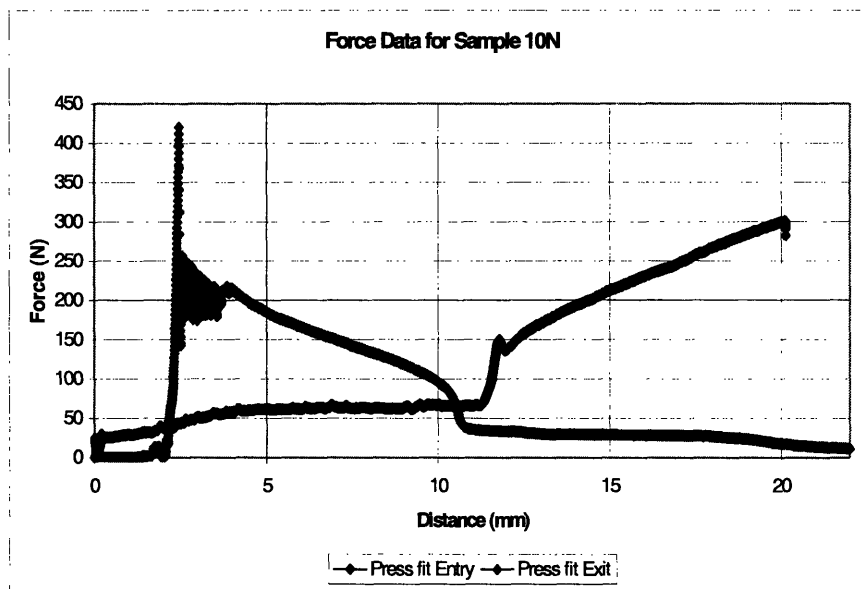


Figure 40. The maximum force measured was 300.7 N. Subtracting entry effects of 144.0 N, the press fit force for a distance of 10.28 mm was determined to be 156.7 N. Removing the steel dowel pin required 420.0 N.

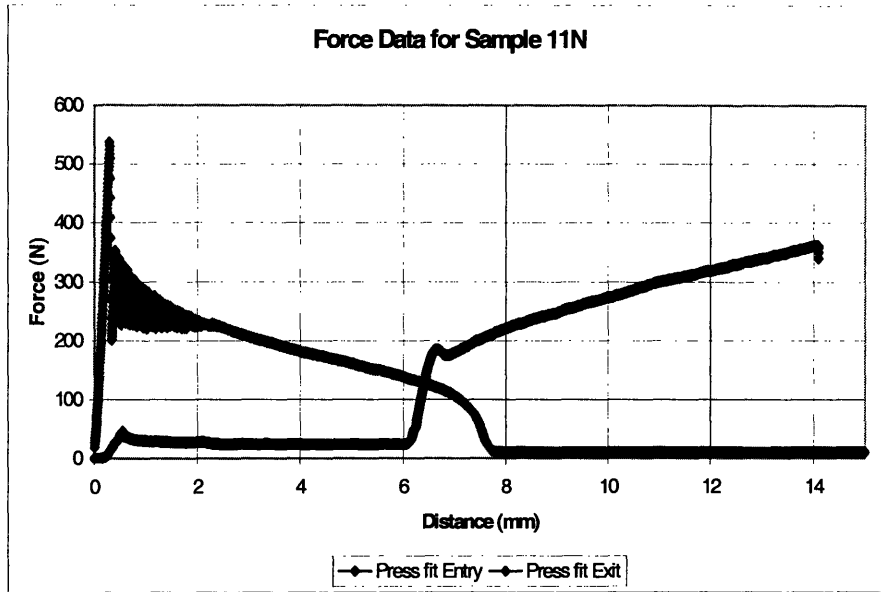


Figure 41. The maximum force measured was 362.2 N. Subtracting entry effects of 183.6 N, the press fit force for a distance of 10.46 mm was determined to be 178.6 N. Removing the steel dowel pin required 536.9 N.

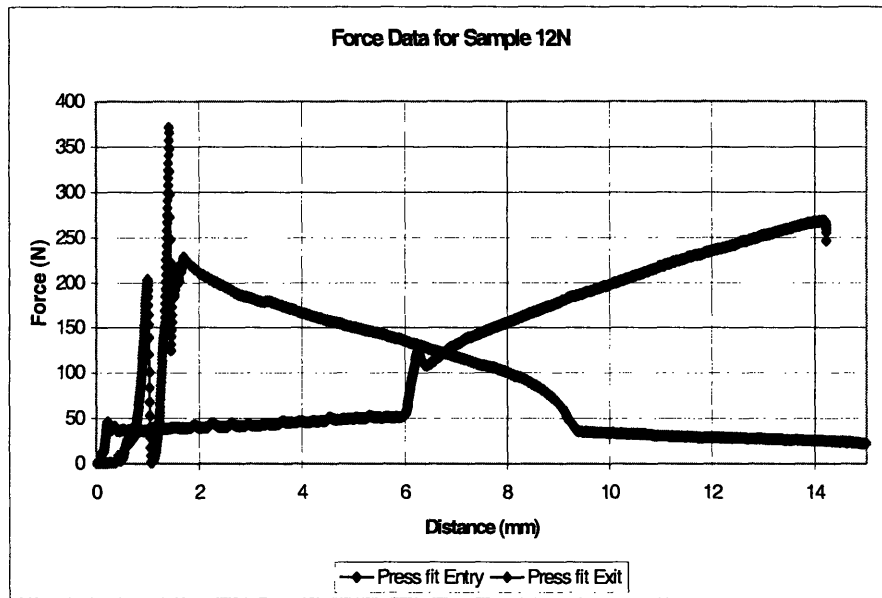


Figure 42. The maximum force measured was 268.4 N. Subtracting entry effects of 120.0 N, the press fit force for a distance of 10.58 mm was determined to be 148.4 N. Removing the steel dowel pin required 371.2 N.

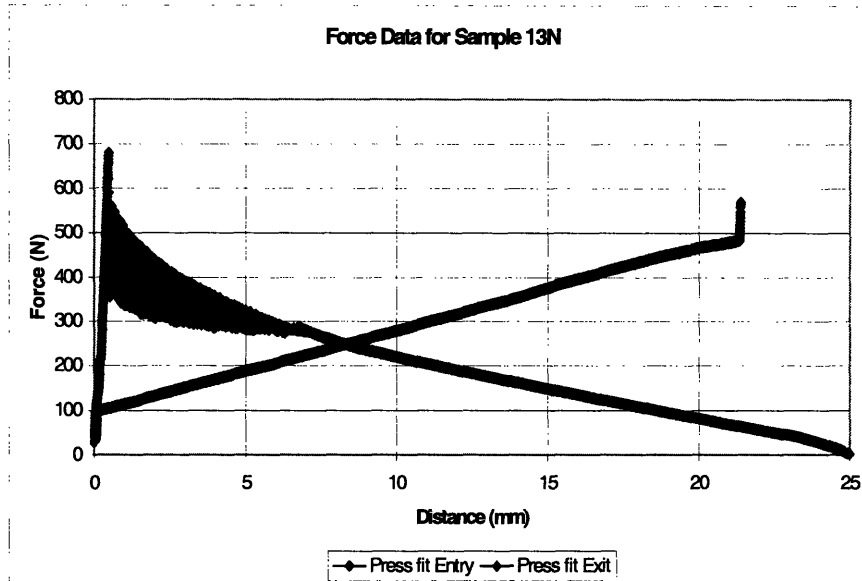


Figure 43. The maximum force measured was 489.5 N. Subtracting entry effects of 104.5 N, the press fit force for a distance of 17.89 mm was determined to be 385.0 N. Removing the steel dowel pin required 679.5 N.

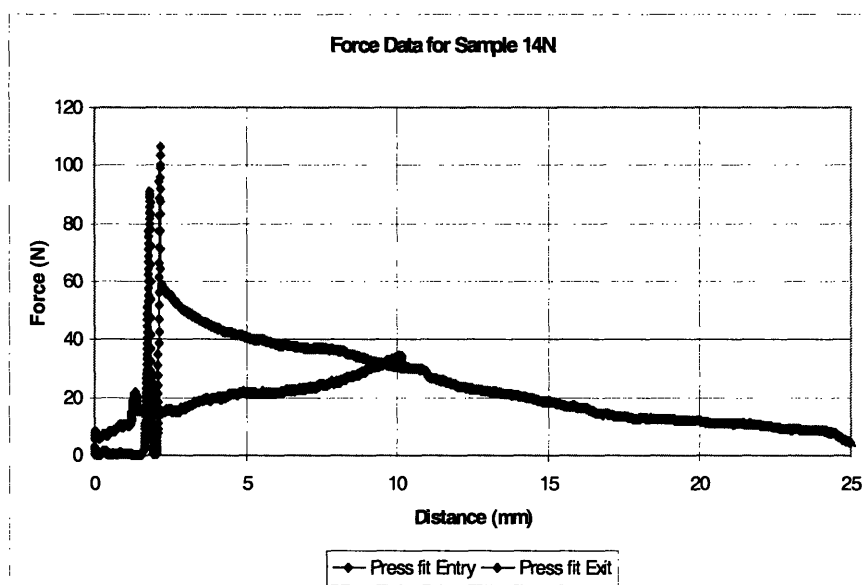


Figure 44. The maximum force measured was 34.5 N. Subtracting entry effects of 15.5 N, the press fit force for a distance of 10.17 mm was determined to be 19.0 N. Removing the steel dowel pin required 106.3 N.

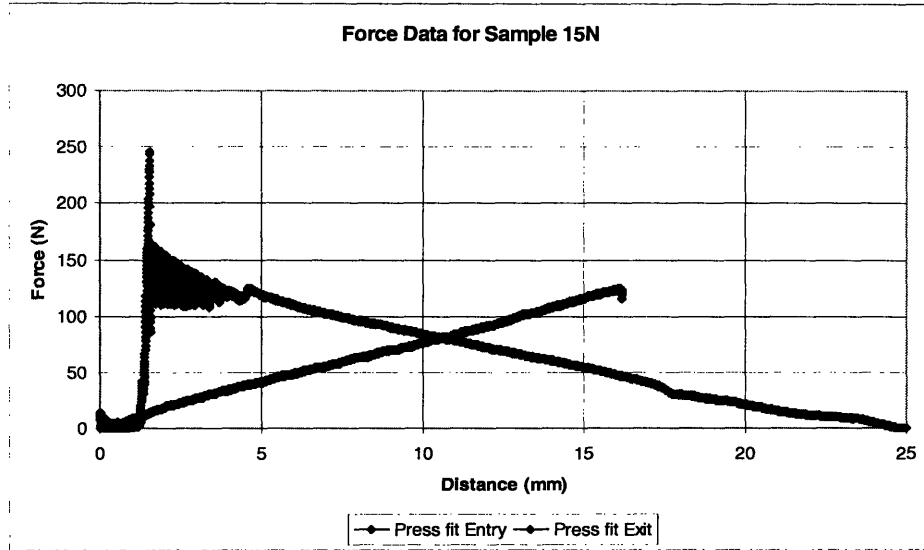


Figure 45. The maximum force measured was 124.3 N. No entry effect was observed. Therefore the press fit force for a distance of 16.16 mm was determined to be 124.3 N. Removing the steel dowel pin required 245.1 N.

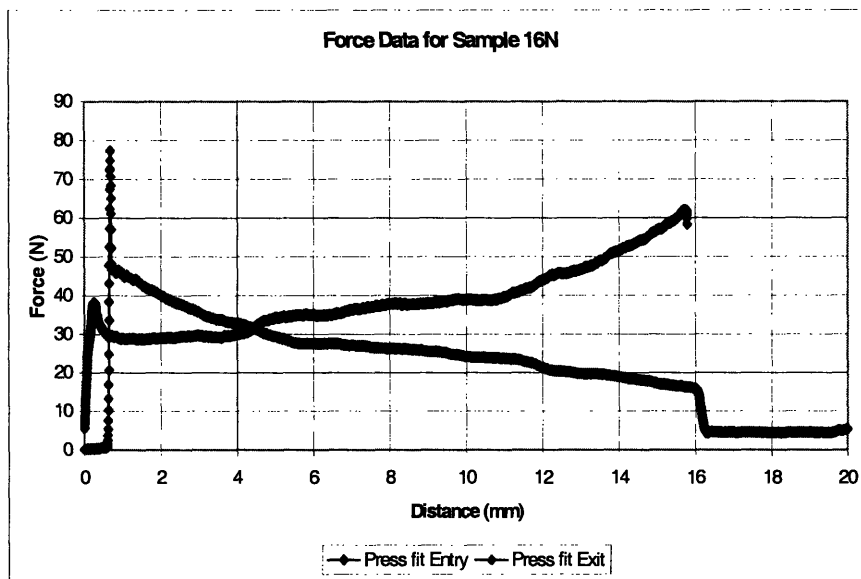


Figure 46. The maximum force measured was 62.0 N. Subtracting entry effects of 30.8 N, the press fit force for a distance of 15.78 mm was determined to be 31.2 N. Removing the steel dowel pin required 77.3 N.

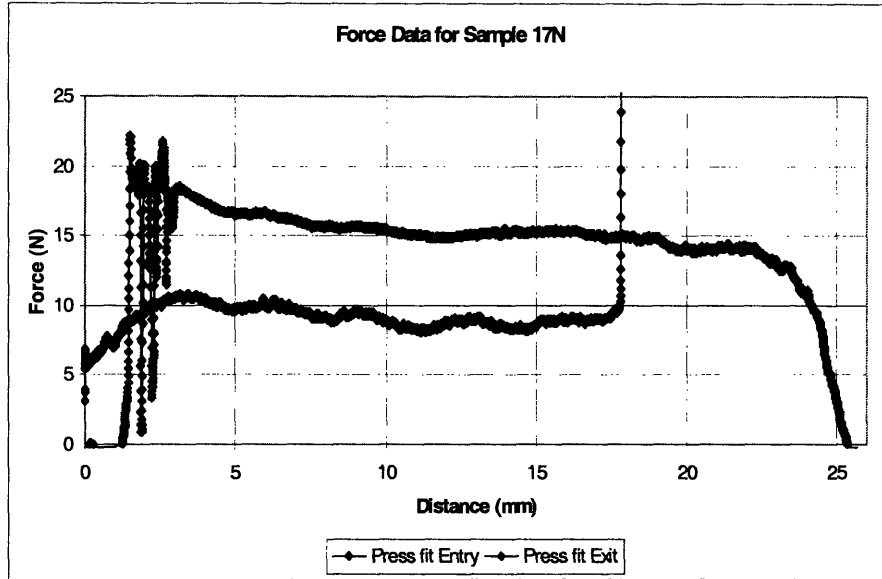


Figure 47. The maximum force measured was 10.0 N. No entry effect was observed. Therefore the press fit force for a distance of 17.90 mm was determined to be 10.0 N. The sharp peak in the press fit entry data at distance 18mm is due to the pin pressing through the nylon hex and into the table. Removing the steel dowel pin required 22.2 N.

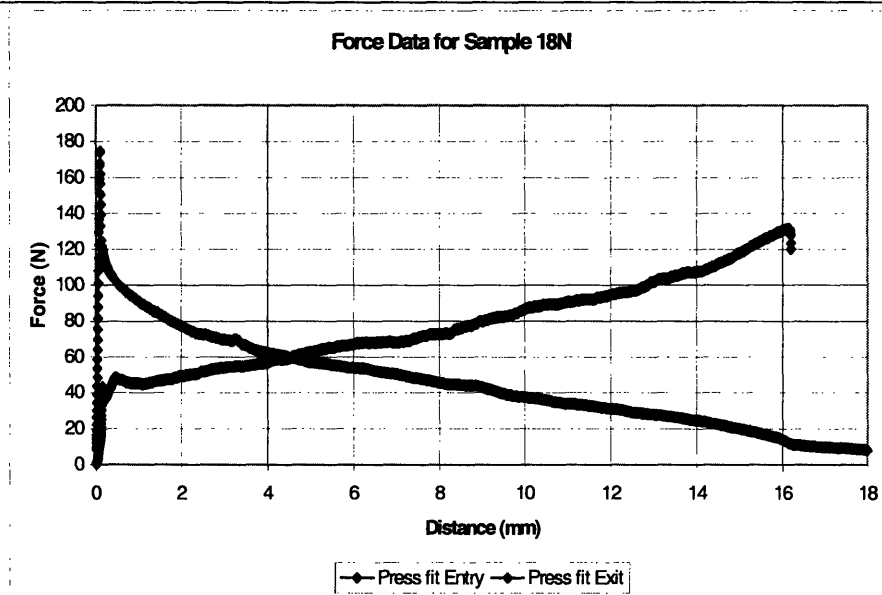


Figure 48. The maximum force measured was 131.7 N. Subtracting entry effects of 48.0 N, the press fit force for a distance of 16.19 mm was determined to be 83.7 N. Removing the steel dowel pin required 174.7 N.

Appendix 4: Nylon Torque Data

The following graphs show the torque vs. time graphs for each sample. From these graphs, the maximum torque was determined for each test as the maximum peak in the graph. There is some noise in the signal, which can be seen as somewhat random data points that do not behave similarly to the points on either side. These outlier data points have not been selected as the maximum torque data points. Please refer to Sect. 4.1 for interpretation of experimental results.

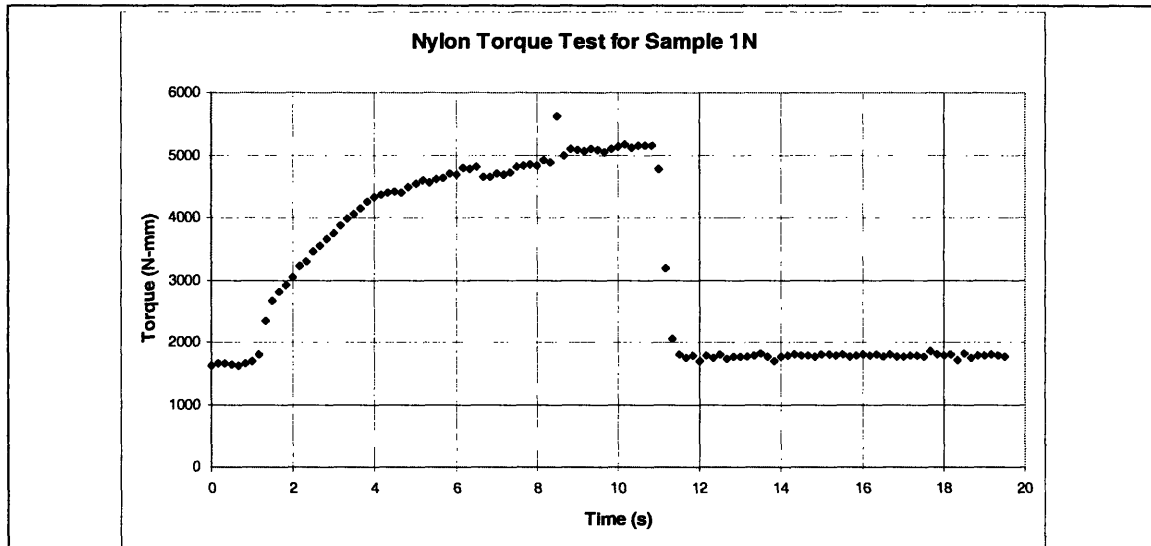


Figure 49. The measured applied torque, shown as the maximum peak on the graph, is 5070.8 N. The residual torque due to the offset of the lever arm was calculated to be 688.9 N. Therefore the net torque is 4381.9 N.

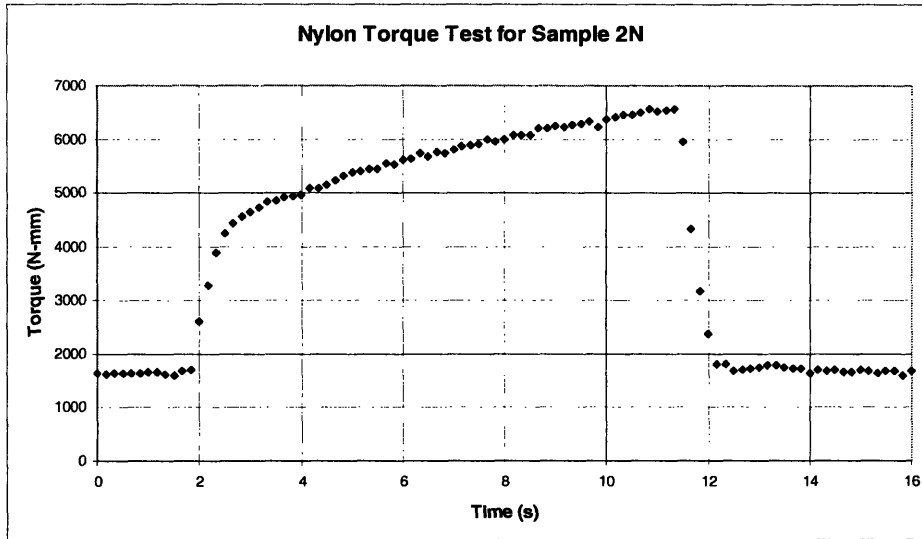


Figure 50. The measured applied torque, shown as the maximum peak on the graph, is 6549.4 N. The residual torque due to the offset of the lever arm was calculated to be 490.6 N. Therefore the net torque is 6058.8 N.

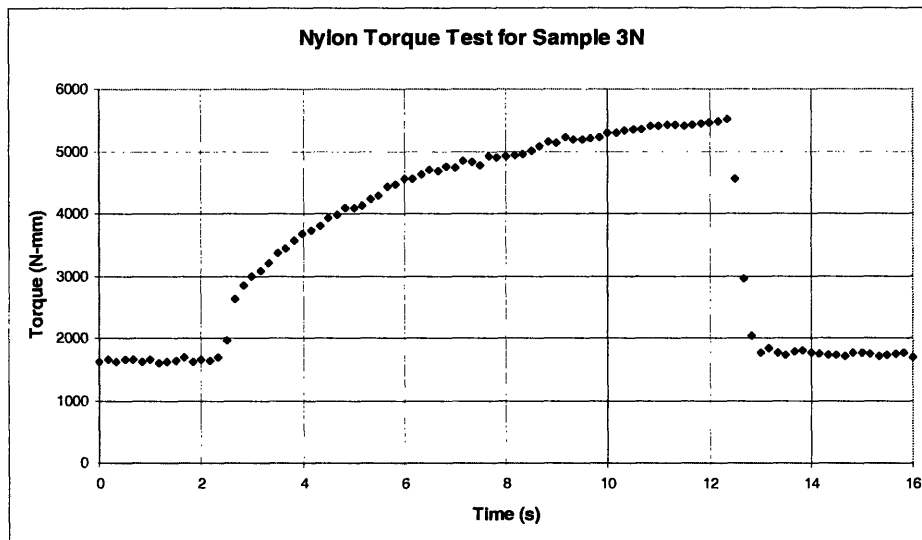


Figure 51. The measured applied torque, shown as the maximum peak on the graph, is 5520.5 N. The residual torque due to the offset of the lever arm was calculated to be 1711.6 N. Therefore the net torque is 3808.9 N.

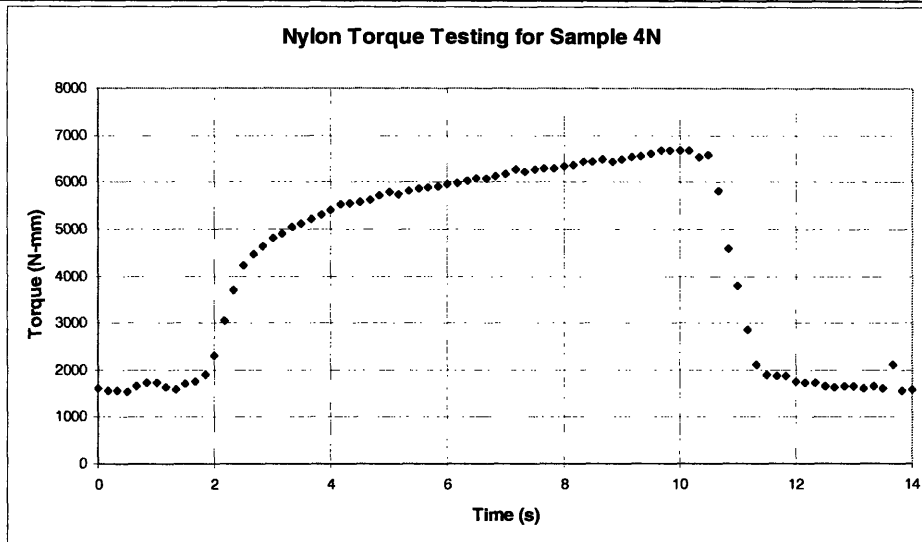


Figure 52. The measured applied torque, shown as the maximum peak on the graph, is 6687.6 N. The residual torque due to the offset of the lever arm was calculated to be 935.6 N. Therefore the net torque is 5752.0 N.

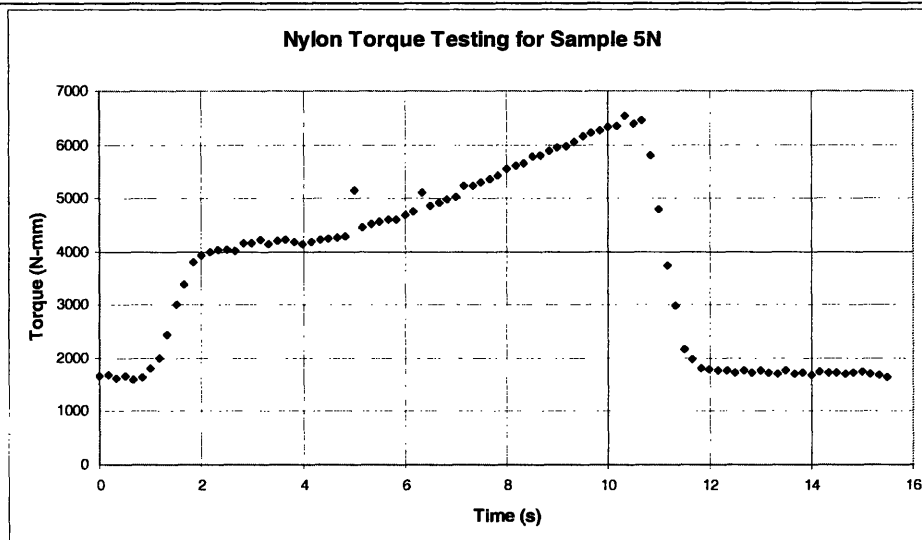


Figure 53. The measured applied torque, shown as the maximum peak on the graph, is 6537.8 N. The residual torque due to the offset of the lever arm was calculated to be 768.2 N. Therefore the net torque is 5769.6 N.

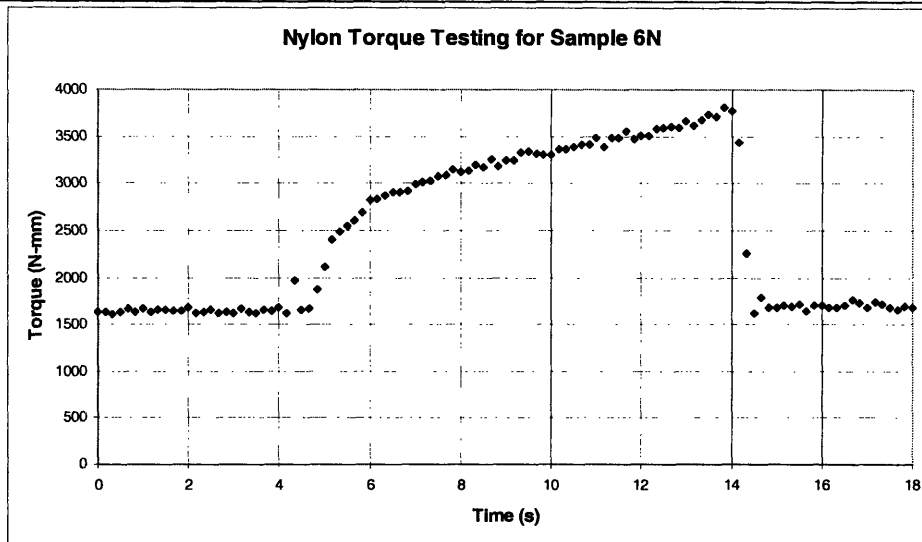


Figure 54. The measured applied torque, shown as the maximum peak on the graph, is 3807.2 N. The residual torque due to the offset of the lever arm was calculated to be 890.8 N. Therefore the net torque is 2916.4 N.

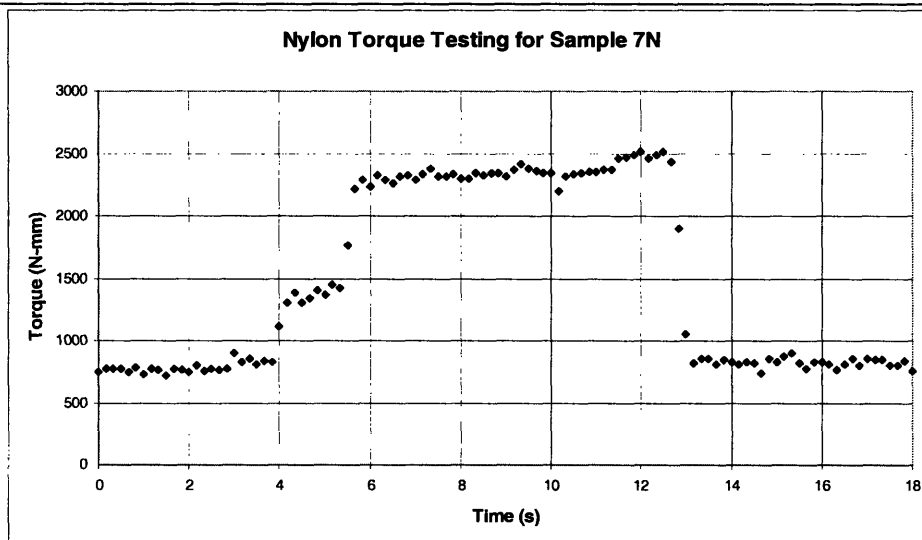


Figure 55. The measured applied torque, shown as the maximum peak on the graph, is 2510.6 N. The residual torque due to the offset of the lever arm was calculated to be 463.1 N. Therefore the net torque is 2047.4 N.

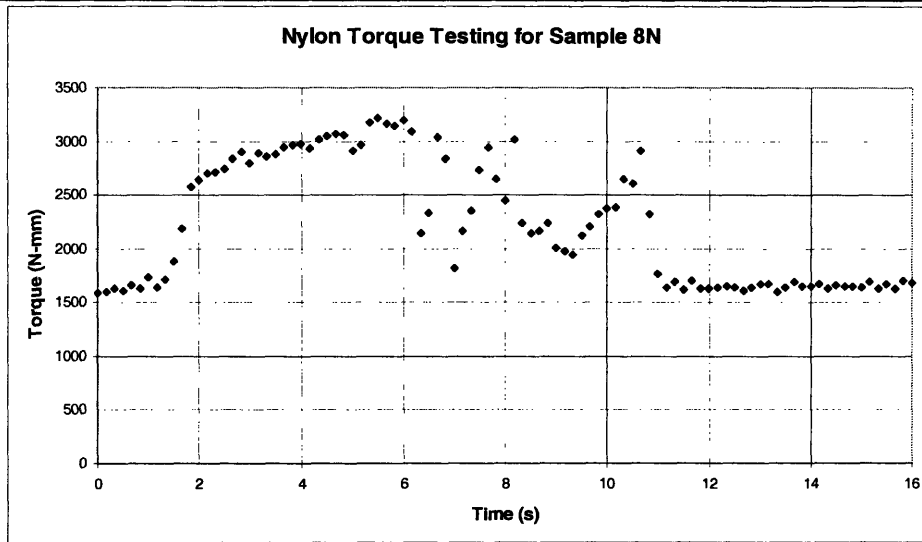


Figure 56. The measured applied torque, shown as the maximum peak on the graph, is 3217.4 N. The residual torque due to the offset of the lever arm was calculated to be 855.6 N. Therefore the net torque is 2361.8 N.

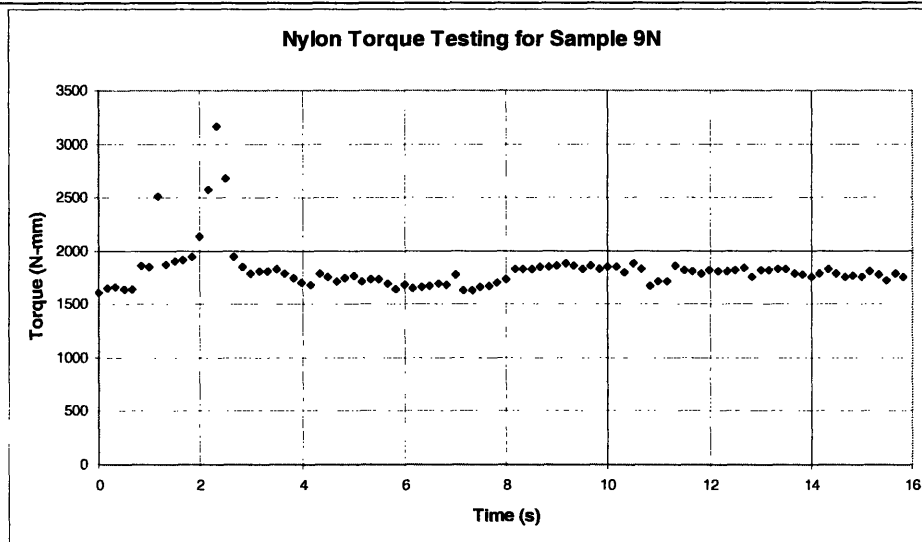


Figure 57. The measured applied torque, shown as the maximum peak on the graph, is 3158.5 N. The residual torque due to the offset of the lever arm was calculated to be 185.0 N. Therefore the net torque is 2973.5 N.

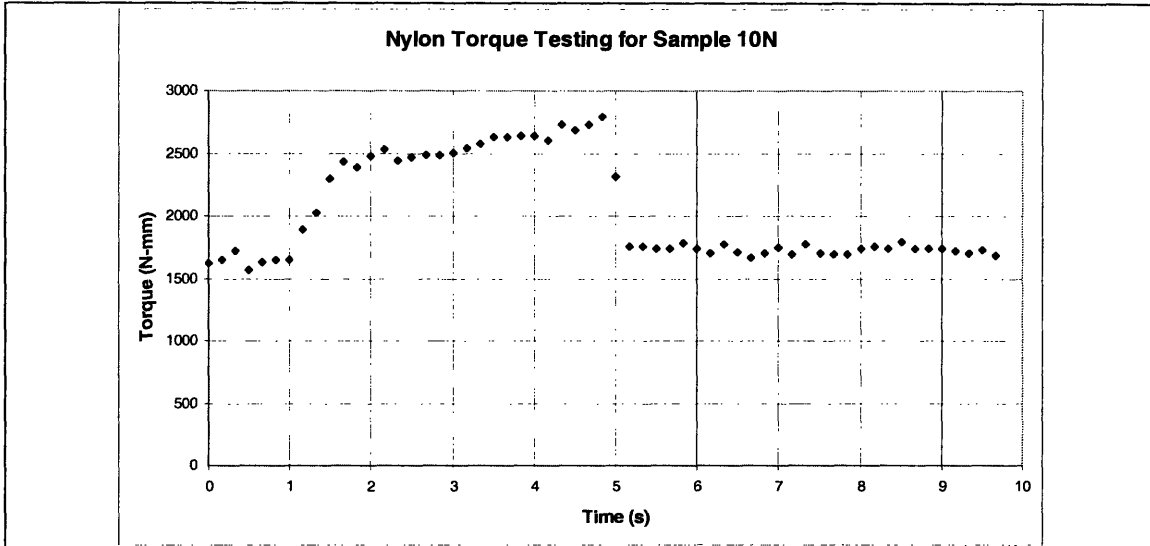


Figure 58. The measured applied torque, shown as the maximum peak on the graph, is 2796.5 N. The residual torque due to the offset of the lever arm was calculated to be 160.0 N. Therefore the net torque is 2636.5 N.

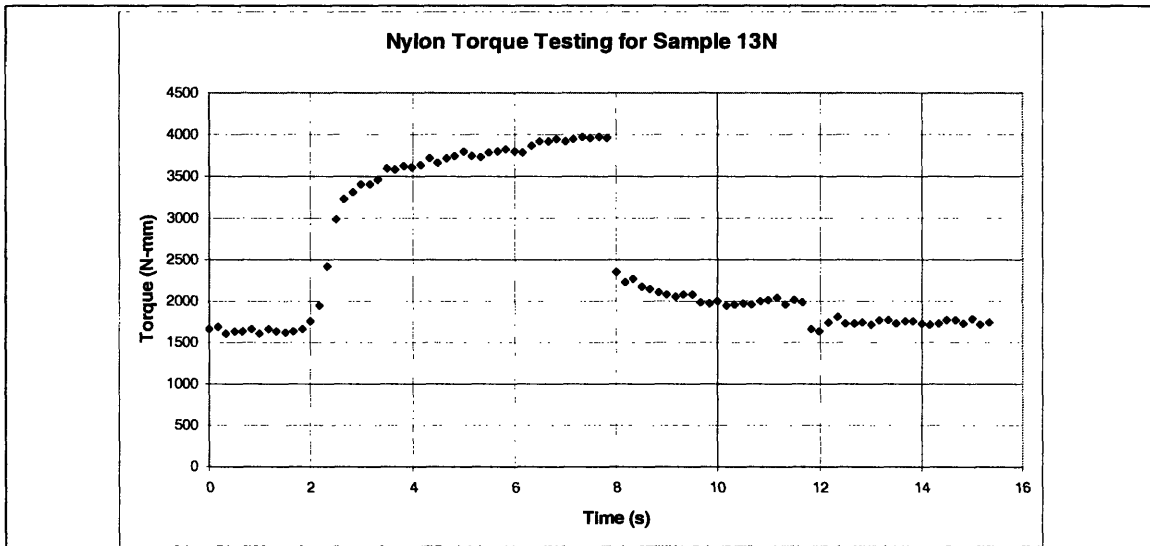


Figure 59. The measured applied torque, shown as the maximum peak on the graph, is 3967.4 N. The residual torque due to the offset of the lever arm was calculated to be 136.0 N. Therefore the net torque is 3831.4 N.

Data for samples 11N, 12N, 14N, 15N, 16N, 17N, and 18N was not collected. These samples required less than the torque of the lever to cause the hex to rotate independent of the dowel pin. Therefore, since the torque of the lever arm is 1617 N-mm, these samples required less than 1617 N-mm.

Appendix 4: Brass Experimental Force Data

The following graphs show the force vs. distance graphs for each sample. From these graphs, the maximum press fit force was determined for each test. Please refer to Sect. 4.1 for interpretation of experimental results.

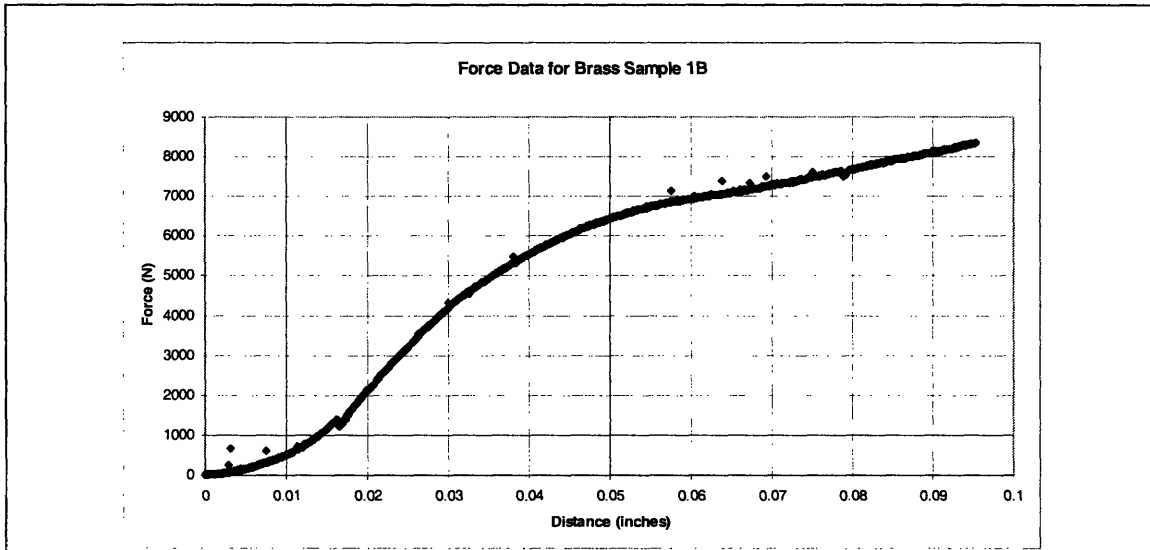


Figure 60. Experimental press fit force required for brass sample 1B. Maximum measured force is 8351 N.

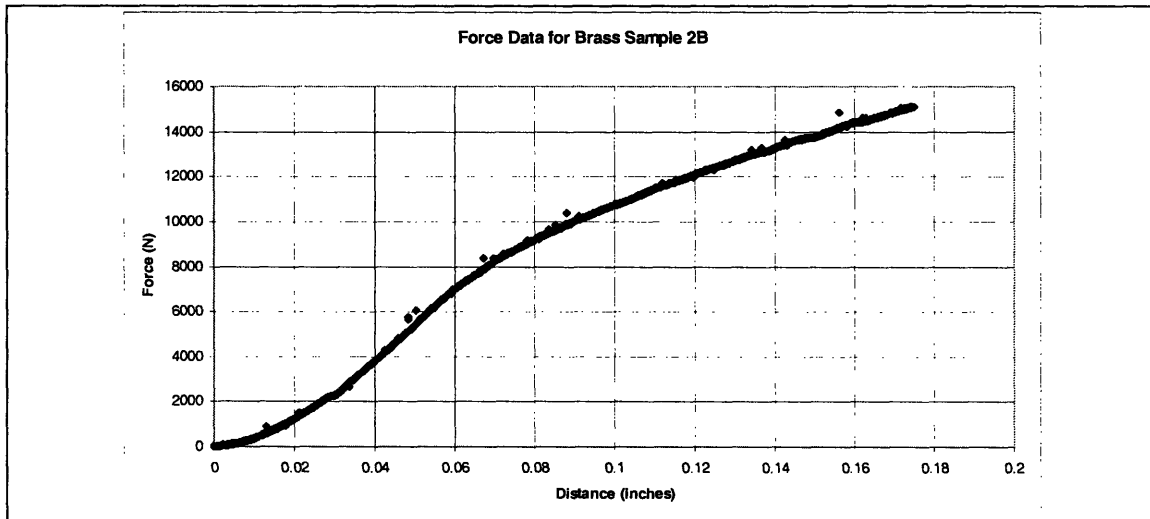
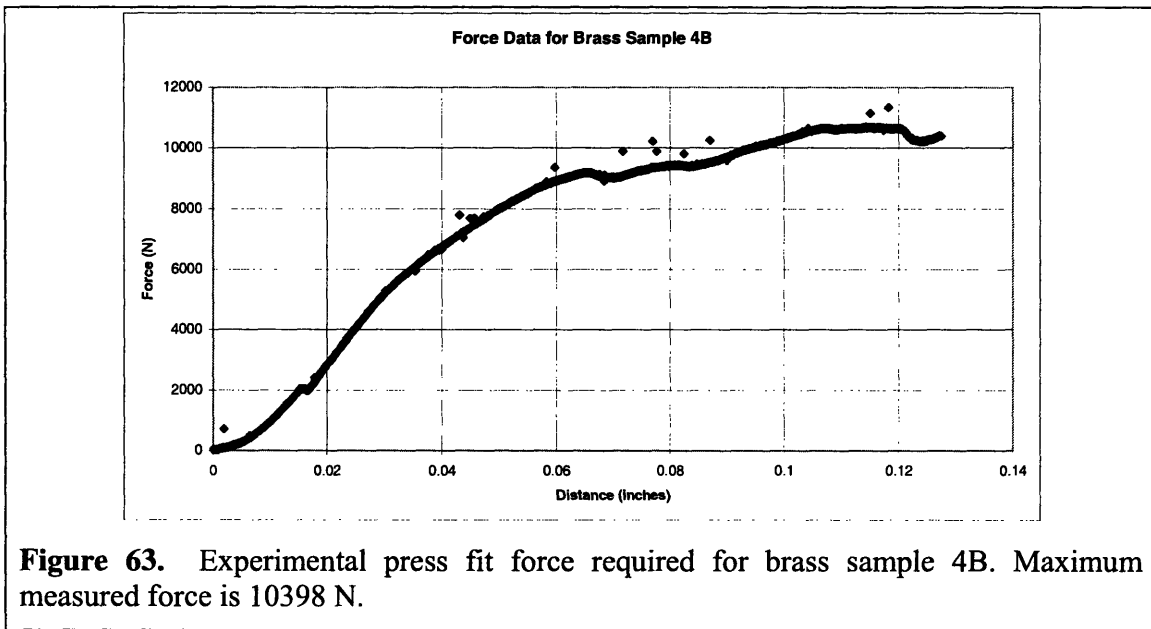
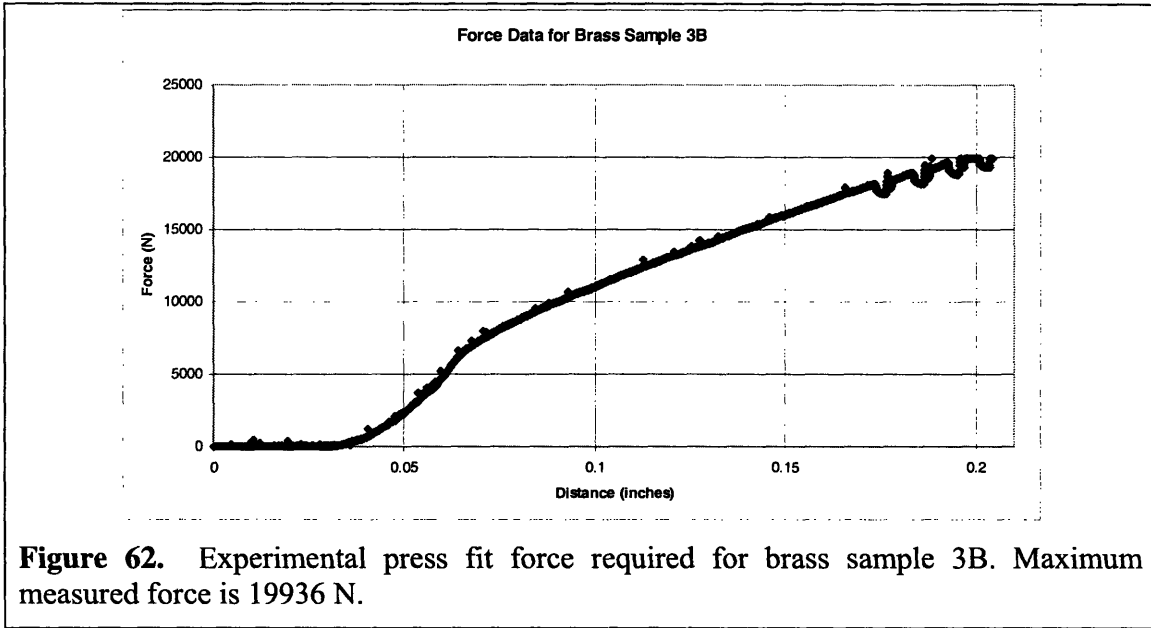
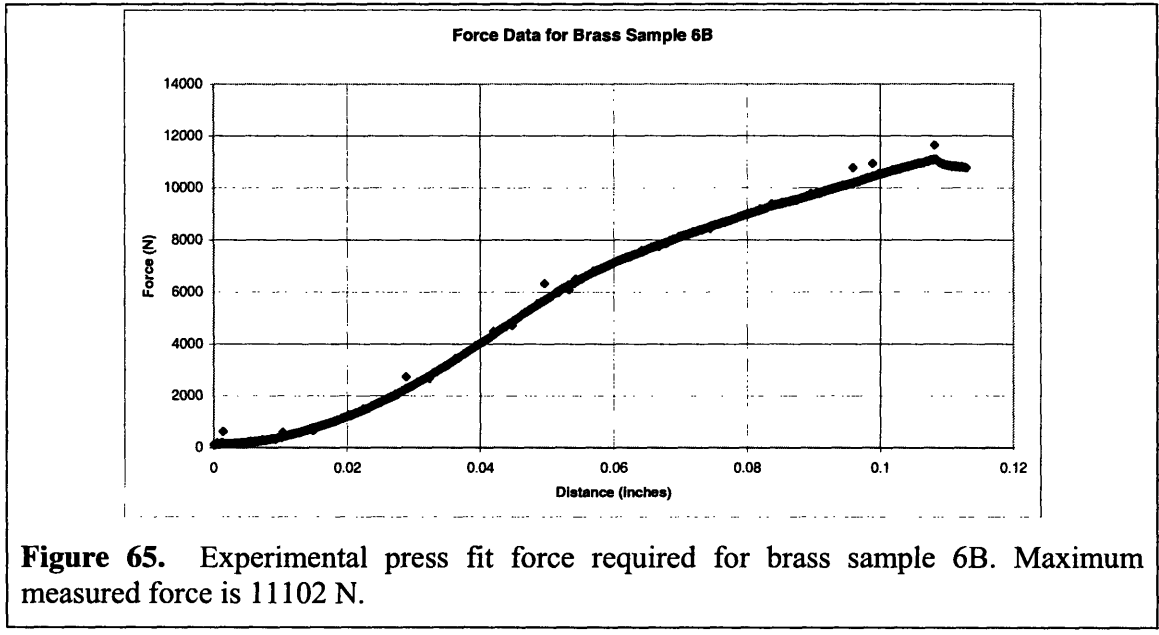
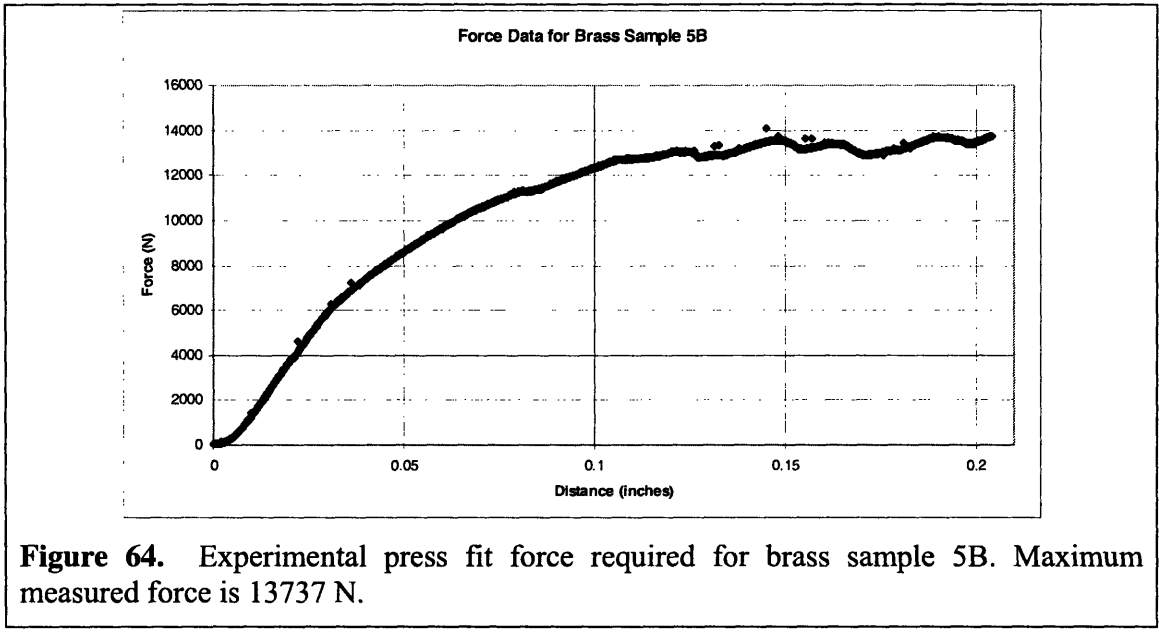
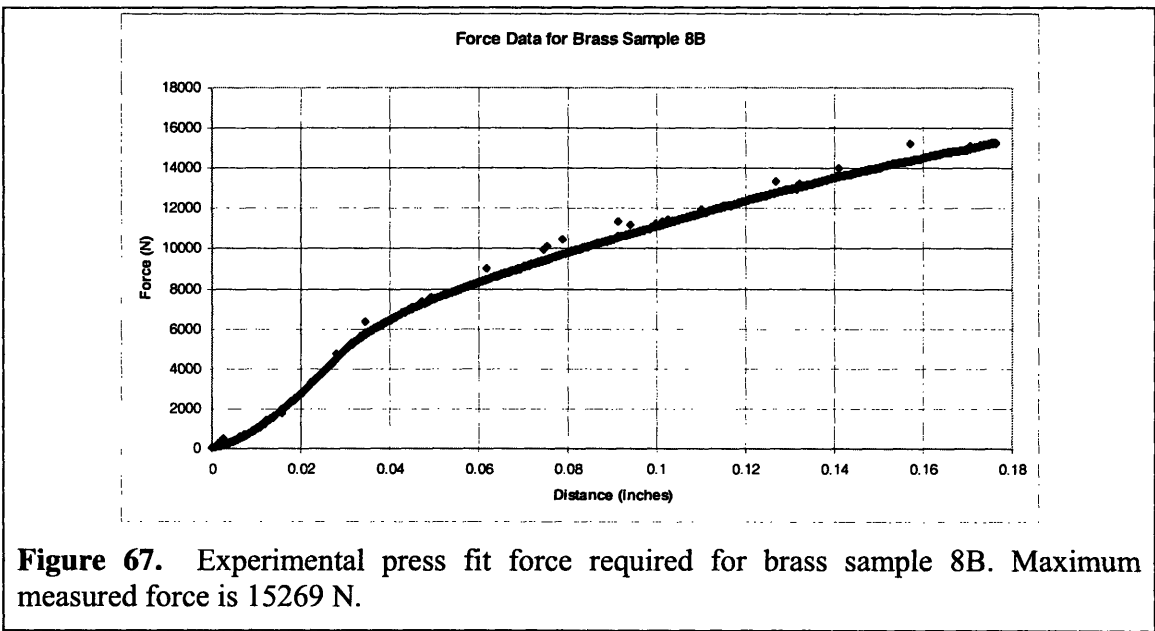
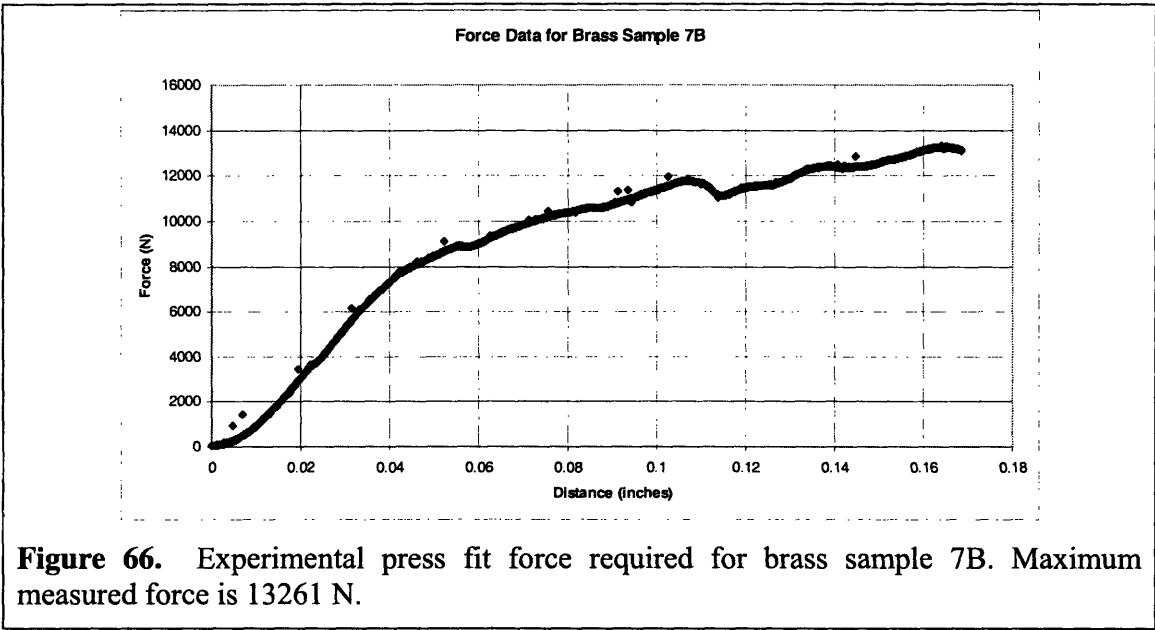
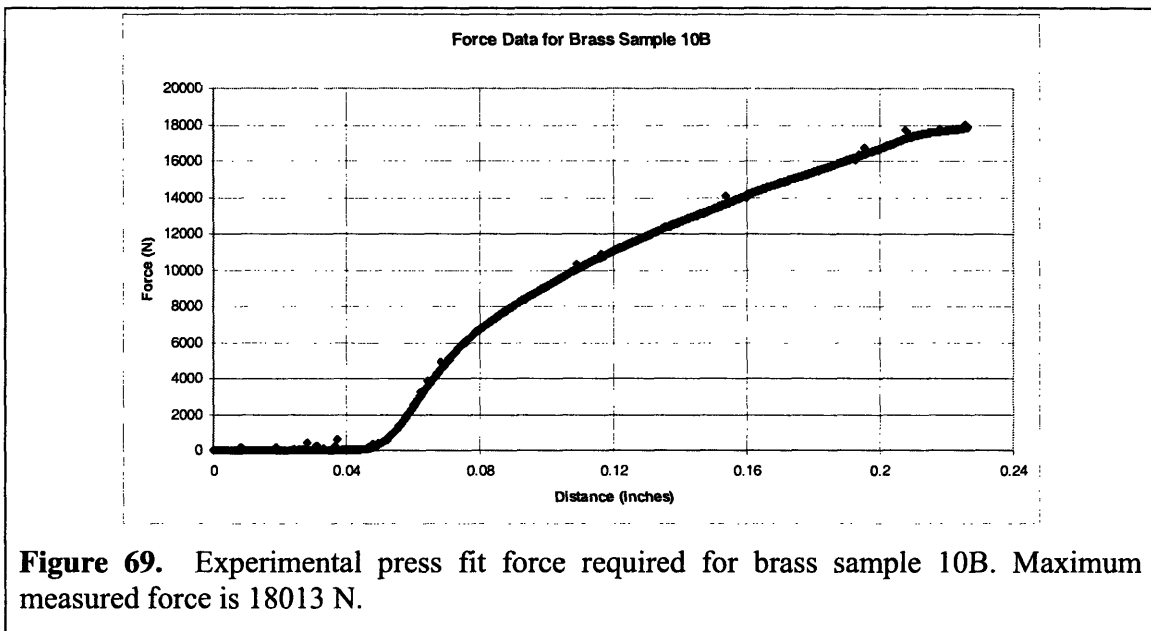
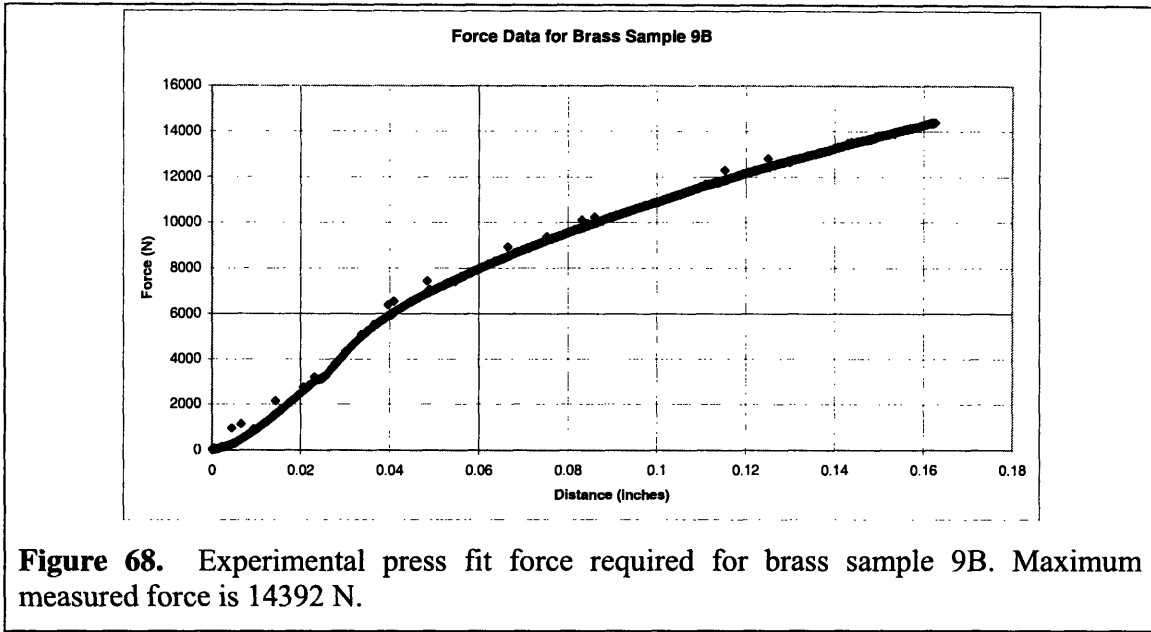


Figure 61. Experimental press fit force required for brass sample 2B. Maximum measured force is 15134 N.









No data for Sample 11.

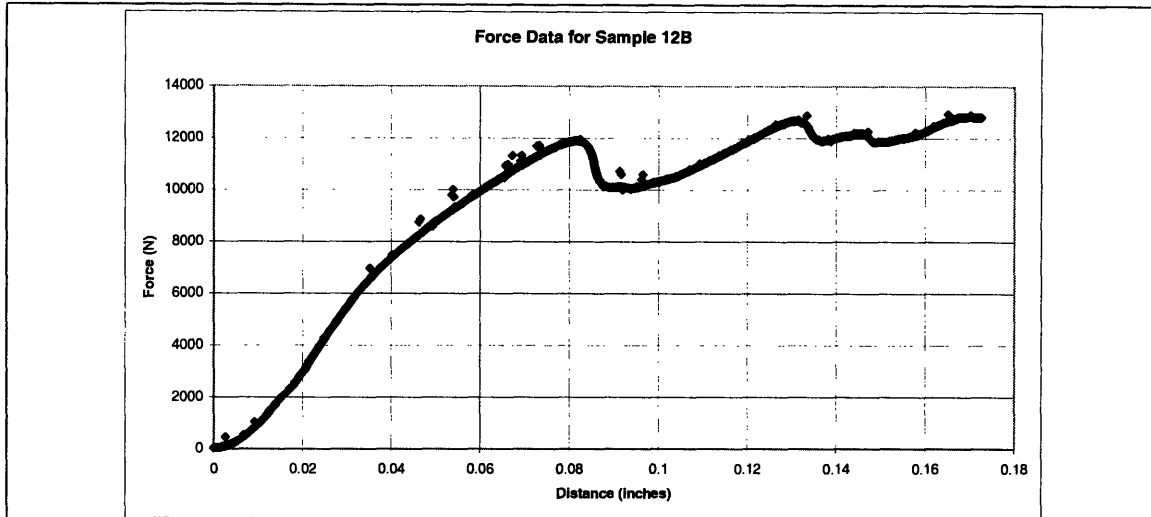


Figure 70. Experimental press fit force required for brass sample 12B. Maximum measured force is 12816 N.

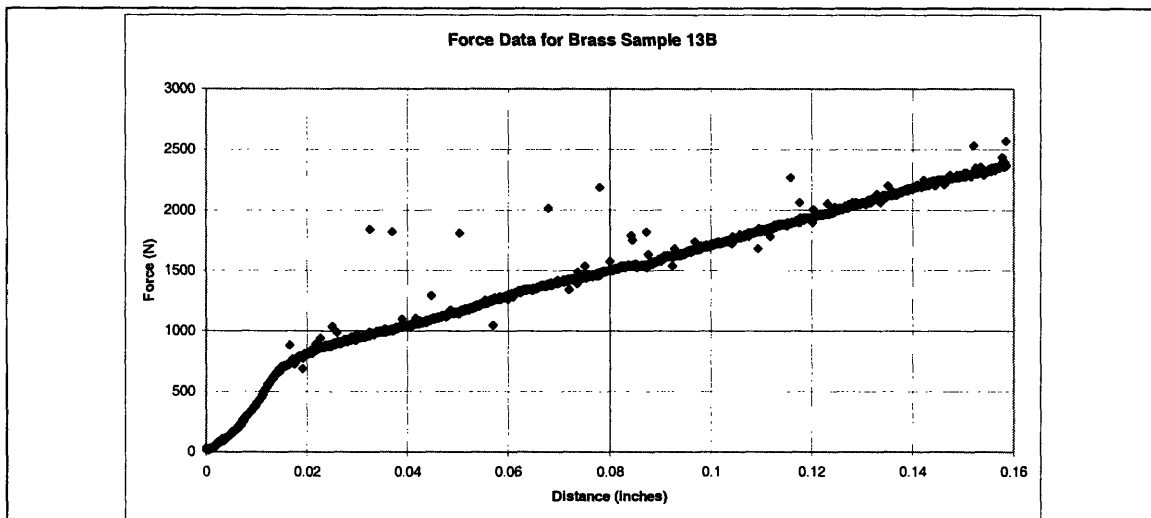


Figure 71. Experimental press fit force required for brass sample 13B. Maximum measured force is 2374 N.

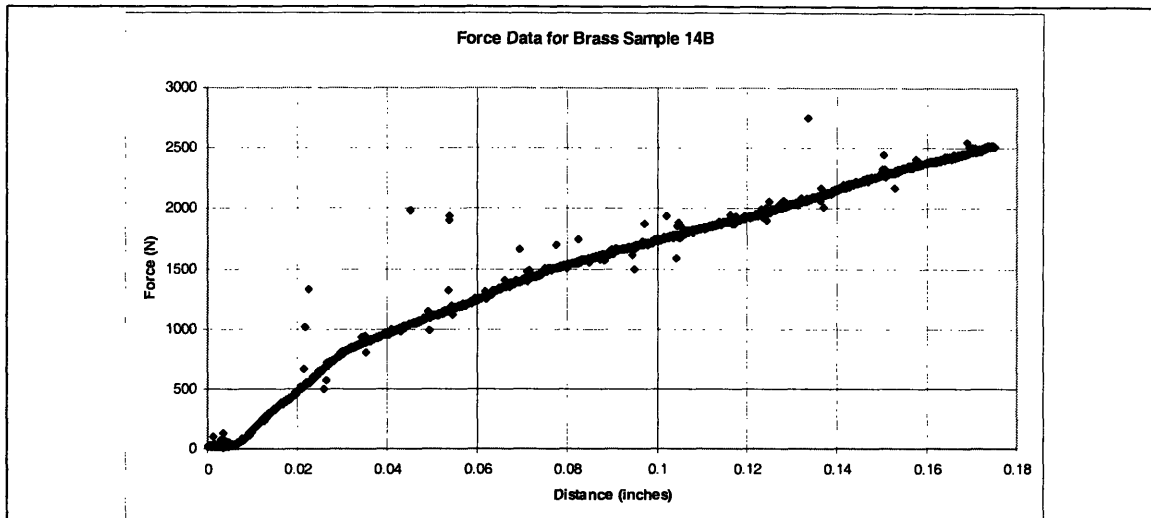


Figure 72. Experimental press fit force required for brass sample 14B. Maximum measured force is 2517 N.

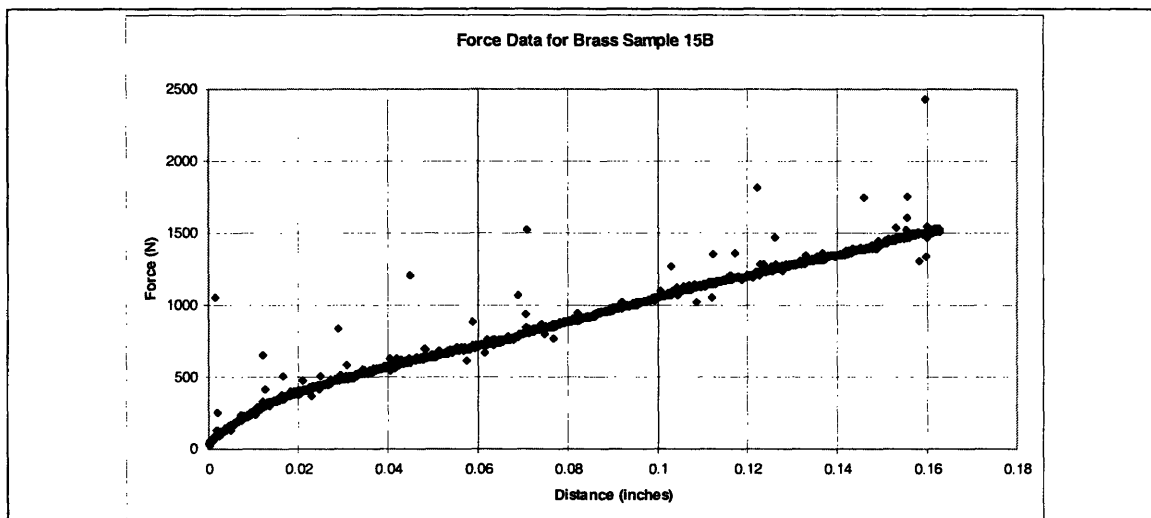
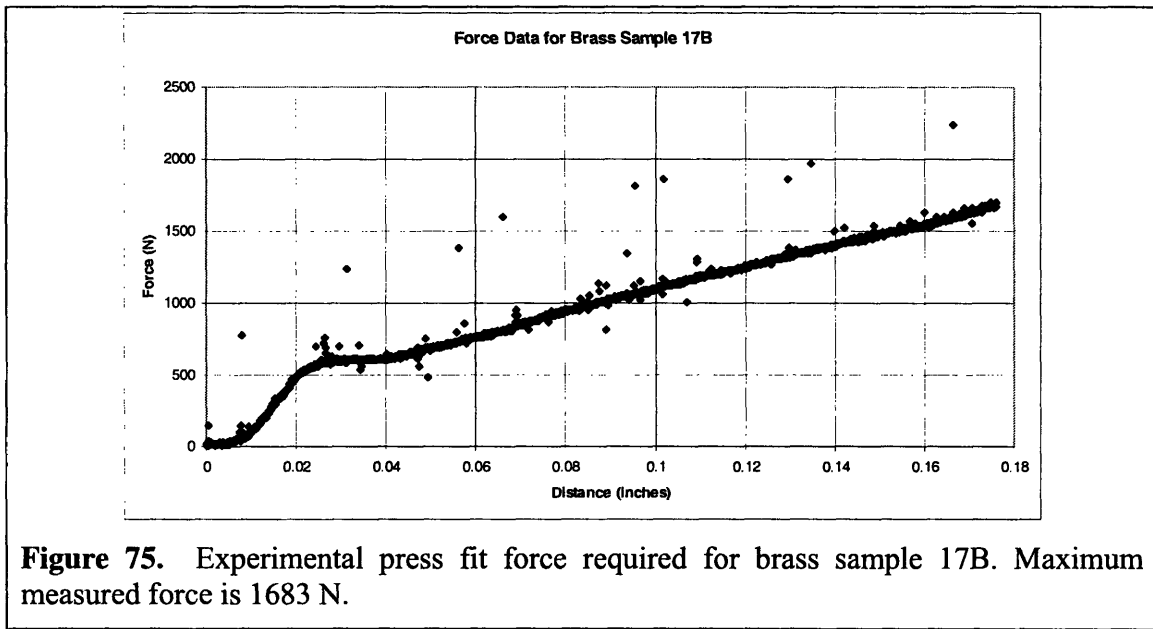
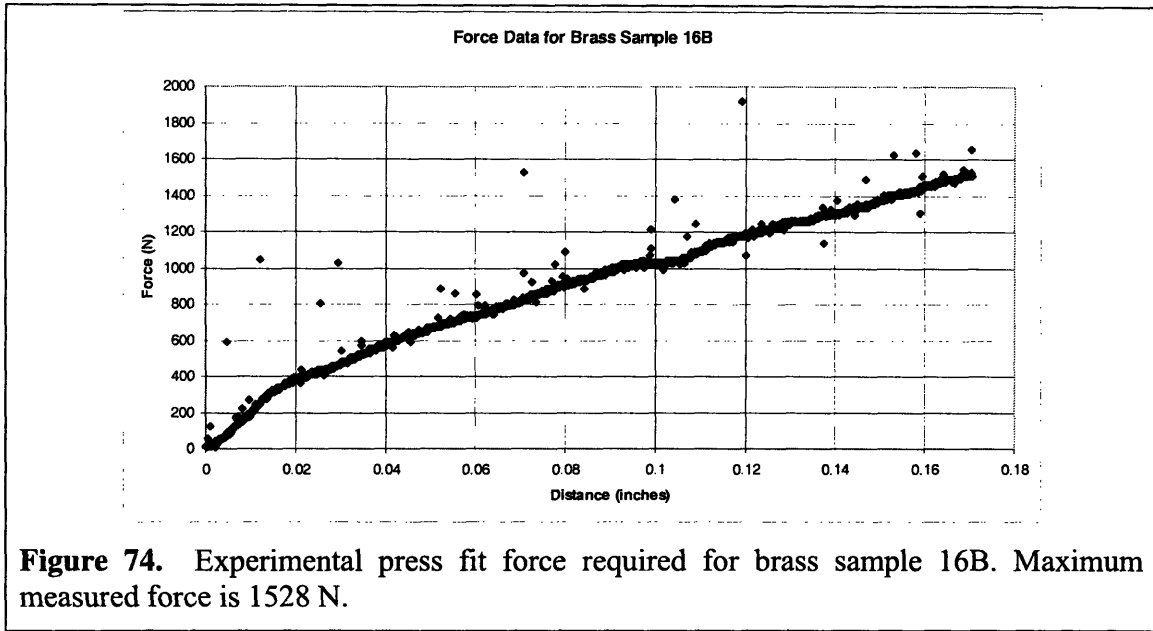


Figure 73. Experimental press fit force required for brass sample 15B. Maximum measured force is 1540 N.



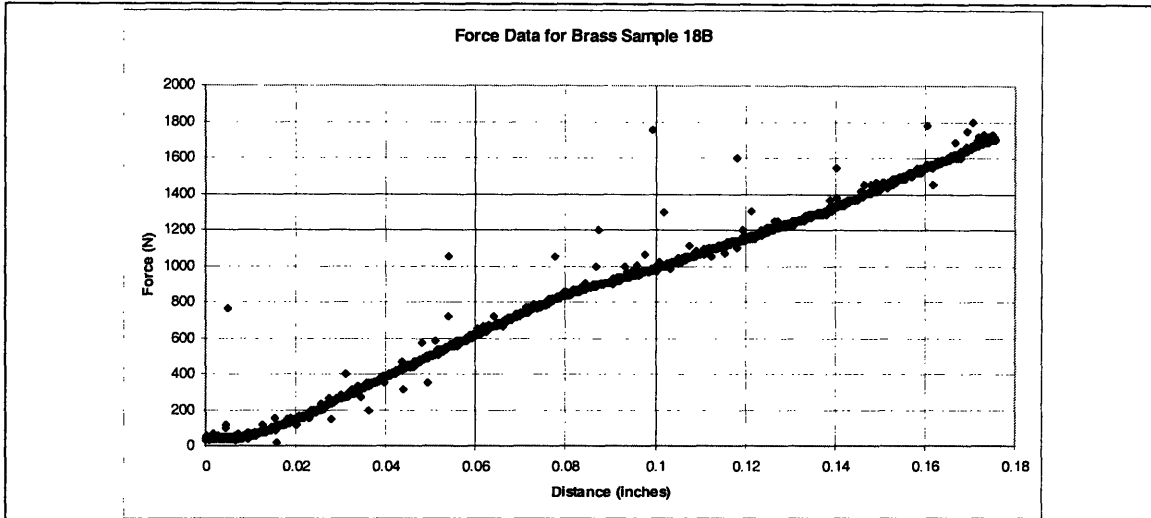


Figure 76. Experimental press fit force required for brass sample 18B. Maximum measured force is 1708 N.

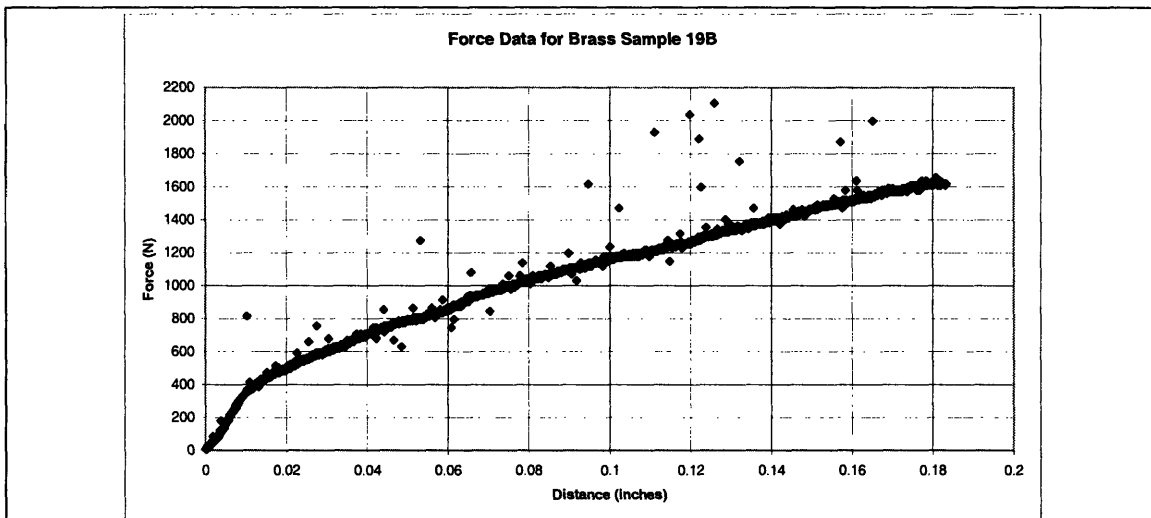


Figure 77. Experimental press fit force required for brass sample 19B. Maximum measured force is 1617 N.

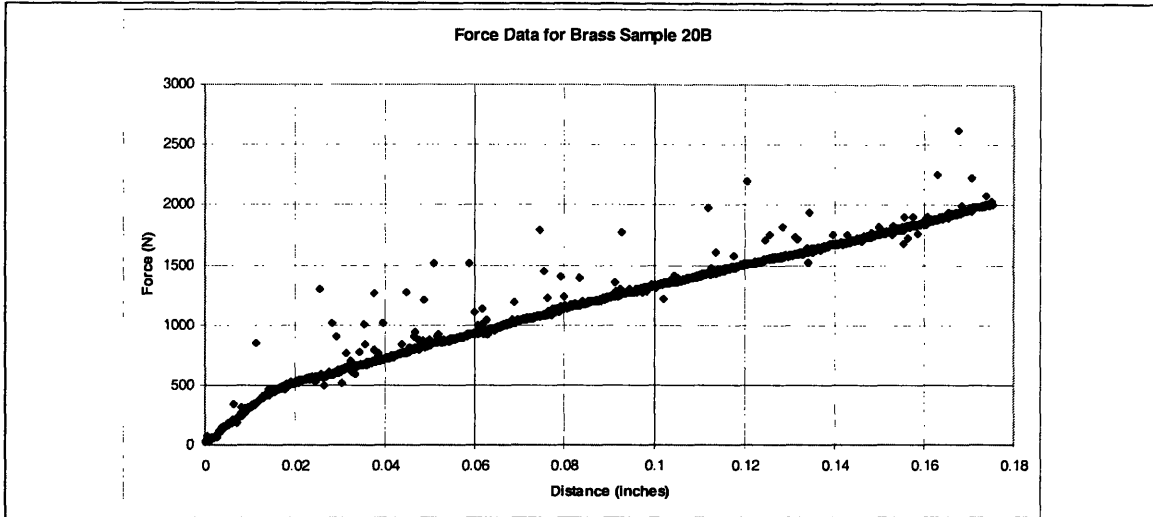


Figure 78. Experimental press fit force required for brass sample 20B. Maximum measured force is 2000 N.

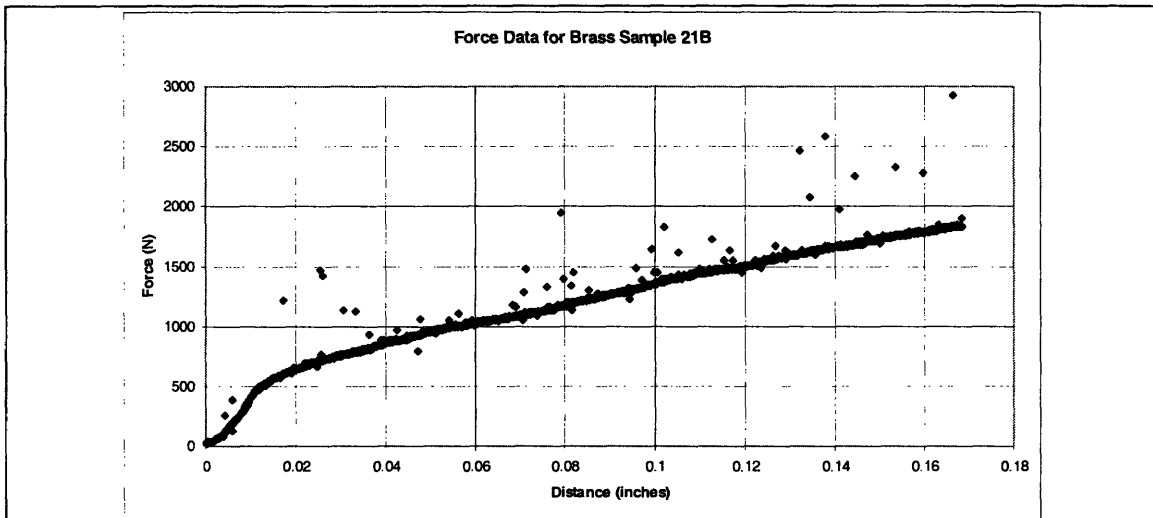


Figure 79. Experimental press fit force required for brass sample 21B. Maximum measured force is 1879 N.

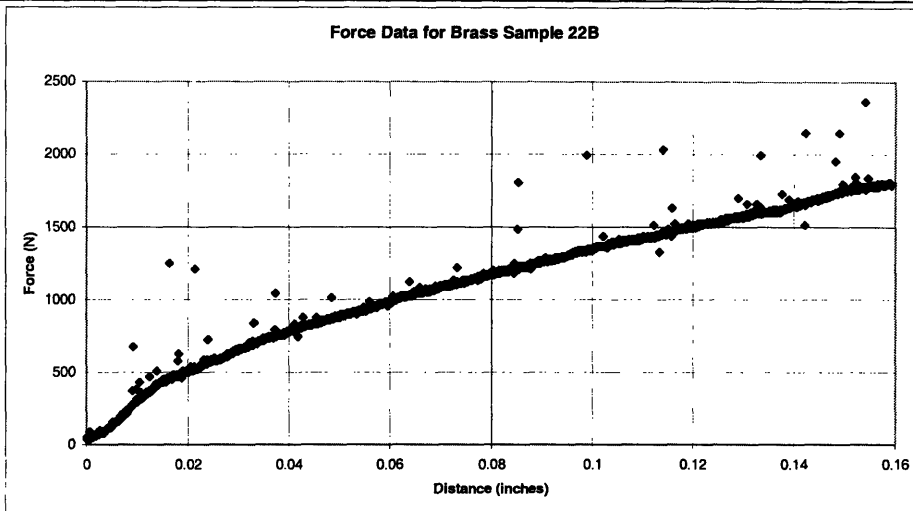


Figure 80. Experimental press fit force required for brass sample 22B. Maximum measured force is 1807 N.

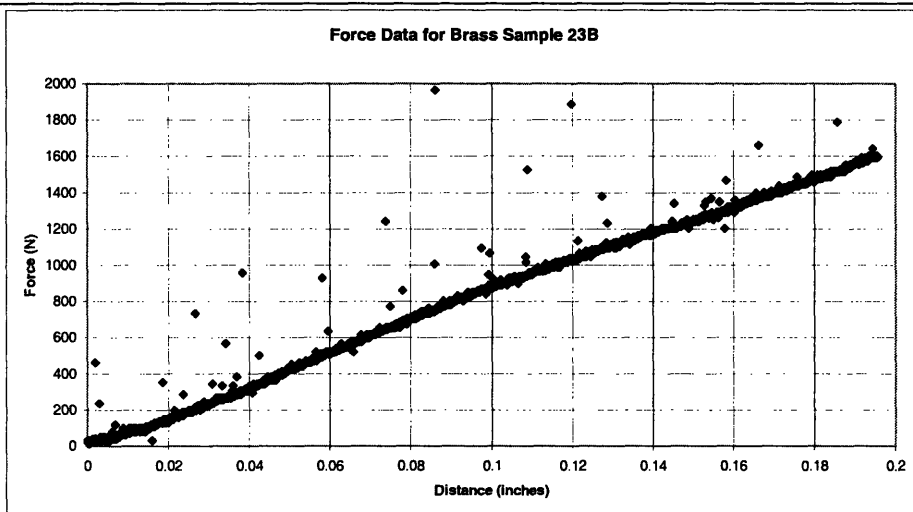


Figure 81. Experimental press fit force required for brass sample 23B. Maximum measured force is 1604 N.

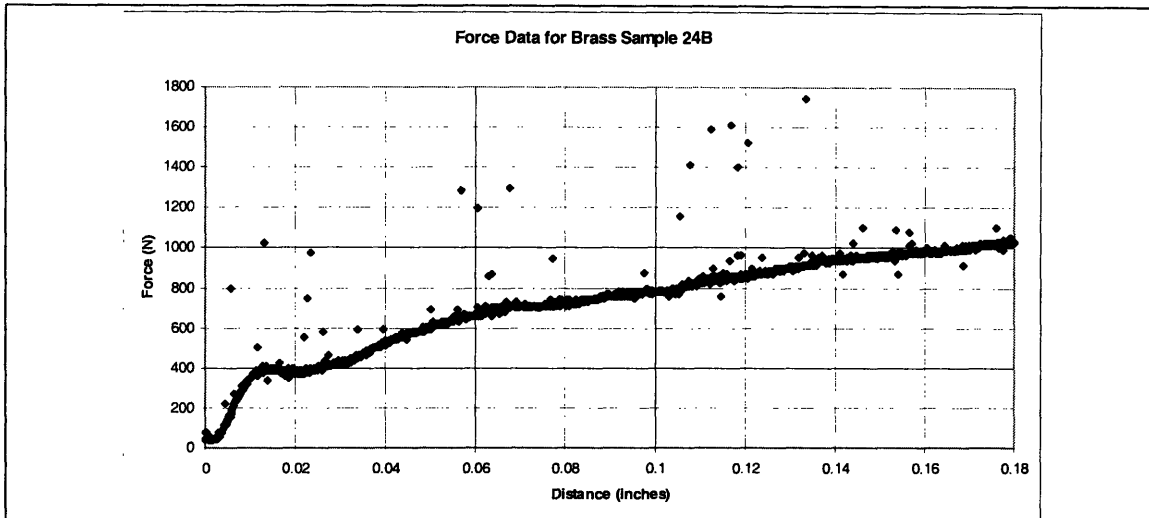


Figure 82. Experimental press fit force required for brass sample 24B. Maximum measured force is 1033 N.

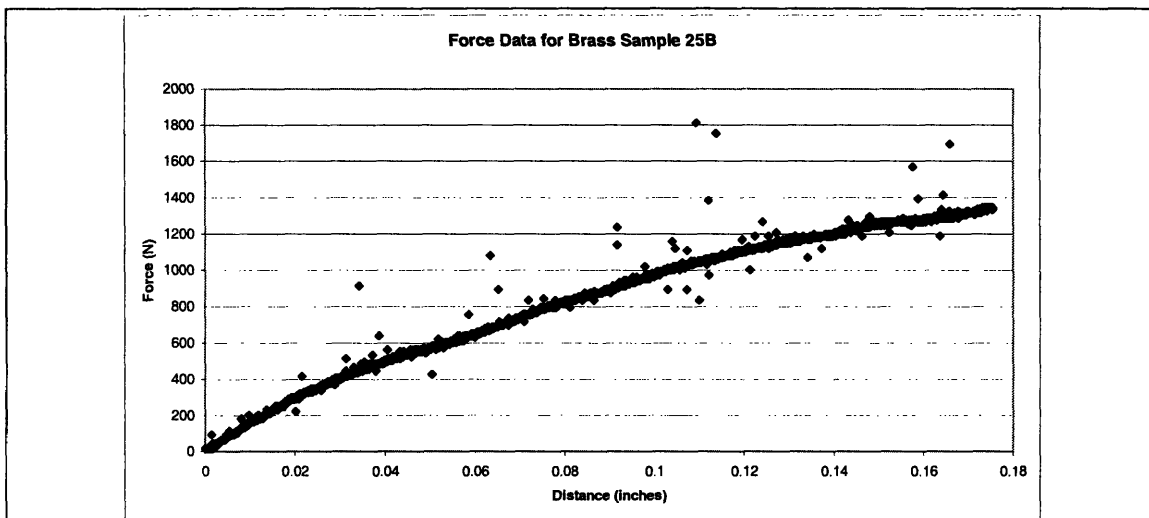


Figure 83. Experimental press fit force required for brass sample 25B. Maximum measured force is 1344 N.

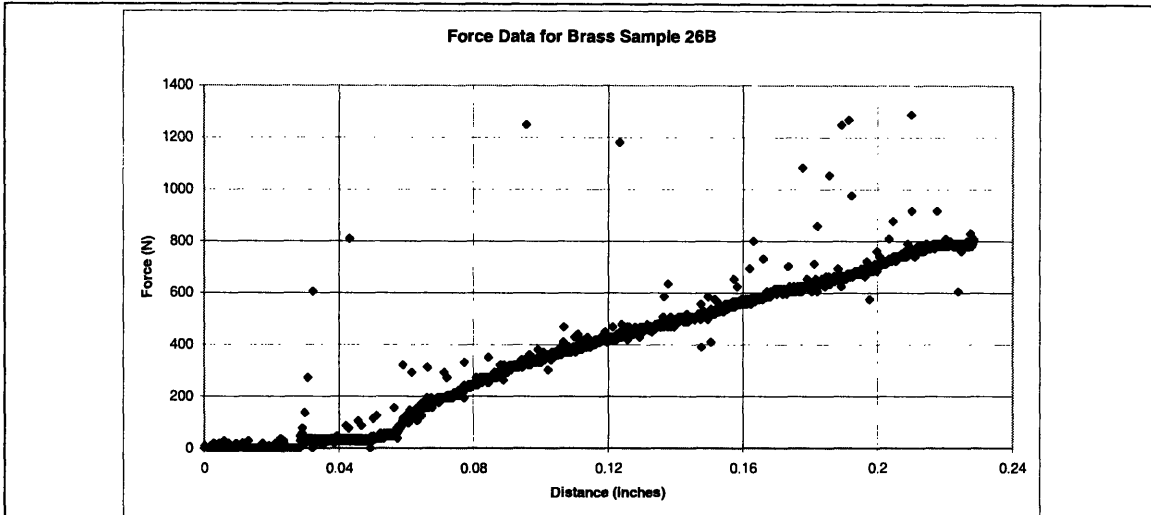


Figure 84. Experimental press fit force required for brass sample 26B. Maximum measured force is 800 N.

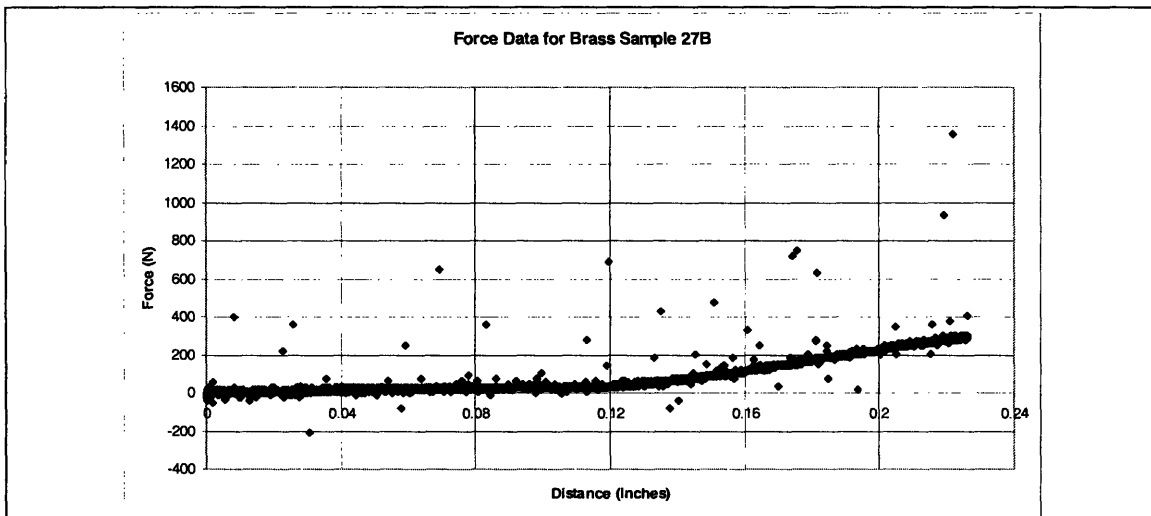


Figure 85. Experimental press fit force required for brass sample 27B. Maximum measured force is 300 N.

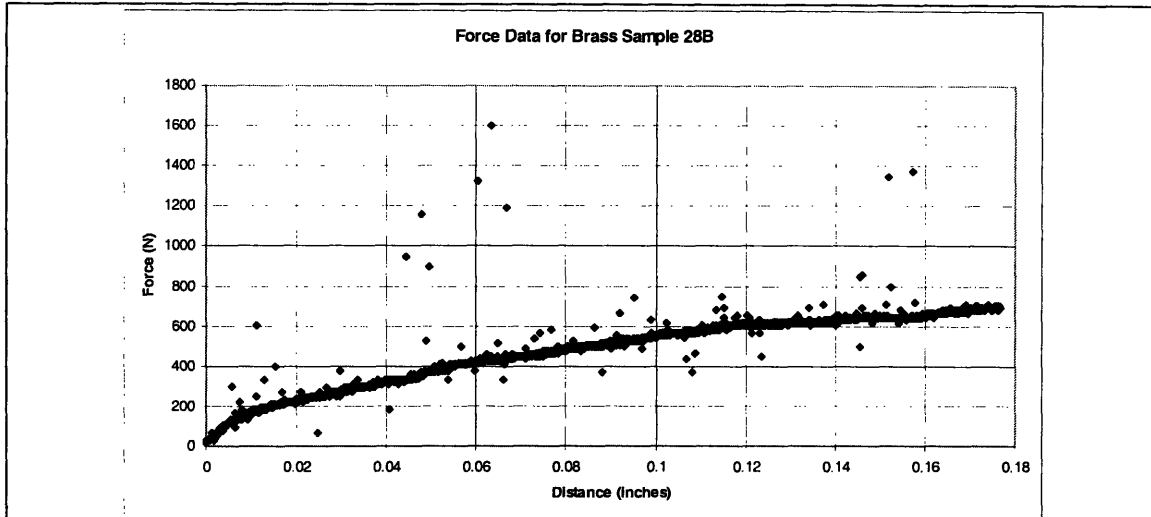


Figure 86. Experimental press fit force required for brass sample 28B. Maximum measured force is 701 N.

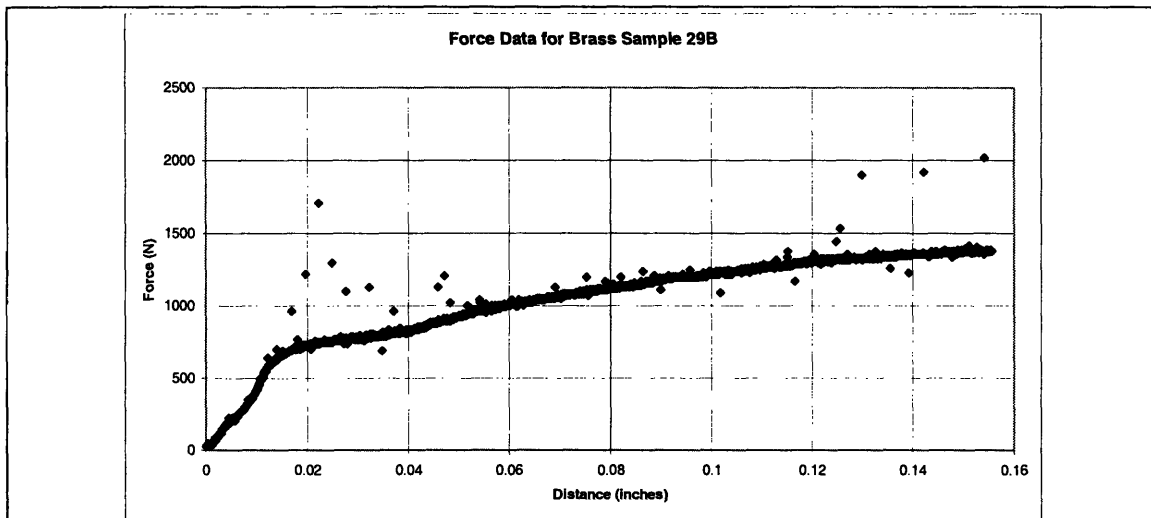


Figure 87. Experimental press fit force required for brass sample 29B. Maximum measured force is 1384 N.

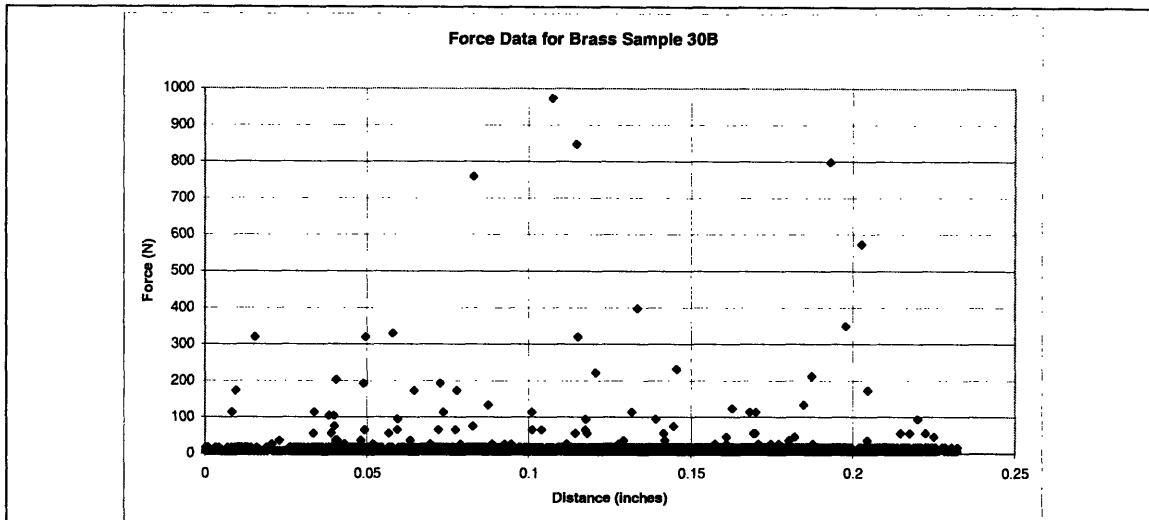


Figure 88. Experimental press fit force required for brass sample 30B. Maximum measured force is 0 N. Force readings were negligible.

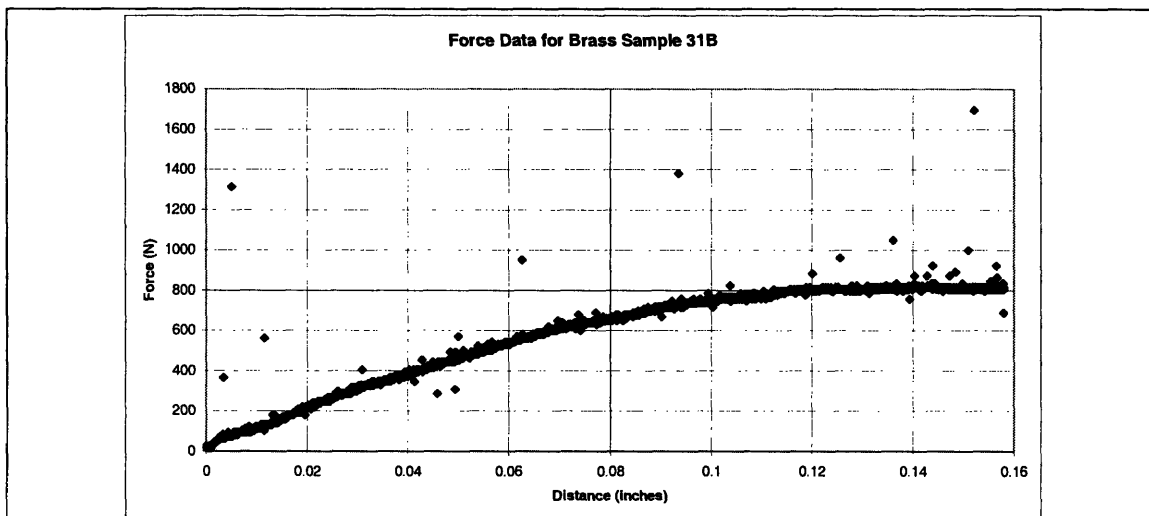


Figure 89. Experimental press fit force required for brass sample 31B. Maximum measured force is 815 N.

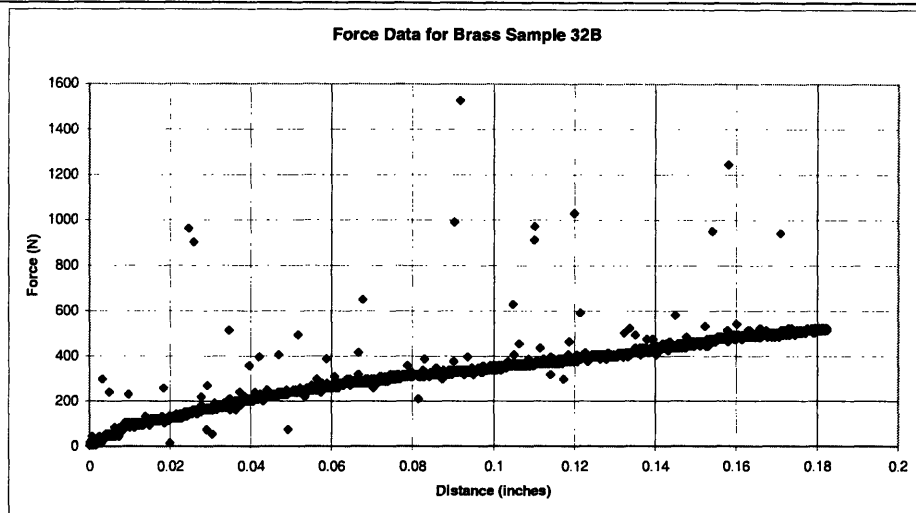


Figure 90. Experimental press fit force required for brass sample 32B. Maximum measured force is 523 N.

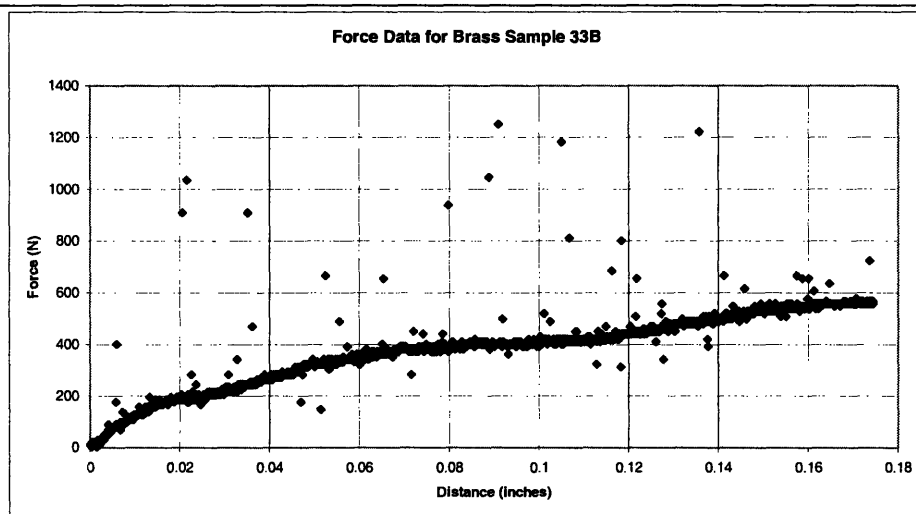
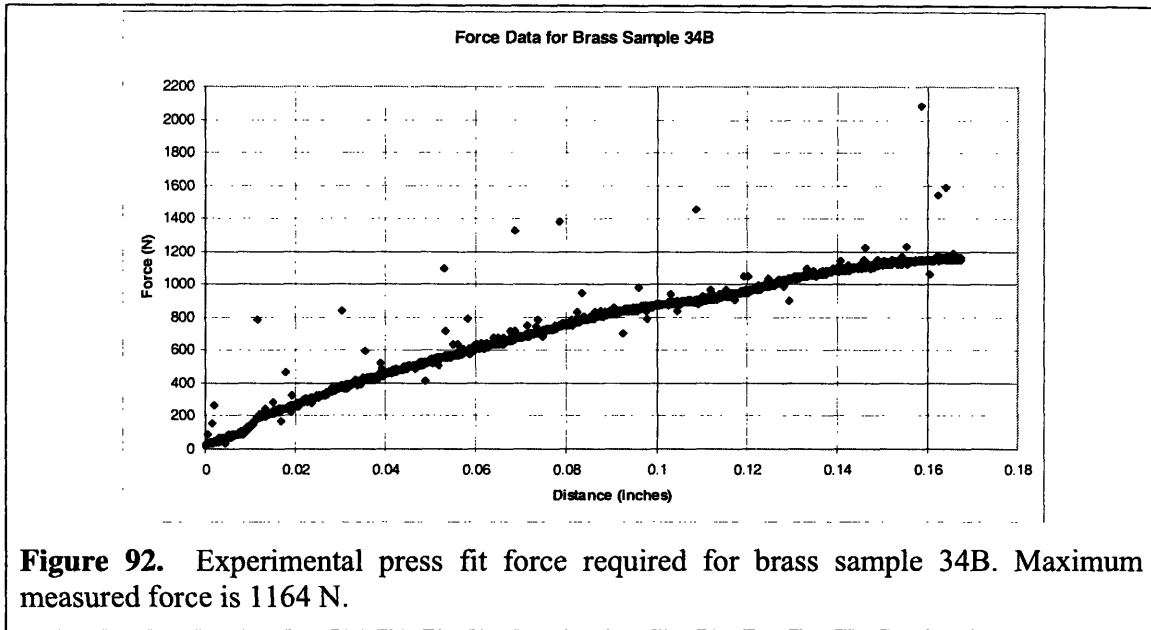


Figure 91. Experimental press fit force required for brass sample 33B. Maximum measured force is 567 N.



Appendix 5: Brass Torque Data

The following graphs show the torque vs. time graphs for each sample. From these graphs, the maximum torque was determined for each test as the maximum peak in the graph. There is some noise in the signal, which can be seen as somewhat random data points that do not behave similarly to the points on either side. These outlier data points have not been selected as the maximum torque data points. Please refer to Sect. 4.1 for interpretation of experimental results.

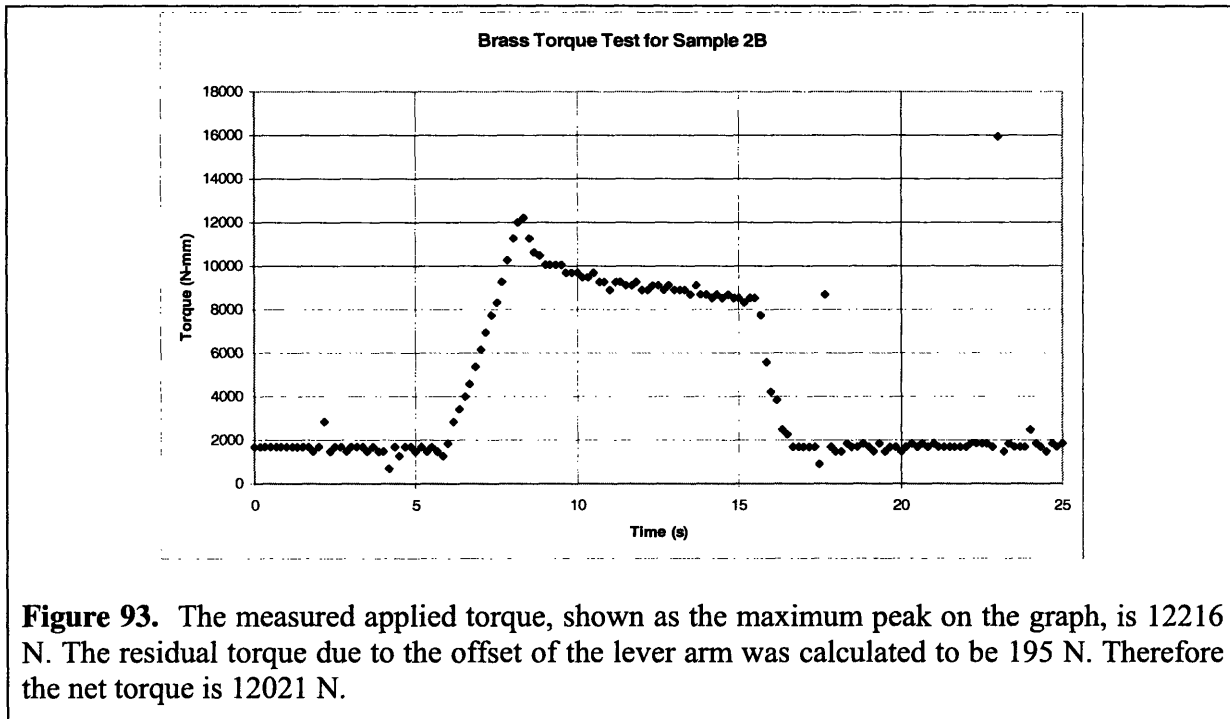


Figure 93. The measured applied torque, shown as the maximum peak on the graph, is 12216 N. The residual torque due to the offset of the lever arm was calculated to be 195 N. Therefore the net torque is 12021 N.

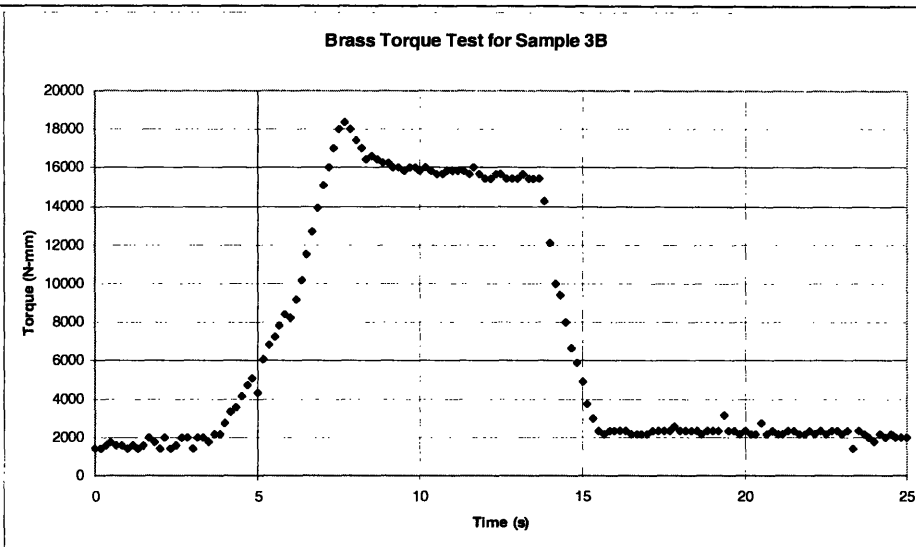


Figure 94. The measured applied torque, shown as the maximum peak on the graph, is 18383 N. The residual torque due to the offset of the lever arm was calculated to be 231 N. Therefore the net torque is 18152 N.

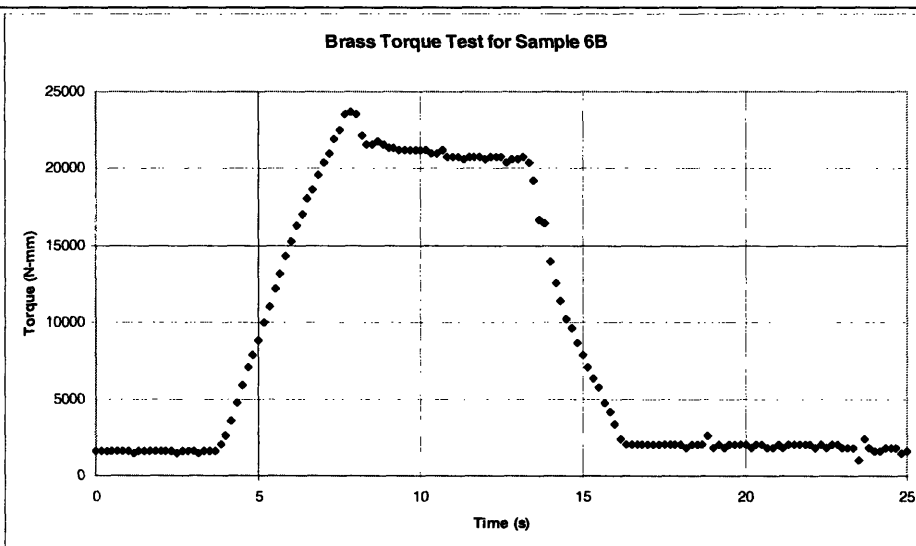


Figure 95. The measured applied torque, shown as the maximum peak on the graph, is 23708 N. The residual torque due to the offset of the lever arm was calculated to be 423 N. Therefore the net torque is 23285 N.

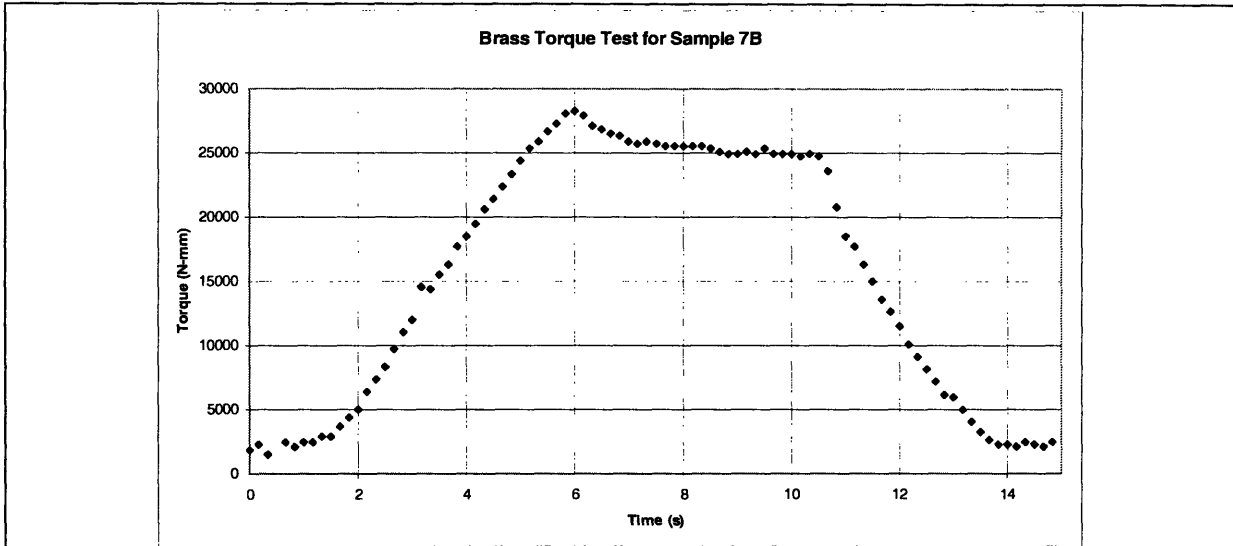


Figure 96. The measured applied torque, shown as the maximum peak on the graph, is 28253 N. The residual torque due to the offset of the lever arm was calculated to be 393 N. Therefore the net torque is 27860 N.

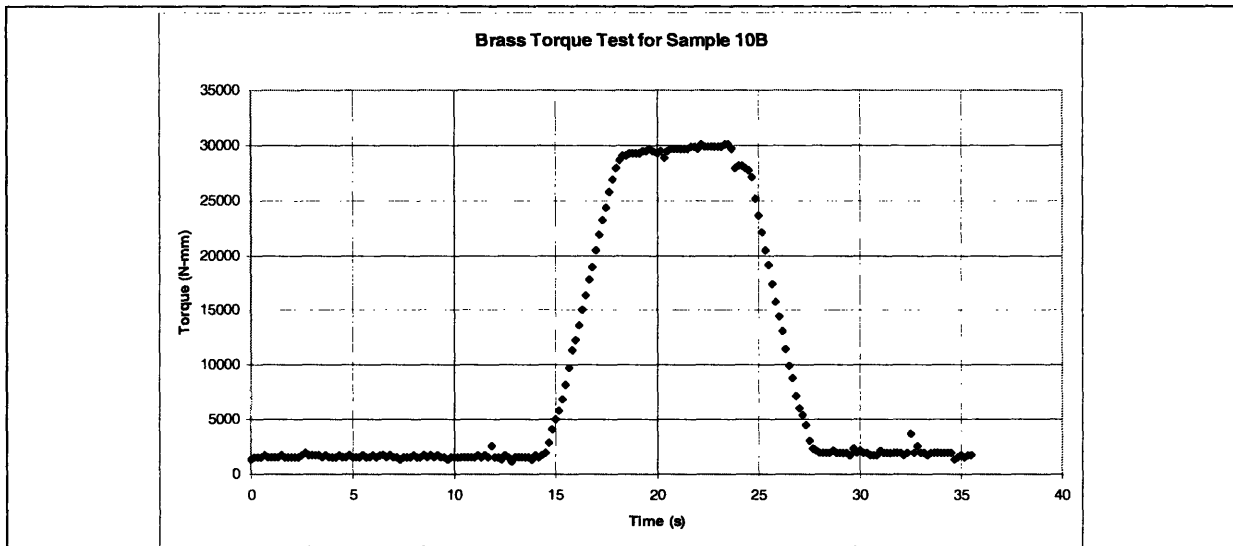


Figure 97. The measured applied torque, shown as the maximum peak on the graph, is 30064 N. The residual torque due to the offset of the lever arm was calculated to be 459 N. Therefore the net torque is 29605 N.

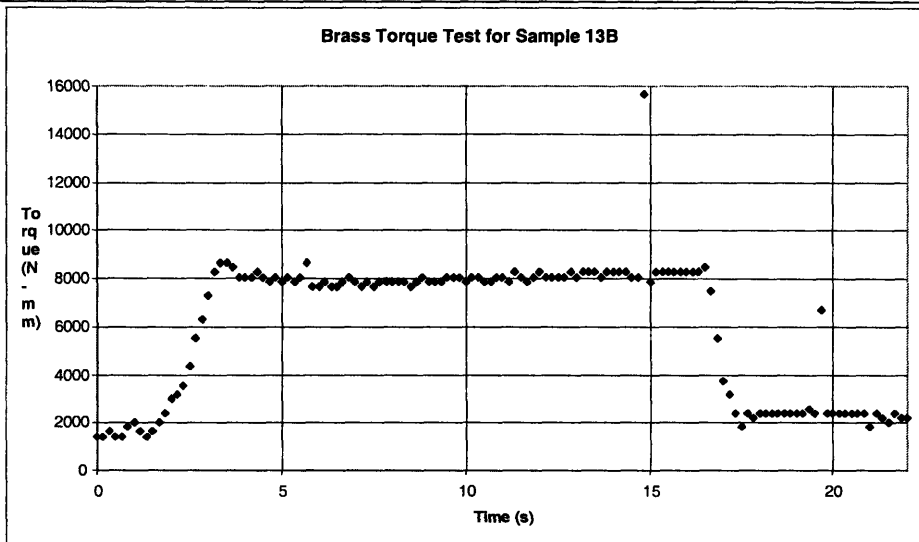


Figure 98. The measured applied torque, shown as the maximum peak on the graph, is 8648 N. The residual torque due to the offset of the lever arm was calculated to be 144 N. Therefore the net torque is 8504 N.

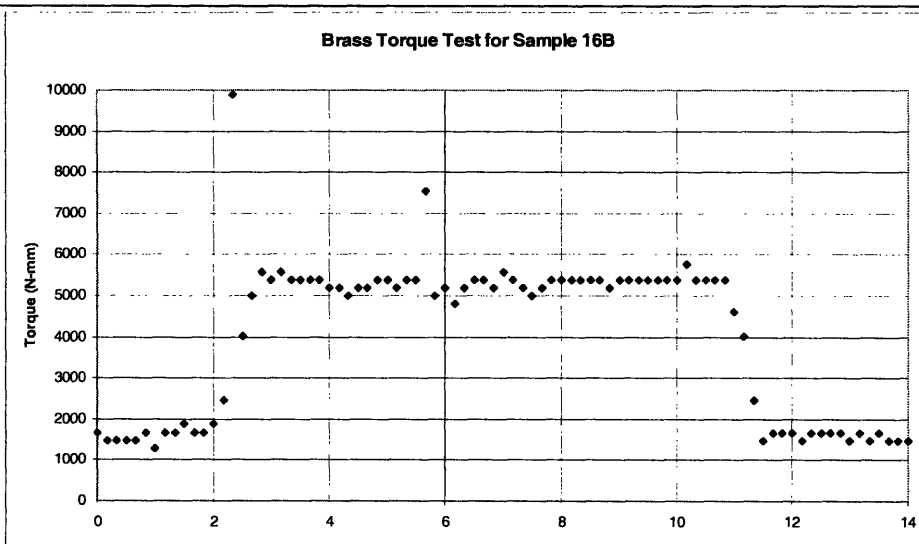


Figure 99. The measured applied torque, shown as the maximum peak on the graph, is 5779 N. The residual torque due to the offset of the lever arm was calculated to be 88 N. Therefore the net torque is 5691 N.

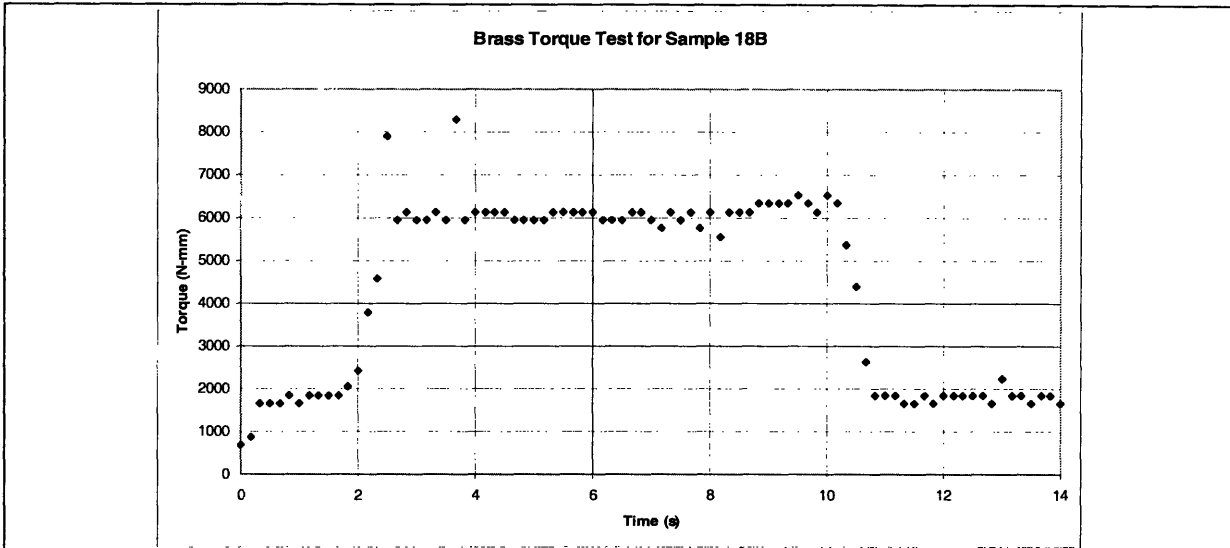


Figure 100. The measured applied torque, shown as the maximum peak on the graph, is 6532 N. The residual torque due to the offset of the lever arm was calculated to be 91 N. Therefore the net torque is 6441 N.

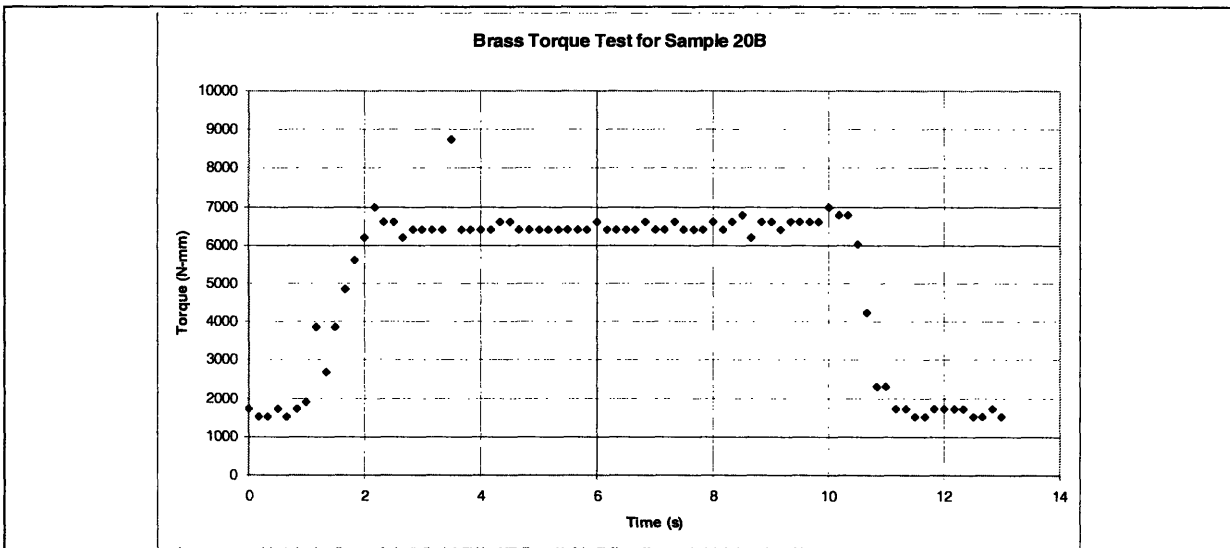


Figure 101. The measured applied torque, shown as the maximum peak on the graph, is 6988 N. The residual torque due to the offset of the lever arm was calculated to be 67 N. Therefore the net torque is 6921 N.

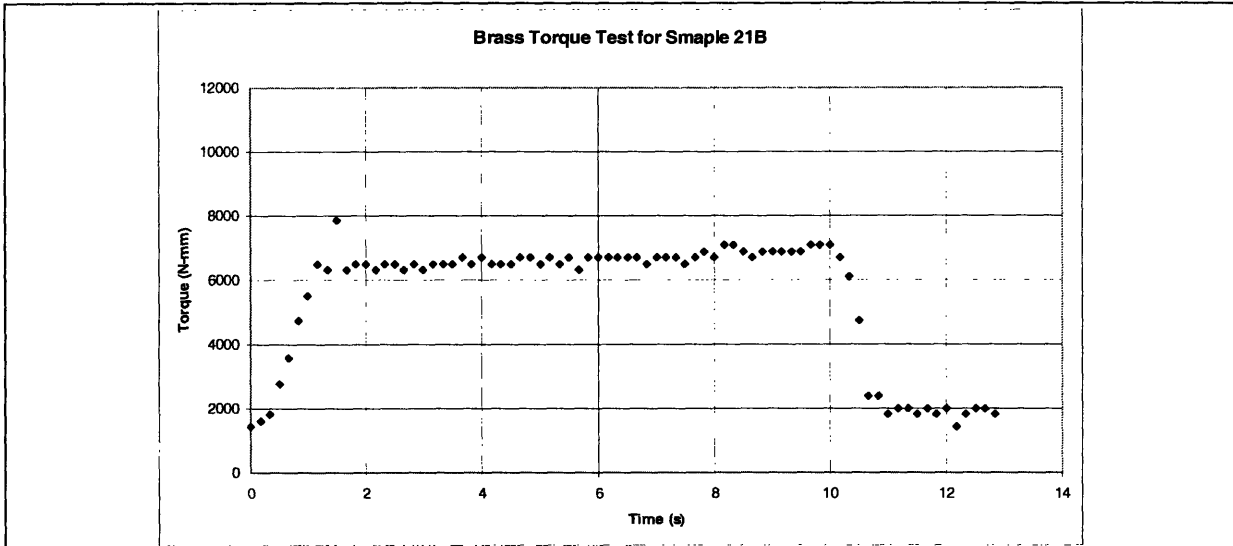


Figure 102. The measured applied torque, shown as the maximum peak on the graph, is 7086 N. The residual torque due to the offset of the lever arm was calculated to be 69 N. Therefore the net torque is 7017 N.

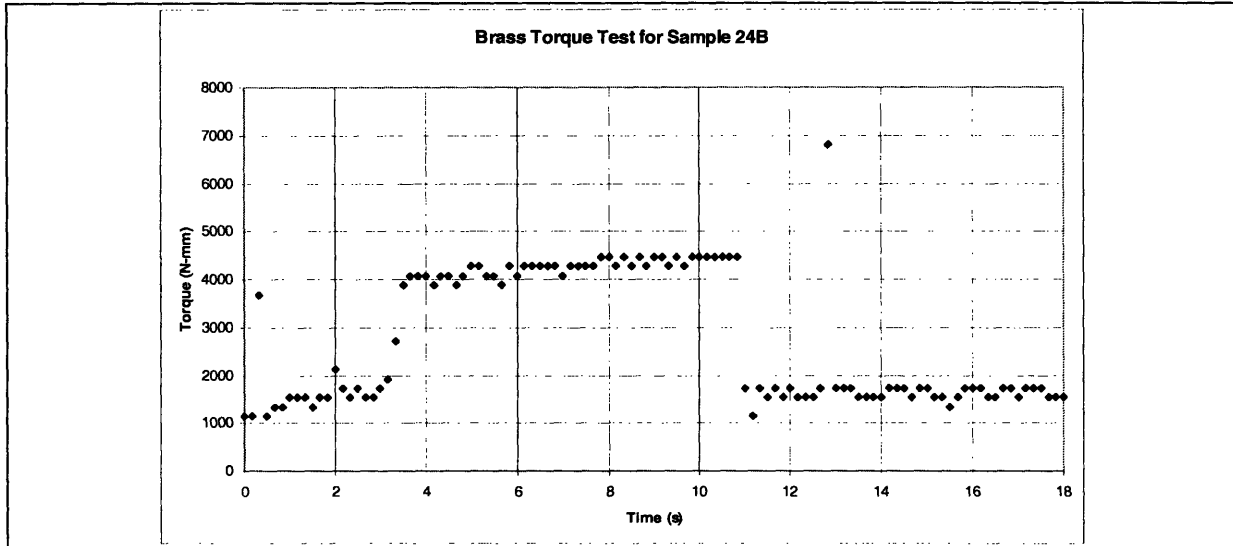


Figure 103. The measured applied torque, shown as the maximum peak on the graph, is 4464 N. The residual torque due to the offset of the lever arm was calculated to be 65 N. Therefore the net torque is 4399 N.

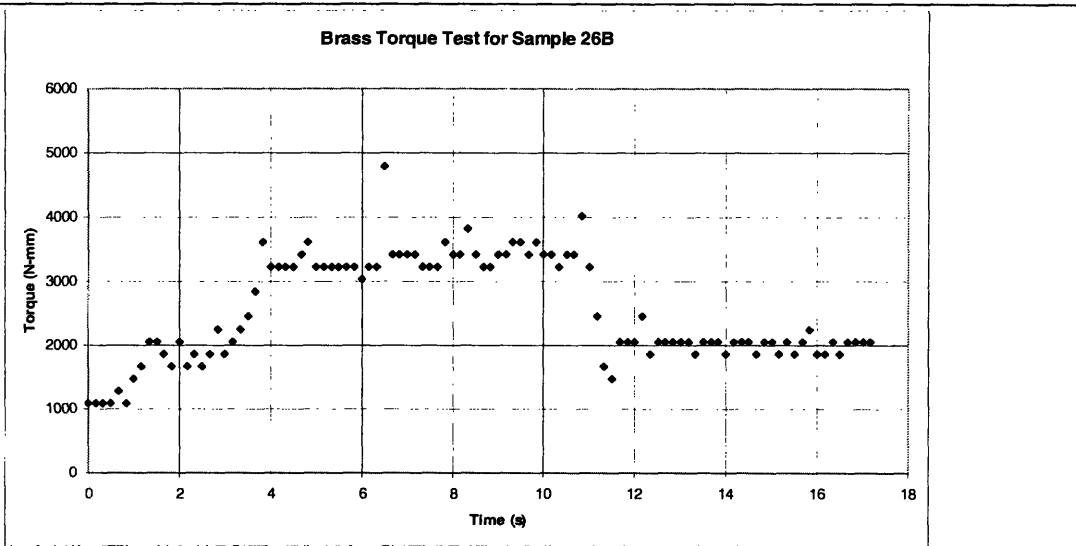


Figure 104. The measured applied torque, shown as the maximum peak on the graph, is 4012 N. The residual torque due to the offset of the lever arm was calculated to be 60 N. Therefore the net torque is 3952 N.

Data for samples 28B, 30B, 32B, and 33B was not collected. These samples required less than the torque of the lever to cause the hex to rotate independent of the dowel pin. Therefore, since the torque of the lever arm is 1617 N-mm, these samples required less than 1617 N-mm.